Copyright Warning & Restrictions

The copyright law of the United States (Title 17, United States Code) governs the making of photocopies or other reproductions of copyrighted material.

Under certain conditions specified in the law, libraries and archives are authorized to furnish a photocopy or other reproduction. One of these specified conditions is that the photocopy or reproduction is not to be "used for any purpose other than private study, scholarship, or research." If a, user makes a request for, or later uses, a photocopy or reproduction for purposes in excess of "fair use" that user may be liable for copyright infringement,

This institution reserves the right to refuse to accept a copying order if, in its judgment, fulfillment of the order would involve violation of copyright law.

Please Note: The author retains the copyright while the New Jersey Institute of Technology reserves the right to distribute this thesis or dissertation

Printing note: If you do not wish to print this page, then select "Pages from: first page # to: last page #" on the print dialog screen

ABSTRACT

DYNAMICS OF PHASE LOCKING IN NEURONAL NETWORKS IN THE PRESENCE OF SYNAPTIC PLASTICITY

by
Zeynep Akcay

The behavior generated by neuronal networks depends on the phase relationships of its individual neurons. Observed phases result from the combined effects of individual cells and synaptic connections whose properties change dynamically. The properties of individual cells and synapses can often be characterized by driving the cell or synapse with inputs that arrive at different phases or frequencies, thus producing a feed-forward description of these properties. In this study, a recurrent network of two oscillatory neurons that are coupled with reciprocal synapses is considered. Feed-forward descriptions of the phase response curves of the neurons and the short-term synaptic plasticity properties are used to define Poincaré maps for the activity of the network. The fixed points of these maps correspond to the phase locked modes of the network. These maps allow analysis of the dependence of the resulting network activity on the properties of network components.

Using a combination of analysis and simulations, how various parameters of the model affect the existence and stability of phase-locked solutions is shown. It is also shown that synaptic plasticity provides flexibility and supports phase maintenance in networks. Conditions are found on the synaptic plasticity profiles and the phase response curves of the neurons for the network to be able to maintain a constant firing period, while varying the relative activity phase of the neurons or vice versa. Synaptic plasticity is shown to yield bistable phase locking modes. These results are geometrically demonstrated using a generalization to cobwebbing for two dimensional maps. Type I neurons modeled with Morris-Lecar and Quadratic Integrate-and-Fire

are used to estimate the predictive power of the analytical results; however, the results hold in general.

The properties of the Negative-Leak model are also studied; a recent conductance-based model which is obtained by replacing a regenerative inward current with a negative-slope-conductance linear current. The map methods are extended to analyze networking properties of Negative-Leak neurons by including burst response curves. Finally, geometric singular perturbation techniques are applied to analyze how a hyperpolarization-activated inward current contributes to the generation of oscillations in this model.

This work introduces a general method to determine how changes in the phase response curves or synaptic dynamics affect phase locking in a recurrent network which can be generalized to study larger networks.

DYNAMICS OF PHASE LOCKING IN NEURONAL NETWORKS IN THE PRESENCE OF SYNAPTIC PLASTICITY

by
Zeynep Akcay

A Dissertation
Submitted to the Faculty of
New Jersey Institute of Technology and
Rutgers, The State University of New Jersey – Newark
in Partial Fulfillment of the Requirements for the Degree of
Doctor of Philosophy in Mathematical Sciences

Department of Mathematical Sciences
Department of Mathematics and Computer Science, Rutgers – Newark

May 2014

APPROVAL PAGE

DYNAMICS OF PHASE LOCKING IN NEURONAL NETWORKS IN THE PRESENCE OF SYNAPTIC PLASTICITY

Zeynep Akcay

Dr. Amitabha Bose, Dissertation Co-Advisor — Date
Professor, Department of Mathematical Sciences, NJIT

Dr. Farzan Nadim, Dissertation Co-Advisor — Date
Professor, Department of Mathematical Sciences and Department of Biological Sciences, NJIT

Dr. Victor V. Matveev, Committee Member — Date
Associate Professor, Department of Mathematical Sciences, NJIT

Dr. Horacio G. Rotstein, Committee Member — Date
Associate Professor, Department of Mathematical Sciences, NJIT

Dr. Dirk M. Bucher, Committee Member — Date
Associate Professor, Department of Biological Sciences, NJIT

BIOGRAPHICAL SKETCH

Author: Zeynep Akcay

Degree: Doctor of Philosophy

Date: May 2014

Undergraduate and Graduate Education:

- Doctor of Philosophy in Mathematical Sciences,
  New Jersey Institute of Technology, Newark, NJ, 2014
- Master of Science in Financial Mathematics,
  Florida State University, Tallahassee, FL, 2009
- Master of Science in Mathematics,
  Koc University, Turkey, 2007
- Bachelor of Science in Mathematics,
  Bogazici University, Turkey, 2005

Major: Mathematical Sciences

Presentations and Publications:

Z. Akcay, A. Bose and F. Nadim, "Effects of Synaptic Plasticity on Phase and Period Locking in a Network of Two Oscillatory Neurons," *The Journal of Mathematical Neuroscience*, 4:8, 2014.

Z. Akcay, "Effects of Synaptic Plasticity on Phase and Period Locking in a Network of Two Oscillatory Neurons," *Joint Mathematics Meeting*, Baltimore, MD, January 2014.

Z. Akcay, "Predicting Neuronal Network Activity with Synaptic Plasticity Using Numerical Phase Response Curves," *Dynamic Neural Networks: The Stomatogastric Nervous System Meeting*, San Diego, CA, November 2013.

Z. Akcay, "Effects of Synaptic Plasticity on Phase and Period Locking in a Network of Two Oscillatory Neurons," *IXth Annual Graduate Student Research Day*, NJIT, October 2013.

Z. Akcay, "Predicting Neuronal Network Activity with Synaptic Plasticity Using Numerical Phase Response Curves," *Student Seminar*, Department of Mathematical Sciences, NJIT, June 2012.

Z. Akcay, "An Agent Based Stock Price Model," *SPA 07: 32nd Conference on Stochastic Processes and their Applications*, University of Illinois at Urbana-Champaign, Champaign, IL, August 2007.

Z. Akcay, "Fractional Brownian Motion in Finance From Arbitrage Point of View," *M.S. Thesis*, Koc University, Turkey, 2007.

All praises and thanks be to God, the Lord of the Universe.

(Qur'an 1:2)

In the memory of my dearest Mom, Nazlı Akçay,
To my sweet Dad, Ali Rıza Akçay,
To my beloved husband, Serkan Özkan.

ACKNOWLEDGMENTS

First, I would like to express my deepest appreciation to my advisors, Professor Amitabha Bose and Professor Farzan Nadim, both of whom were sources of inspiration and knowledge during my graduate career. Specifically, I would like to thank Professor Bose, who provided invaluable insight, motivation and guidance during our weekly meetings. His kindness and patience during my journey in completing my research, provided a strongly productive environment. Also, I would like to thank Professor Nadim, for his strong encouragement, understanding and his fascinating ideas. He found time to meet with me whenever I needed him, and nurtured my growth as a scientist by providing support to attend many scientific conferences and meetings. I feel very fortunate to have had the opportunity to work with both of them.

I would like to extend my appreciation to my committee members, Professor Victor Matveev, Professor Horacio Rotstein and Professor Dirk Bucher, for taking the time to learn about my work and share their valuable comments. I would like to thank Professor Matveev and Professor Rotstein, also for helping me build the foundations for establishing ideas useful for my research through the courses they taught. Even if not a member of my committee, I would also like to thank Professor Jorge Golowasch, for sharing his original perspectives during lab meetings. Together, they have created a friendly environment of collaboration and support.

I would like to thank the members of the Nadim Lab, especially Diana Martinez and Yang Zhang, the members of Golowasch Lab and Bucher Lab and all the graduate students in the Department of Mathematical Sciences, NJIT, for their company and for exchanging ideas.

I would like to thank my professors at Florida State University, especially Professor Giray Ökten, Professor Penelope Kirby and Professor Betty Anne Case, for their support and encouragement from the beginning to the end of my graduate

career. I would also like to thank my friend and colleague, Tuğba Karabıyık, for her sincere company since my years at FSU.

I would like to thank my father, Ali Rıza Akçay, for believing in me and supporting me for many years. He was a model hard-working person, who inspired me, through his successful perseverance during the many hard times throughout his life. I would like to thank my mother-in-law, Şükriye Özkan, who cared for me during my illness and while I was preparing for my dissertation. I would like to thank my brother, Tuğrul Akçay and his wife, Ayzer Akçay, for cheering me up with their company. I would also like to thank all my loyal friends in the US and in Turkey.

Finally, I would like to thank my husband, Serkan Özkan, for supporting me in every aspect, and, especially, for filling my life with love, peace and energy.

TABLE OF CONTENTS

TABLE OF CONTENTS
(Continued)

Chapter **Page**

LIST OF FIGURES

LIST OF FIGURES
(Continued)

Figure **Page**

CHAPTER 1

INTRODUCTION

1.1 Background and Significance

The problem of understanding how neuronal networks generate behavior is a major subject of interest in neuroscience. The importance of this problem comes from the fact that many kinds of behavior in animals are generated by oscillatory neuronal networks. The output of a neuronal network is determined in part by the relative spiking times of its individual neurons. Therefore, how period and relative phase relations of the neurons in an oscillatory neuronal network corresponding to different behaviors are achieved and maintained is a question of considerable interest.

The phase relations in an oscillatory network correspond to the relation between the firing times of the neurons in the network. Any kind of phase relationship observed in a neuronal network results from the combined effects of individual cells and synaptic connections. These components have a variety of properties some of which change dynamically. They are also subject to neuromodulation that alters these properties. These neurons that can have very different intrinsic properties can sometimes spike in synchrony, in anti-phase, or in another fixed phasic relationship [23]. The different characteristics of the neurons and synapses all work together to determine a phase relation which corresponds to a meaningful network activity.

1.1.1 Factors Determining The Output of a Neuronal Network

The individual neurons in a network can differ in their intrinsic properties. For example, when isolated from their network, they can be silent, tonically spiking or bursting. Different neurons can have different responses to the synaptic inputs they receive. These different characteristics all play a role in determining the resulting network activity.

The neurons in a network communicate with each other through synaptic connections, therefore as important as the cellular properties are the synaptic properties in determining the network activity. The resulting period and phase relations of the network depend on the synaptic properties such as whether the synapse is excitatory or inhibitory, its strength and time course. Some of these synaptic properties might not be fixed but rather change dynamically for a given synaptic connection. The time dependent changes in the synaptic strength are referred as synaptic plasticity. If the strength increases with consecutive spikes of the presynaptic neuron, it is called short-term synaptic facilitation and if it decreases, it is called short-term synaptic depression [1].

Short-term synaptic depression is a property observed in many synaptic connections in human and animals. While the role of synaptic depression has to some extend been identified [28], it is not totally understood yet [1]. Apart from synaptic depression being observed commonly, some synapses show a combination of both depressing and facilitating effects. A presynaptic cell can send synaptic outputs to two different cells one of which has facilitating and the other has depressing property [1]. Some synapses show a combination of both depressing and facilitating effects. If a presynaptic cell fires at a fixed frequency, the synaptic strength reaches a steady value. The steady-state synaptic strength increases with presynaptic firing frequency, if the synapse is facilitating, and decreases if it is depressing. In some synapses, this value reaches a maximum at an intermediate frequency, referred to as the preferred frequency of the synapse [37]. This effect is assumed to be the result of the competing effects of depression and facilitation.

Neuromodulation plays an important role in determining the output of a network. It is the altering of cellular or synaptic properties through some released chemicals called neuromodulators [40]. Examples of neuromodulators are noradrenaline and serotonin which are proposed to change the firing pattern of the relay neurons

in thalamus [49]. Through neuromodulation, the same neuronal network can have different outputs. It is a means to reconfigure the functions of neuronal circuits and make them more flexible [4]. Hence, it is not possible to predict the network output without knowing which neuromodulators the network is under the influence of [32].

1.1.2 Methods to Study the Neuronal Activity

A useful approach to define and analyze the activity of neuronal networks is a Poincaré map derived from the properties of the neurons [2, 9, 10, 11, 12, 14, 17, 20, 21, 22, 36, 45, 58, 60, 62, 63, 61, 72, 73, 85, 88]. A map in general is a function $\Pi : M \to M$ through the relation $x_n = \Pi(x_{n-1})$ for a discrete time set $n \in \mathbb{Z}$ [51]. A Poincaré map takes a variable from a cross-section S of a flow back to S itself. Neurons are nonlinear oscillators and their activity can be modeled using a set of ordinary differential equations. These equations describe the change of the membrane potential and gating variables with respect to time [33, 53]. The oscillating neuronal activity corresponds to a periodic orbit of this dynamical system. Poincaré maps are used to simplify the network activity and obtain a relation for the variables from one firing cycle to the next.

When analyzing the neuronal activity by Poincaré maps, one of the main tools used is the phase response (or resetting) curve (PRC) of an individual neuron. The PRC quantifies the responses of an oscillatory neuron to perturbations [87]. It is a measurement of the relative changes in the period of an oscillating neuron due to brief and weak perturbations received at different phases of its cycle. According to this measurement, an oscillatory neuron can be categorized as Type I or Type II. The firing time of Type I neurons is always delayed (advanced) with an inhibitory (excitatory) perturbation regardless of the phase they receive it. On the other hand, both delay and advance of the firing time can be observed in Type II neurons [22]. The PRCs in general can be computed numerically (for model neurons) or experimentally

(for real neurons) [81]. If the perturbation is infinitesimally small, then the PRC of a model neuron can be obtained by linearizing the governing differential equations about the limit cycle and solving the adjoint equation [70]. We will call the PRC obtained from the adjoint method the infinitesimal phase response curve (iPRC). We will use the term PRC to refer to responses obtained by inputs that imitate synaptic inputs and that are not necessarily brief or weak.

In a small network, the PRC can be used to define a 1D map that measures the degree of network synchrony [17]. The PRCs of the individual neurons are combined to obtain maps for the evolution of frequency and phase relations in a network. The fixed point of these maps correspond to the possible oscillatory modes of the network. Such maps allow for the analysis of the network activity in a reduced system by considering only the effect of the synaptic inputs on cycle length, rather than considering multiple dynamic variables.

Several studies used these methods to study the activity of neuronal networks [2, 9, 10, 12, 14, 17, 20, 45, 55, 56, 62, 63, 61, 65, 72, 73, 85]. Some of these studies assumed infinitesimal perturbations and used iPRCs [11, 21] while others used more general PRCs [60, 63]. Although this theory assumes the neurons are intrinsic oscillators, it can be generalized to include non-oscillatory cells [72]. This allows analysis in networks consisting of both kinds of neurons.

PRC-based maps were also used to incorporate some properties of neurons or synapses. This approach was applied to understand synchronization of adapting neurons [14, 72]. The effect of conduction delays on network synchrony can also be analyzed using PRC based maps [85, 88]. The changes in the burst duration of neurons and their possible effects on the network activity are studied in [62] using a similar approach. In addition to a PRC, a burst resetting (response) curve (BRC) is used to define a map for the network activity when the burst duration changes in a network [62].

Another mathematical method commonly used to study the activity of a model neuron is geometric singular perturbation theory [69, 74, 80, 86]. This technique uses the fact that the activity of a neuron involves processes that occur at two different time scales. This fact allows one to analyze the activity of a neuron in reduced systems for fast and slow time scales. This technique, for example, was applied in a network of two reciprocally inhibitory cells to understand how oscillations are generated [80, 86] or to describe mechanisms that determine frequency in such networks [74].

1.1.3 Bistability in the Nervous System

Neuronal networks are dynamical systems, due to the dynamically changing nature of the neurons and the synaptic connections. Multistability in a dynamical system is the existence of multiple stable steady states. In other words, it is the simultaneous existence of multiple separate attractors in the phase space [15]. Multistability is generally observed in neuronal systems as bistability, the existence of two stable steady states. Bistability is observed in many neuronal systems, such as the voltage activity of individual neurons [13, 71, 83], the activity of the neuronal networks [6, 52] and the period of network oscillations [57].

It is shown in both experimental [13, 35, 83] and modeling [71, 78] studies that bistability can occur in the activity of individual neurons. Bistable firing behavior, either shifting between silence and low-freq firing or between two levels of tonic discharge frequencies is experimentally shown to exist in cat motor neurons [35]. It is shown in [13] that the patterns of neuronal activity in mammalian spinal motoneurons exhibit bistability. STG neurons demonstrate either tonic firing or bursting activity depending on certain ionic conductances [83]. These finding motivated modeling studies which studied the mechanisms of bistability in the firing patterns of the model neurons [71].

Bistability is associated with various roles. It is experimentally shown to play a role in the perception of visual stimuli [19, 84] and in pulse propogation [29]. It is required for the normal functioning of the human brain. The bistable state of the nucleus accumbens, a part of the human brain, displays bistability, which is crucial for proper gating of information [26]. An improper functioning of these neurons is associated with schizophrenia [30]. The interneuron network of the auditory cortex is another example of a bistable network [52]. The two states of the network are believed to be associated with the perception of different frequencies in sound waves by individuals.

Bistability can be achived through various mechanisms. The bistability of a neuron could be due to intrinsic properties of the neuron such as ion gated channels [13, 31, 35]. It is argued in [52] that the bistability of a neuron could be due to the bistability of a network. The mechanisms for bistability of a network are studied in many modeling studies [6, 44, 57]. Short term synaptic depression is shown to create bistability in oscillatory network of model neurons [6, 57]. It is argued that a single depressing synapse can produce two distinct oscillatory regimes and both regimes exist simultaneously for a range of synaptic coupling strength giving rise to bistability. It is shown in [44] that a hybrid network, consisting of a real neuron and computational neurons, coupled with model synapses yields bistability when both synapses are depressing.

1.1.4 Individual Neuron Dynamics

Since the neurons are the main components that compose neuronal networks, the factors that determine the dynamics of individual neurons are extremely important. How oscillations are obtained in a single neuron through the contribution of several ionic currents has been studied widely. Regenerative inward currents are known to be essential in the generation of oscillations [5]. Examples of such currents include I_{NaP},

I_{Ca}, and some non-specific cation currents such as I_{MI}. These currents have inverted bell-shaped I-V curves. It is shown experimentally in [89] that the crucial component of I_{MI} for the generation of oscillatory activity is only the linear portion of the I-V relationship with negative slope. This ionic current with a negative conductance is referred as the negative-leak current (I_{N-L}). Bose et al. show analytically that a model neuron is able to generate oscillations with only the potassium current and I_{N-L} [5]. We will refer to this model as the Negative-Leak (N-L) model.

Another important ionic current in the generation of oscillations is the hyper-polarization activated current (I_h) [64]. Its contribution to generation of oscillations has been studied widely [50, 68]. It has been shown in [5] that I_h plays a role in stabilizing oscillatory activity in N-L model neurons.

1.1.5 A Motivating Example: Pyloric Network

Central pattern generators (CPG) have been studied widely to understand how rhythmic motor output is obtained by the interaction of cellular and synaptic properties [18, 46, 59, 79]. CPGs are networks of interacting neurons that control rhythmic motor activity such as respiration, locomotion and chewing [16]. All CPGs in vertebrates and invertebrates share a common principle that they continue their activity in the absence of patterned input, when isolated from the nervous system [47, 59].

The pyloric network of the crustaceans is an example of a CPG. It controls the movements of the crustacean pyloric muscles. This system provides many advantages for studying CPGs; for example, the neurons and their connections in the network are readily identifiable and their voltage activities can be simultaneously recorded. It produces regular stable ongoing activity *in vitro* that is similar to the activity *in vivo*. It is also easy to subject this system to experimental manipulations; for example, it is possible to introduce specific ionic or synaptic currents by using dynamic clamp

techniques. Another attribute of this system is that the output of the network is easily observable through recording from motor neurons [46]. Hence, the pyloric network is a useful system to study the mechanisms used in phase determination. Lessons learned from it can be applied to more complex circuits like those in the human brain.

The pyloric network has a tri-phasic rhythm generated by a pacemaker group of neurons: the anterior burster (AB) and the pyloric dilator (PD) [46]. These neurons fire in the absence of any synaptic connections hence are intrinsic bursters. The rest of the neurons in the pyloric network (referred to as the follower neurons) are either quiescent or produce tonic activity when they are isolated from their synaptic connections. The electrical couplings between some cells cause their firing times to synchronize. Hence, such a group is treated as one cell for ease in modeling. The AB/PD group fires first, the lateral pyloric (LP) neuron fires next followed by the pyloric (PY) neuron in each cycle, causing the tri-phasic activity of the network.

The AB/PD group sends inhibitory synapses to all the other pyloric cells while the only chemical synapse they receive from the pyloric network is the inhibitory synapse from LP to PD. As the synapse from LP to PD is the only chemical synaptic feedback to the pacemakers, it has been studied widely [42, 55, 56, 66]. In some recent studies, the role of this feedback synapse was shown to promote stability [42, 55, 56].

The synaptic connections between PD and LP have some important plasticity properties. Both synapses have short-term depression in the biological range of frequencies (0.5-3 Hz). If a larger range of frequencies (0.1-4 Hz) is considered, both synapses demonstrate frequency preferences: when the membrane potential of the presynaptic neuron is voltage clamped using sine waves with changing frequency, the inhibitory post synaptic currents (IPSCs) from both cells have maximum responses at a preferred frequency [18, 82]. Both modeling and experimental studies were done to understand the effects of dynamic synaptic strength on phase locking of the network [43, 57]. It was proposed by Nadim et al. that it acted as a switch mechanism in the

regulation of the network frequency [57]. It was further proposed that the depressing property of the PD to LP synapse synapses acted to enhance phase maintenance [43].

The pyloric network is subject to extensive neuromodulation that modify the properties of the cells and synapses hence alter the network output [16, 46, 59]. With neuromodulatory effects, the network can run in a wide range of frequencies. Although the network frequency changes, the tri-phasic relation among the neurons stays unchanged. They are kept fixed with changing frequency. The absolute time delays between bursting activities of cells change with network frequency in a manner that enables the phase relations to stay fixed [8, 34]. There have been modeling studies to analyze the effects of several factors such as the electrical coupling between pacemakers [39, 75], synaptic or cellular properties [66, 79] on determination of the network frequency. Other studies combined modeling tools with geometric singular perturbation analysis to understand the factors having a role in phase and frequency determination [3, 7, 54]. In [67], it was proposed that LP and PY phases are determined by the intrinsic properties of the neurons rather than the synaptic connections. In [7], A-current and synaptic depression were proposed to act together to maintain phase. However, the mechanisms underlying the phase maintenance across a range of frequencies are still not understood.

1.1.6 Our Aim and Approach

Our motivation comes from the properties observed in the pyloric network. We consider a recurrent network of two neurons that represent AB/PD and LP. We include in our model network the synaptic plasticity property observed between the pyloric cells. With this simplified model, we would like to shed light to the mechanisms underlying phase maintenance in the pyloric network.

We combine the phase response information of the neurons with the properties of the synapses to define Poincaré maps for the activity of an oscillatory network of two

neurons. The synaptic properties we consider are the synaptic strength and duration that changes dynamically with frequency according to the models we propose. On the other hand, these properties have an effect on determining the network frequency. We combine these two pieces of feed forward information, the dependence of synaptic properties on network frequency and the dependence of the network frequency on synaptic properties to obtain feedback maps. These maps give the relative phases of the neurons and the network period as well as the dynamics of the synaptic properties from cycle to cycle. Fixed points of these maps correspond to the phase locked modes of the network. The stability of these modes can be analyzed by linearizing the maps around these points. These maps allow us to analyze the dependence of the resulting network activity on the properties of network components. In general, we do our analysis on simplified models for networks of two cells. This analysis advances our understanding of how dynamics of different network components contribute to phase and frequency determination in an oscillatory network.

Through experiments, it is easy to measure the steady-state response of a synapse at different input frequencies without knowing what the underlying dynamics are that give rise to this steady-state value. On the other hand, we define our maps for the evolution of the phase and synaptic properties from cycle to cycle when the network is not in the steady state. Therefore, using the steady-state measurements in building the maps can yield erroneous results. However, the results at the fixed point of these steady-state maps should be consistent with the measured data. We define maps that either use the steady-state values for the synaptic strength or its dynamics. We compare the results of the maps where the synaptic strength have dynamics or it obeys a steady-state relation. Hence, we show with an example that using steady-state relations is equivalent to using dynamics for synaptic strength.

The main advance in our work is the derivation of tools for analyzing higher-dimensional maps that incorporate the effects of synaptic plasticity and

provide predictions on circumstances under which an oscillatory network of neurons will phase-lock and at what period. In particular, we consider a network of two neurons, mutually coupled by inhibition in which the synaptic strength is frequency dependent. In deriving these maps, we must not only track the phases of each cell, but also the strength of each synapse. As a result, the 1D map that sufficed in prior studies needs to be replaced with 2D or 3D maps. For 2D maps, we derive a geometric method that generalizes the idea of cobwebbing. Namely, we show how iterations of the map can be tracked through different 2D surfaces. Moreover, projections of these surfaces onto a common plane yields two curves whose intersection is a fixed point of the map that corresponds to a phase-locked solution. We derive conditions on the PRCs and the plasticity profiles of the neurons to show how a network can have a range of parameters over which the network period remains constant, but the phase of locking between cells changes, or vice versa. We also use this map to show that short-term synaptic depression acts as a mechanism for bistability in the network activity. If the depression is strong enough, it may yield bistable phase locked solutions. So, in addition to supporting phase maintenance, synaptic plasticity provides flexibility to neuronal networks by serving as a mechanism for bistable phase locked solutions.

We extend the studies on the Negative-Leak model. We replace the standard calcium current in a Morris-Lecar (M-L) neuron with I_{N-L}, a linear current with negative slope and show that the two models have similar characteristics. We also consider the networking properties of N-L model neurons using maps. Since the burst duration changes in coupled N-L neurons, we use a burst response curve, in addition to PRCs. We derive a map that takes into account this change in the burst duration and obtain results consistent with simulations. Finally, we consider the effects of the h-current on generating oscillations in N-L neurons. We find conditions on the properties of the h-current that enables the oscillations to emerge and study the dynamics of the oscillations.

1.2 Overview of Thesis

Most of the thesis is dedicated to study the phase locking in a network of two neurons that are reciprocally coupled with inhibitory synapses. We study how the period and the phase relations of this network are effected with changes in the plasticity properties of the synapses.

We start by defining the mathematical models we use throughout the thesis in Chapter 2. We use Morris-Lecar model [53] to model the burst envelope of bursting neurons and Quadratic Integrate-and-Fire model [27] for spiking neurons. We use Negative-Leak model [5] for neurons with changing burst durations. Although we show our results for these specific models, the methods we develop do not depend on a specific type of model. Next, we give a formal definition of phase response curves and compare the PRCs for the two neuron models. Finally, we describe how plasticity can be modeled in spiking and bursting neurons in Chapter 2.

In Chapter 3, we first give the derivation of the Poincaré map when the synapses are static. When the synaptic conductances are equal, this map yields anti-phase results in identical neurons. We then include plasticity in the synapse between one of the two cells. We assume a model for generalized synaptic plasticity, with depression and facilitation components. We study the activity of this network in two ways. In the first approach, we use the plasticity model we assumed in the derivation of the map. In the second approach, we ignore the dynamics of this plasticity model but use only the values they reach at the steady-state in the map. We numerically show that the two maps yield the same steady-state solutions. When dynamics of the plasticity variables are used, the map has three dimensions, while using the steady-state values provides a decrease in the dimension, hence an ease in computing.

In Chapter 4, we consider the case when both of the neurons in the network have synaptic plasticity. We make use of the result shown in Chapter 3, that the maps using dynamics or the steady-state values of the plasticity variables yield equivalent results.

Using this result, we are able to analyze the evolution of the network period and the phase relations with a 2D map when both synapses show plasticity. First, we show geometrically how phase and period evolve. This is a generalization of cobwebbing to 2D maps. We also show geometrically how the fixed points of this map are obtained by the intersection of the surfaces defined by the map with the diagonal planes. Next, we compare the phase and period locking of networks with identical neurons and different synaptic plasticity profiles. We observe how the phase relation can stay fixed while the network period changes, and vice versa, with changes in the synaptic plasticity profile. We show the dependence of these network variables on the plasticity profiles of the neurons using contour plots. Then we find conditions for a network to have a fixed phase relation between its neurons while varying its period, or vice versa, using the Implicit Function Theorem. We conclude this chapter by showing the contribution of heterogeneity in the neurons to phase and period determination of the network. These findings provide an insight to the phase maintenance observed in real biological networks.

We use the same map approach in Chapter 5, to study other contributions of synaptic plasticity to phase locking. Different than Chapters 3 and 4, instead of a generalized synaptic plasticity, we only consider depression, and only in one direction. We define a 2D map where depression variable changes dynamically in each iteration. This map is also studied in [36]. The relation between the fixed points of this map and a static map is derived. We show that if the depression property is strong enough, it may cause bistable phase locking solutions in the network, where only one stable solution is observed in networks with static synapses. By numerically finding the eigenvalues of the 2D map, we show that the map undergoes a saddle-node bifurcation causing the fixed points lose stability.

Finally, in Chapter 6, we study the recent derived Negative-Leak model [5]. After we describe the model, we look at the networking properties of a network of

two N-L neurons coupled with inhibition. Using simulations, we observe that the burst duration of these neurons are not fixed but change with firing frequency. The maps we derived to study the network activity in earlier chapters assumed a fixed burst duration, which is the case in M-L neurons. Here, we describe the burst response curve that tracks the changes in the burst duration due to a synaptic perturbation. We use BRCs together with PRCs to define a 2D map for the activity of two neurons whose burst durations are not fixed and compare the results with simulations. We next compare the N-L model with the M-L model. We show a method of approximating the Ca^{2+} current in M-L model with a N-L current and compare the oscillations obtained from the two models. Lastly, we study the contribution of the h-current in the generation of oscillations in the N-L model. Using geometric singular perturbation techniques, we analyze how changes in the h-current parameters shape the oscillations.

CHAPTER 2

MATHEMATICAL MODELS FOR NEURONS AND SYNAPSES

In this chapter, we introduce mathematical models to describe neuronal and synaptic dynamics. Models for neuronal dynamics are described in Section 2.1. The phase and burst response curves are introduced in Sections 2.2 and 2.3, respectively. Finally, we describe models for synaptic dynamics in Section 2.4.

2.1 Dynamics of Neurons

2.1.1 Quadratic Integrate and Fire Model

The Quadratic Integrate-and-Fire [27] model is given by the equations

$$\frac{dV}{dt} = 1 + V^2 \tag{2.1}$$

$$V^+ = V_r \text{ when } V^- = V_{th} \ (V_r < V_{th}). \tag{2.2}$$

The first equation describes the dynamics of the membrane potential V. When V reaches the threshold V_{th}, a spike occurs and V is immediately set to the resting potential V_r. The advantage of using this model is that the firing period of the neuron can be analytically calculated. The intrinsic period of the neuron with dynamics given in Equations (2.1) is given by

$$P_0 = \arctan V_{th} - \arctan V_r. \tag{2.3}$$

If the presynaptic cell fires a sequence of spikes, then the term n^{th} cycle refers to the time duration between the n^{th} and $n + 1^{st}$ crossings of V_{th}. When the neurons are synaptically coupled, the time between subsequent firing of the same neuron may change. This time is called the cycle length, denoted by P_n in cycle n. When a perturbation with strength a is received by the neuron at time t_s, the first equation

in (2.1) becomes

$$\frac{dV}{dt} = 1 + V^2 + a\delta(t - t_s)$$

In this case, the cycle period of the neuron changes to

$$P_n = \arctan V_{th} - \arctan(\tan(P_0\phi + \arctan V_r) + a) + P_0\phi. \tag{2.4}$$

2.1.2 Morris-Lecar Model

An isolated Morris-Lecar [53] neuron is a conductance-based model neuron that contains the leak (L), potassium (K) and calcium (Ca) currents. The conductance and reversal potential of a given current X are denoted by $\bar{g}_X$ and E_X, respectively. The Ca current depends on an instantaneous function m_∞ of the membrane voltage (V) and is given by $I_{Ca} = \bar{g}_{Ca} m_\infty(V)(V - E_{Ca})$ where $m_\infty(V) = 0.5\,(1 + \tanh((V - V_a)/V_b))$. The parameters V_a and V_b govern the kinetics of the Ca current. The leak current is given by $I_L = \bar{g}_L(V - E_L)$. The K current is driven by a dynamic activation variable w and is given by $I_K = \bar{g}_K w(V - E_K)$. The equations for the membrane voltage V and K activation variable w are given by

$$\begin{aligned} \frac{dV}{dt} &= (I_{app} - I_L - I_K - I_{Ca})\,/C \\ \frac{dw}{dt} &= \frac{w_\infty(V) - w}{\tau_w(V)} \end{aligned} \tag{2.5}$$

where $w_\infty(V) = 0.5(1 + \tanh((V - V_c)/V_d))$ and $\tau_w(V) = 1/(\phi \cosh((V - V_c)/2V_d))$. The parameters V_a, V_b and ϕ govern the K kinetics. The parameter for the neuronal dynamics, C, denotes the membrane capacitance and I_{app} denotes the current externally injected to the neuron.

2.1.3 Negative Leak Model

A regenerative inward current has a nonlinear inverted bell shaped I-V curve (Figure 2.1). This current turns off at negative voltages and the curve has a positive slope at

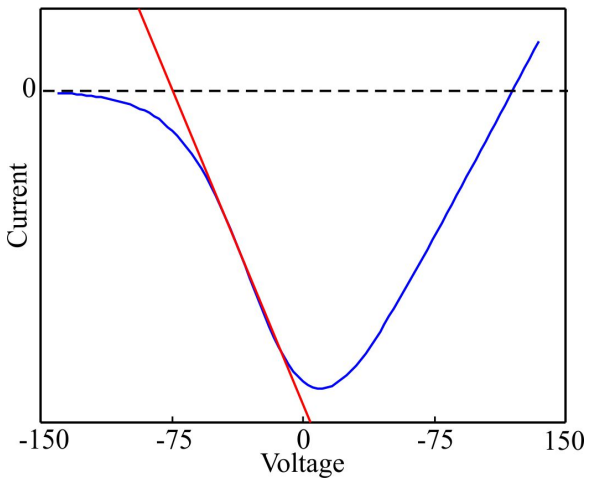

Figure 2.1 I-V curve of regenerative inward current and approximation by I_{N-L}.

higher voltages. It has a negative slope in-between. It is shown in a recent study that oscillations can be obtained when this current is replaced by a linear current which approximates this negative-sloped region [5]. This result gave rise to the hypothesis that "regenerative inward currents contribute to neuronal and network oscillations mainly through their negative-slope-conductance linear range of their I-V curve".

Therefore, if the regenerative inward current is replaced by a linear current which approximates the negative-slope region of the regenerative inward current's I-V curve (Figure 2.1), then such a model is capable of maintaining oscillatory activity. Using I_{N-L} instead of a curve with a nonlinear I-V curve enables us to analytically study how the interaction of several ionic currents contributes to oscillatory activity.

It has been shown in [5] that a model neuron having only a K and a $N-L$ current is capable of generating oscillations. Observe that one can combine the two linear leak currents I_L and I_{N-L} in a neuron model under one total leak current $I_{T-L} = g_{T-L}(V - E_{T-L})$ where g_{T-L} and E_{T-L} satisfies

$$\begin{aligned} g_{T-L} &= g_{N-L} + g_L \\ g_{T-L}E_{T-L} &= g_{N-L}E_{N-L} + g_L E_L. \end{aligned}$$

When the total leak conductance g_{T-L} is negative, it has a destabilizing effect on the membrane voltage. With this notation, the equations of this basic N-L model are

$$\begin{aligned} \frac{dV}{dt} &= -(I_K + I_{T-L})/C \\ \frac{dw}{dt} &= \frac{w_\infty - w}{\tau_w(V)}. \end{aligned} \tag{2.6}$$

where $I_K = g_K w(V - E_K)$ and $I_{T-L} = g_{T-L}(V - E_{T-L})$. The conductance g_{T-L} is less than zero which has a destabilizing effect on the membrane voltage. When certain relationships between the parameters are satisfied, Equations 2.6 yield stable oscillations [5].

The N-L model with the h-current is described in Chapter 6 where the effect of the h-current in the creation of oscillations in N-L neurons is discussed.

2.2 Phase Response Curves

The phase response curve of an oscillator describes how the period of the oscillator changes depending on the phase at which it receives a perturbation (Figure 2.2). In general, the PRC can be computed numerically (for model neurons) or experimentally (for biological neurons) by injecting a brief perturbing current (such as a small current pulse) and measuring the effect of this perturbation on the cycle length as a function of the phase of the perturbing input. If the perturbation is infinitesimally small, then an infinitesimal phase response curve (iPRC) of the model neuron can be obtained by linearizing the governing differential equations about the limit cycle and solving the adjoint equation. Throughout this thesis, we use the term PRC to refer to responses calculated by direct perturbations, for example ones that imitate synaptic inputs.

Denote by P_0 the intrinsic period of a cell. Suppose a perturbation is given at time dt after the firing of the cell. This yields a phase $\phi = dt/P_0$ of the perturbation. Denote by $\tilde{P}$ the time between when a cell fires prior to a perturbation and the

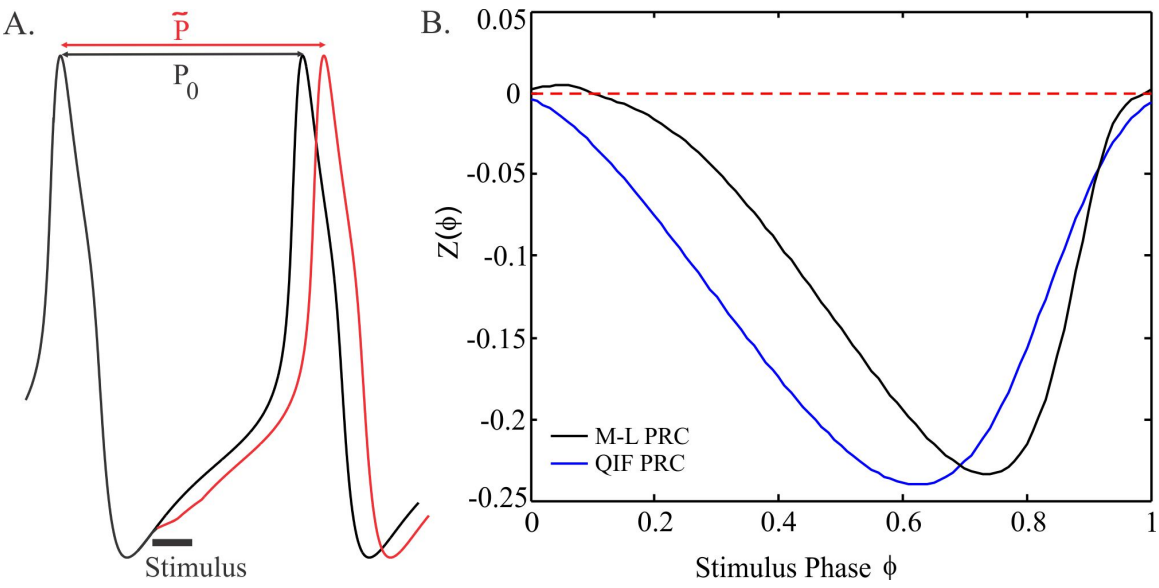

Figure 2.2 PRC due to synaptic input. A. A brief perturbing current pulse stimulus is used to measure the PRC as described in equation (2.7). B. The PRCs obtained from the Morris-Lecar model (2.5) and QIF model (2.1).

subsequent firing of the cell when a perturbation is given at phase ϕ. Then we define the PRC as

$$Z(\phi) = \frac{P_0 - P_n}{P_0} \tag{2.7}$$

In general, the effects of a perturbation to the current cycle of a neuron is referred as the first order PRC, while the effects to the following cycle is referred as the second order PRC. The PRC refers to the first order PRC unless noted otherwise. The PRC of a QIF neuron can analytically be calculated using equations (2.3) and (2.4). It is given by

$$Z(\phi) = \frac{\arctan(\tan(P_0\phi + \arctan V_r) + a) - \arctan V_r}{P_0} - \phi \tag{2.8}$$

The PRC of a M-L model neuron (2.5) can numerically be computed. We choose parameters so that the oscillations arise through a saddle node on invariant circle (SNIC) bifurcation. Neurons that oscillate through a SNIC bifurcation have a Type

1 iPRC [23], which is always of one sign. In the case of an inhibitory perturbation received by the neuron, the Type 1 iPRC is never positive and the next firing time is therefore delayed. A PRC obtained from our model neurons for a specific synaptic strength is shown in Figure 2.2. It is computed by applying a perturbation of the form

$$I_{syn} = g_{pre \to post} \mathrm{H}(\mathrm{V_{pre}} - \mathrm{V_{th}})(\mathrm{V_{post}} - \mathrm{E_{syn}}). \tag{2.9}$$

The reference point to compute the PRC is chosen to be when V crosses V_{th} in the positive direction. Note again that this method of computing the PRC is different from computing the iPRC of a spiking neuron which yields a strictly Type 1 PRC. The PRC we obtain is very similar, but there is a region of the PRC that is positive near small stimulus phases due to the longer active duration of the neuron. The PRCs of the M-L and QIF model neurons we use throughout this work are qualitatively the same.

Selection of PRCs

In Chapters 3 and 4, for our analytical estimates to match the results of numerical simulations of the model, we took advantage of the computability of a PRC for the M-L neuron. In each iteration, we numerically computed the response of a neuron to a synaptic input of a specific strength at a specific phase. Although this method yields accurate results, it is computationally slow and it is almost impossible to implement on biological neurons. For this purpose, we created a meshed PRC measured at discrete phase points and for a discrete set of predetermined synaptic strengths. We used mesh sizes of 0.1 for the phase and 0.0125 for the synaptic strength to obtain a total of 77 points of numerically-computed phase response values. The responses to the phases and strengths not on the mesh points were calculated by linear interpolation.

2.3 Burst Response Curves

In addition to the cycle period, the burst duration of a neuron may change due to perturbations received. This is tracked by a burst response curve which is defined in a similar fashion with a PRC. A BRC measures how much the burst duration alters with perturbations received [62]. The first and second order BRC is defined by,

$$W^i = \frac{b_0 - b_i}{b_0} \tag{2.10}$$

for $i = 1, 2$, where b_i denotes the altered burst duration in the i^{th} cycle of the neuron, when a perturbation is received in the 1^{st} cycle.

2.4 Models for Synaptic Plasticity

In this section, we describe some models for synaptic plasticity. The short-term synaptic plasticity in spiking cells can be described by a phenomenological model [48],

$$\begin{aligned} r' &= (1-r)/D - ru\delta(t-t_n) \\ u' &= (U-u)/F + U(1-u)\delta(t-t_n). \end{aligned} \tag{2.11}$$

Here, r is called the depression variable, which represents the available synaptic sources while u is called the facilitation variable, which represents the fraction of the resources activated by the action potential. The recovery time constants for the r and u variables are D and F, respectively. When an action potential occurs at time $t = t_n$, an amount ru of synaptic resources is activated and this amount is reduced from the amount of available resources. At the same time, the facilitation variable is increased by $U(1-u)$ as a result of the action potential. This model is capable of describing depressing synapses when the facilitation variable u is fixed and facilitating synapses when the depression variable r is fixed. When both of them are

allowed to vary, the synaptic conductance reaches a maximum at an intermediate firing frequency, referred as the preferred or resonant frequency.

2.4.1 Synaptic Depression Model for Instantaneous Spikes

The model (2.11) for short-term synaptic depression is modified in [36] using the following equations

$$\begin{cases} \frac{dr}{dt} = \frac{1-r}{\tau_r} & \text{after neuron fires} \\ r^+ = f \cdot r^- & \text{when neuron fires.} \end{cases} \tag{2.12}$$

Here, the amount of available synaptic resources is reset by a fraction $f(0 < f < 1)$ at the instant that the neuron fires and recovers to 1 with time constant τ_r after the spike. Hence, the value of the depression variable r heavily depends on the firing period of the neuron. When the neuron is firing with a fixed period of P, then, the depression variable r oscillates between a minimum value r_{min} and a maximum value r_{max} at the steady state. Therefore, the value of depression at the onset of a spike at the steady state can be obtained from equation (2.12) as

$$r_{max} = \frac{1 - e^{-P/\tau_r}}{1 - fe^{-P/\tau_r}}. \tag{2.13}$$

Observe that if P is large, r approaches 1, otherwise it approaches 0.

2.4.2 Synaptic Plasticity Model for Bursting Neurons

We modify the synaptic plasticity model [48] for neurons that have broader action potentials or those for which the burst envelope instead of individual spikes are modeled. We again assume that there are two variables which determine the strength of the synapses when a neuron fires; the depression variable r and a facilitation variable u. They change according to the activity of the presynaptic cell and together

determine the synaptic strength. These variables obey the following dynamics

$$\begin{aligned} \frac{dr}{dt} &= \begin{cases} \frac{-r}{\tau_1}, & V \geq V_{th} \\ \frac{1-r}{\tau_2}, & V < V_{th} \end{cases} \\ \frac{du}{dt} &= \begin{cases} \frac{1-u}{\tau_3}, & V \geq V_{th} \\ \frac{U-u}{\tau_4}, & V < V_{th}. \end{cases} \end{aligned} \tag{2.14}$$

When the membrane voltage of the presynaptic cell is above the synaptic threshold V_{th}, the depression variable r approaches 0 with the time constant τ_1, representing the depletion of available synaptic resources. During this time interval, the facilitation variable u approaches 1 with the time constant τ_3, representing the increase in utilized resources. When the membrane voltage is below the synaptic threshold, these variables recover to their steady state values of 1 and U, with the time constants τ_2 and τ_4, respectively. The strength of the synapses is determined by scaling the maximal synaptic conductance by the product of the values of these variables at the onset of a burst. Hence, the synaptic conductance is given by $g_{pre\to post} = \bar{g}_{pre\to post} r_n u_n$, where r_n and u_n are the values of r and u when the presynaptic membrane potential passes synaptic threshold in the n^{th} cycle (n is defined below).

2.4.3 Steady State Synaptic Plasticity Profiles

If the cell is firing with a fixed frequency and a fixed burst duration, then it reaches an oscillatory steady state. The values r and u also reach steady states and each oscillates between a minimum and a maximum value. At steady state, when crossing the synaptic threshold, the values of r_n and u_n are, respectively, r_{max} and u_{min}. These values can be calculated from equations (2.15) as

$$\begin{aligned} r_{max} &= \frac{1 - e^{-t_b/\tau_2}}{1 - e^{-t_a/\tau_1} e^{-t_b/\tau_2}} \\ u_{min} &= \frac{U + e^{-t_b/\tau_4} - e^{-t_b/\tau_4}(U + e^{-t_a/\tau_3})}{1 - e^{t_a/\tau_3} e^{-t_b/\tau_4}} \end{aligned} \tag{2.15}$$

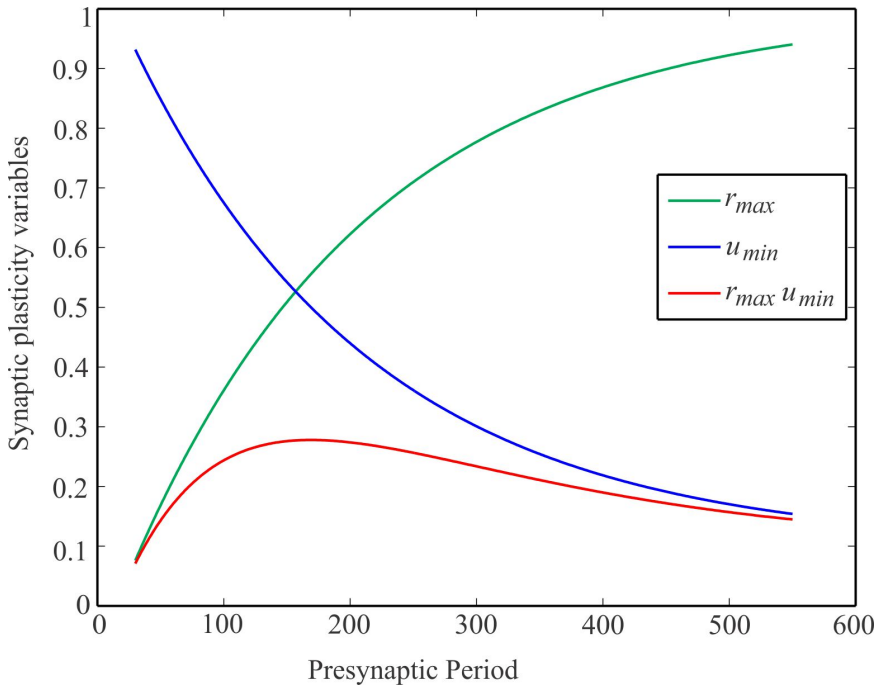

Figure 2.3 Steady state values of plasticity variables. The maximum value r_{max} that the depression variable r and the minimum value u_{min} that the facilitation variable u reach at the steady state at the onset of presynaptic activity plotted against the presynaptic period. The plasticity profile of the synapse is given by their product.

where t_a and t_b are the durations that the cell spends above or below V_{th}, respectively.

It is often possible to measure the strength of the synaptic output when the presynaptic neuron is driven in a range of frequencies. The values of r_{max} and u_{min} as defined above are dependent on the presynaptic frequency and an appropriate choice of time constants allows for our model to fit a variety of frequency-dependent synaptic outputs. In particular, we are interested in synapses whose strength is maximal at a unique preferred frequency as we have observed in experimental measurements [18]. In our results presented below, we will use period instead of frequency for ease of analysis. By choosing appropriate parameters, therefore, we can match the period at which the peak of the product $r_{max}u_{min}$ is maximized with the experimentally-measured

preferred period of the synapse. We define the function

$$g(P) = \bar{g} r_{max}(P) u_{min}(P) \tag{2.16}$$

as the synaptic strength at the time of firing of a presynaptic neuron with constant period $P = t_a + t_b$. We will assume that the changes in period of the bursting neurons affect only the inter-burst duration (i.e., t_a is fixed). We will henceforth refer to this relationship (2.16) as the steady-state synaptic plasticity profile.

Figure 2.3 shows plots of the steady state values of r_{max}, u_{min} and the full synaptic plasticity profile ($r_{max}u_{min}$) of a synapse as a function of the firing period, for a given set of parameters. Here $t_a = 15$. The peak of the synaptic plasticity profile in this case occurs at $P = 170$. For ease of analysis, we use a Gaussian function approximation for the steady state synaptic plasticity profile $g(P)$ in Chapter 4 :

$$g(P) = 0.75 e^{\frac{-(P-P_{pref})^2}{2\sigma^2}} + 0.75 \tag{2.17}$$

where P_{pref} is the peak of the profile corresponding to the preferred period of the synapse and σ determines the spread.

CHAPTER 3

DISCRETE MAPS DESCRIBING THE DYNAMICS OF A TWO-CELL RECURRENT NETWORK WITH SYNAPTIC PLASTICITY IN ONE DIRECTION

We derive Poincaré maps that relate the firing times of a network of two neurons coupled with reciprocal inhibition. We assume a predetermined one-to-one firing order between the neurons. The fixed points of these maps correspond to one-to-one firings of the neurons at the steady state. It is possible to derive similar maps assuming orders of firing that are not one-to-one, but these derivations are beyond the scope of the current study. We first assume a fixed synaptic strength between the neurons in Section 3.1. When the synapses have a fixed strength, only the phase response information of the neurons is used to determine the network activity, as has been shown previously [17]. In Section 3.2 we derive maps that describe the network activity when the synapses between the neurons are plastic. We compare two cases. In one case, we assume that the synapses obey the plasticity dynamics given in equation (2.15). In the second case, we consider synapses that obey the corresponding steady-state values given in equation (2.16). The latter case results in a lower-dimensional map.

3.1 Maps with Static Synapses

We start with a network of two oscillatory neurons reciprocally inhibiting each other with constant synaptic strength. We will derive a 1D map that measures the phase difference between the burst onset of the two cells. A fixed point of the map corresponds to a 1:1 phase locked solution. We then derive the criteria for existence and stability of fixed points. Finally, we test the map in a network of two M-L model neurons.

Consider a network of two oscillatory cells, A and B, coupled with reciprocal inhibition (Figure 3.1A). Assume that the synaptic strengths between the cells are constant in each spike, i.e., $g_{A\to B} = g_{B\to A} = \bar{g}$. The intrinsic period of cell A and cell B are denoted by P_0 and Q_0, respectively. When the neurons are synaptically coupled, the time between subsequent firing of the same neuron may change. This time is called the cycle length, denoted by P_n and Q_n in cycle n, respectively for A and B.

We derive a Poincaré map for the relative firing times of the neurons when they are synaptically connected. We choose the Poincaré section to be at $V_A = V_{th}$. The amount of time that passes after cell A fires until cell B fires is denoted by dt_n, while the amount of time after cell B until cell A fires is denoted by $d\tau_n$ (Figure 3.1B). The (activity) phase of neuron A (or B) is defined as the firing time dt_n (or $d\tau_n$) normalized by the cycle length. Therefore, the phases of A and B are, respectively, given by

$$\tilde{\phi}_n = dt_n/P_n \tag{3.1}$$

$$\tilde{\theta}_n = d\tau_n/Q_n. \tag{3.2}$$

In the derivations of the maps, we will make use of the PRCs of A and B which are defined in terms of P_0 and Q_0, the intrinsic periods of A and B. To simplify these derivations we introduce the notation of the "intrinsic phase" of neurons A and B which are defined, respectively, as

$$\phi_n = dt_n/P_0 \tag{3.3}$$

$$\theta_n = d\tau_n/Q_0.. \tag{3.4}$$

We denote the PRC of cell A and cell B as $Z_A(\cdot)$ and $Z_B(\cdot)$, respectively, for synaptic inputs with a fixed strength. Rewriting the PRC relationship (2.7) for the

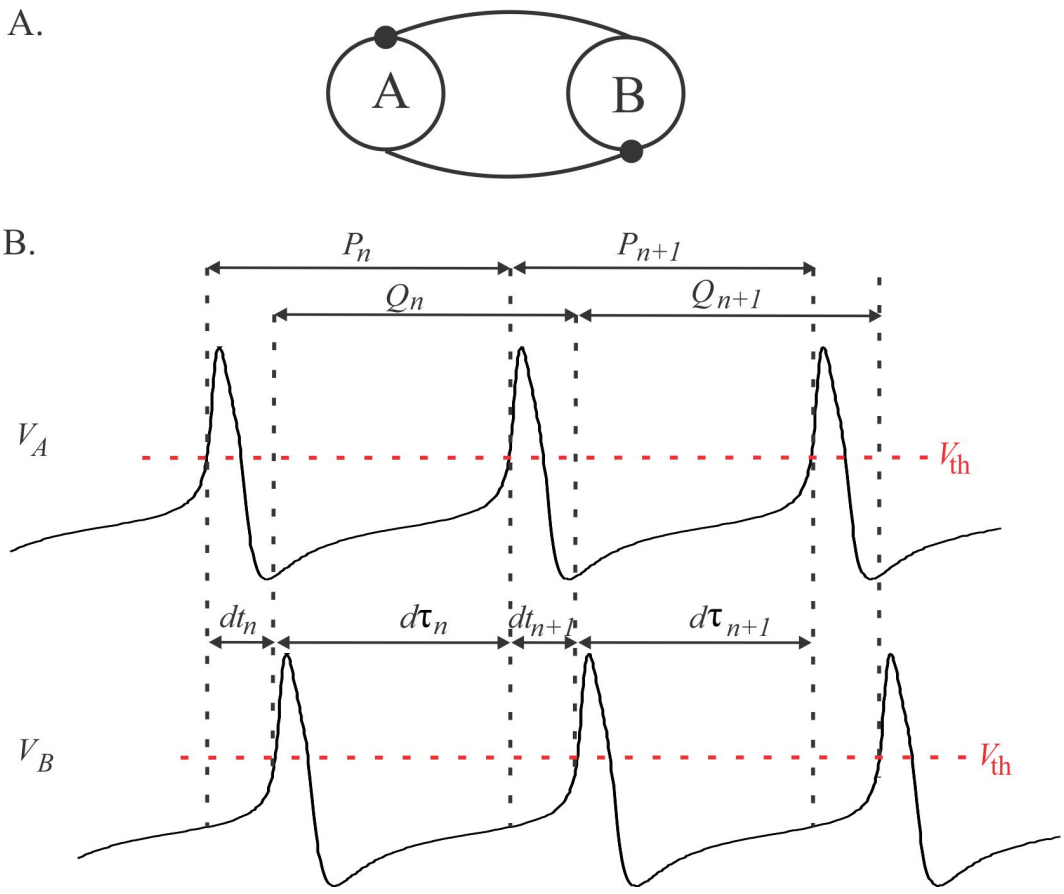

Figure 3.1 Schematic diagram of the coupled network and the map variables. A. Schematic of the network connectivity diagram. B. The cycle length P_n of cell A in cycle n (measured for the M-L simulations when voltage crosses V_{th}) can be divided into the delay between cell A activity to cell B activity (dt_n) and the opposite ($d\tau_n$). The cycle period Q_n of cell B in cycle n is $d\tau_n + dt_{n+1}$.

cycle lengths, we can obtain the cycle lengths of each cell in cycle n as

$$P_n = P_0(1 - Z_A(\phi_n)) \tag{3.5}$$

$$Q_n = Q_0(1 - Z_B(\theta_n)). \tag{3.6}$$

The following equations relate the firing times of the two cells

$$dt_n + d\tau_n = P_n \tag{3.7}$$

$$d\tau_n + dt_{n+1} = Q_n. \tag{3.8}$$

From the equations (3.5) and (3.7), θ_n can be written in terms of ϕ_n:

$$\begin{aligned}\theta_n &= \frac{d\tau_n}{Q_0} = \frac{1}{Q_0}(P_n - dt_n) = \frac{1}{Q_0}\left[P_0(1 - Z_A(\phi_n)) - P_0\phi_n\right] \\ &= \frac{P_0}{Q_0}(1 - Z_A(\phi_n) - \phi_n). \end{aligned} \tag{3.9}$$

Similarly, ϕ_{n+1} can be expressed in terms of θ_n:

$$\begin{aligned}\phi_{n+1} &= \frac{dt_{n+1}}{P_0} = \frac{1}{P_0}(Q_n - d\tau_n) = \frac{1}{P_0}\left[Q_0(1 - Z_B(\theta_n)) - Q_0\theta_n\right] \\ &= \frac{Q_0}{P_0}(1 - Z_B(\theta_n) - \theta_n). \end{aligned} \tag{3.10}$$

using the equations (3.6) and (3.8). Thus, plugging equation (3.9) into equation (3.10) defines the following 1D map for the intrinsic phase of cell A (3.3) when the 1:1 firing order between the cells is maintained:

$$\begin{aligned}\phi_{n+1} &= \Pi(\phi_n) \\ &= \frac{Q_0}{P_0}\left[1 - Z_B\left(\frac{P_0}{Q_0}(1 - Z_A(\phi_n) - \phi_n)\right)\right] - 1 + Z_A(\phi_n) + \phi_n. \end{aligned} \tag{3.11}$$

The condition for a 1:1 phase locking solution is $\phi_n = \phi_{n+1} = \phi^*$. Plugging this into the map gives the condition for a fixed point as

$$P_0(1 - Z_A(\phi^*)) = Q_0(1 - Z_B(\theta^*)) \tag{3.12}$$

where $\theta^* = \frac{P_0}{Q_0}(1 - Z_A(\phi^*) - \phi^*)$. The fixed point is stable if $|\Pi'(\phi^*)| < 1$, hence the stability condition is

$$|(Z'_A(\phi^*) + 1)(Z'_B(\theta^*) + 1)| < 1 \tag{3.13}$$

This result was also found by Dror et al. [17]. If the neurons are identical, $P_0 = Q_0$ and $Z_A(\cdot) = Z_B(\cdot) = Z(\cdot)$. Then the map (3.11) reduces to

$$\begin{aligned}\phi_{n+1} &= \Pi(\phi_n) \\ &= Z(1 - Z(\phi_n) - \phi_n) + Z(\phi_n) + \phi_n. \end{aligned} \tag{3.14}$$

The fixed point equation (3.12) becomes

$$Z(\phi^*) = Z(1 - Z(\phi^*) - \phi^*) \tag{3.15}$$

and the stability condition (3.7) becomes

$$|(Z'(\phi^*) + 1)(Z'(1 - Z(\phi^*) - \phi^*) + 1)| < 1.$$

In this symmetric case, the phase locking of the network does not depend on the intrinsic periods P_0 of the network neurons. The phase of cell A (3.1) in cycle n can be obtained from the relation

$$\tilde{\phi}_n = \frac{dt_n}{P_n} = \frac{\phi_n P_0}{P_n},$$

which can be simplified using equation (3.5) to

$$\tilde{\phi}_n = \frac{\phi_n}{1 - Z(\phi_n)} \equiv f(\phi_n) \tag{3.16}$$

Given the map (3.14) for ϕ_n, in order to derive a map for $\tilde{\phi}_{n+1}$, we need the function given in (3.16) to be invertible. The function f is monotone increasing in $[0, 1]$ if and only if $f'(\phi) \geq 0$ on this interval where

$$f'(\phi) = \frac{1 - Z(\phi) + \phi Z'(\phi)}{(1 - Z(\phi))^2}.$$

The denominator is always positive. The numerator is positive if $Z'(\phi) \geq 0$. For a standard Type I PRC (with a single local extremum), this will occur if ϕ is large enough (i.e., larger than the minimum point of the PRC; see Figure 2.2B). For our choice of parameters this occurs when $\phi > 0.75$ (Figure 2.2B) where the PRC is increasing. On the remaining interval, the expression $1 - Z(\phi)$ is ≥ 1. So if $Z'(\phi) \geq -1/\phi \geq -4/3$ on $[0, 0.75]$, then $f'(\phi)$ would also be positive and f could then be inverted on $[0, 1]$ (Figure 3.2B). However, it is not possible to analytically make this

estimate since we have no closed form expression for $Z(\phi)$. We confirmed numerically though that $Z'(\phi) \geq -4/3$ in this interval, hence $f'(\phi)$ is positive on $[0, 1]$. Therefore, the function f can be inverted on $[0, 1]$. The numerically obtained inverse function f^{-1} is shown in Figure 3.2B. Hence, the phase of cell A (3.1) in cycle $n + 1$ can be obtained from its value in cycle n from

$$\tilde{\phi}_{n+1} = f(\Pi(f^{-1}(\tilde{\phi}_n))) = \tilde{\Pi}(\tilde{\phi}_n) \tag{3.17}$$

In general, the function f (3.16) and the map (3.17) can be defined for networks consisting of either identical or non-identical neurons. We have only considered the networks of identical neurons in this section. The generalization to networks of non-identical neurons is considered below in Chapter 4.

We can now assess the existence and stability of fixed points of the maps (3.14) and (3.17). We numerically solved the map (3.14) using MATLAB to predict the activity of two identical M-L neurons coupled with reciprocal inhibition. We also numerically solved the differential equations governing the activity of the neurons using XPPAUT [21]. We let $\bar{g} = 0.1$ and use the PRCs of the neurons obtained for this value of synaptic strength. We first find the fixed points of the map by solving the fixed point equation (3.15). The two sides of equation (3.15) are plotted in Figure 3.2A. They intersect only at one point $\phi^* = 0.598$, which corresponds to the intrinsic phase of cell A (3.3) at the steady state. The firing period of cell A can be obtained from equation (3.5) evaluated at this intrinsic phase. This value is also equal to the period of B and will be referred to as the period of the coupled network (P_{st}). The activity phase $\tilde{\phi}^*$ of cell A (3.1) at the steady state is 0.5 and is obtained by using (3.16), corresponding to the anti-phase solution, which agrees with the simulations (not shown). In Figure 3.2C, the right and left hand sides of the fixed point equation (3.15) are plotted as functions of the activity phase using (3.16). They intersect at $\tilde{\phi}^* = 0.5$. In Figure 3.2D, we show the cobweb diagram for the map (3.17), starting

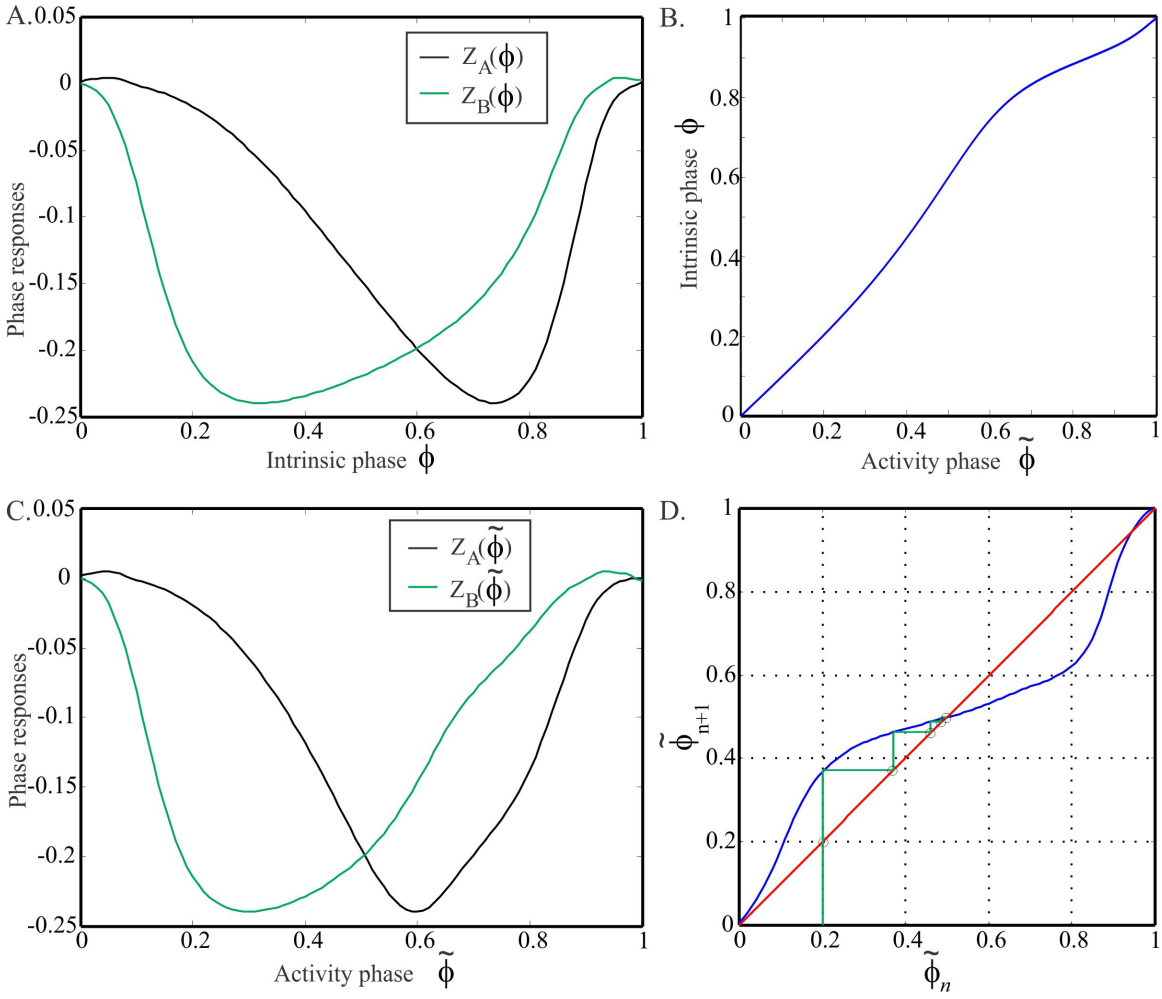

Figure 3.2 Phase locking for static synapses. A. The left and right hand sides of the fixed point equation (3.15) for two identical neurons. The left hand side (black) is the response of neuron A and the right hand side is the response of neuron B at steady state. The intersection gives the fixed point. Note that the black curve is the PRC of both neurons. B. The relation f^{-1} between the intrinsic phase ϕ (3.3) and the activity phase $\tilde{\phi}$ (3.1). C. The same graph as panel A plotted as functions of the activity phase $\tilde{\phi}$ using the transformation from ϕ to $\tilde{\phi}$ shown in panel B. D. Convergence of the iterates starting with the initial condition $\tilde{\phi} = 0.2$ is shown in a cobweb diagram. The iterates (in green) converge to the fixed point at the intersection of the graph of $\tilde{\phi}_{n+1} = \Pi(\tilde{\phi}_n)$ with the line $\tilde{\phi}_n = \tilde{\phi}_{n+1}$.

with the initial condition leading to convergence to the stable steady-state of $\tilde{\phi}^* = 0.5$. For this case, the system locks in the anti-phase state because the two neurons and the two synaptic strengths are identical.

3.2 Maps with Dynamic Synapses in One Direction

In this section, we derive maps to predict the network activity in the presence of synaptic plasticity. We again assume that we have two cells, A and B. We now let the synaptic strength from cell A to cell B be constant and the strength from cell B to cell A exhibit plasticity.

The more appropriate method for deriving the map is to assume that the strength of the synapse from B to A changes according to plasticity dynamics given in equations (2.15). However, often in experiments it is easy to measure the steady-state response of a synapse at different input frequencies without knowing what the underlying dynamics are that give rise to this steady-state value. That is, it is possible to measure the steady-state synaptic plasticity profile $g(P)$ obtained from equation (2.16). We therefore, consider two different approaches in the derivation of the map. In the first derivation we assume that the strength of the B to A synapse is determined by the plasticity dynamics given in equations (2.15), whereas, in the second approach, we assume that the strength of this synapse obeys the steady-state synaptic plasticity profile $g_B(P)$ (Figs. 3.3B and 3.3E). The first approach allows the transients due to different initial conditions to potentially play a role in the convergence of the map to a fixed point. We show, however, that both approaches produce the same result.

When plasticity is included in the B to A synapse, the synaptic strength is no longer constant. Hence, we cannot use a unique PRC for neuron A. Instead, we define a PRC as a function of two variables, where the phase at which the synapse is received and the strength of the synapse determine the response of the neuron. We

denote this by $Z_A(\varphi, g)$. The PRC of neuron B is obtained for a constant synaptic strength $\bar{g}_{A\to B}$ and is denoted by $Z_B(\theta)$.

We will now determine the phase of neuron A and the network period for the two models where the B to A synapse either

i. changes according to the dynamics of the plasticity variables r and u and is given by $\bar{g}_{B\to A} r_n u_n$, or,

ii. obeys the steady-state synaptic plasticity profile $g_B(P) = \bar{g}_{B\to A} r_{max}(P) u_{min}(P)$.

We start with the derivation of the map using the dynamics of plasticity variables (case i). The voltage traces of the neurons A and B and the evolution of the plasticity variables of neuron B obtained from simulations are shown in Figure 3.3A and 3.3C, respectively. In this case, the response of neuron A in cycle n depends on the values of the plasticity variables in this cycle. Assume that we know the values ϕ_n, r_n and u_n. Then we can compute the period of neuron A in cycle n using the expression

$$P_n = P_0(1 - Z_A(\phi_n, \bar{g}_{B\to A} r_n u_n)). \tag{3.18}$$

We can next modify equation (3.9) by rewriting P_n as given in (3.18) to obtain the phase of neuron B in cycle n as

$$\theta_n = \frac{P_0}{Q_0}(1 - Z_A(\phi_n, \bar{g}_{B\to A} r_n u_n) - \phi_n). \tag{3.19}$$

The equation (3.6) giving the cycle length of neuron B becomes

$$Q_n = Q_0 \left(1 - Z_B \left(\frac{P_0}{Q_0}(1 - Z_A(\phi_n, \bar{g}_{B\to A} r_n u_n) - \phi_n)\right)\right). \tag{3.20}$$

in cycle n. Using the equation (3.11) together with the above equations gives a 3D map for the evolution of the intrinsic phase of cell A (3.3) and the synaptic plasticity

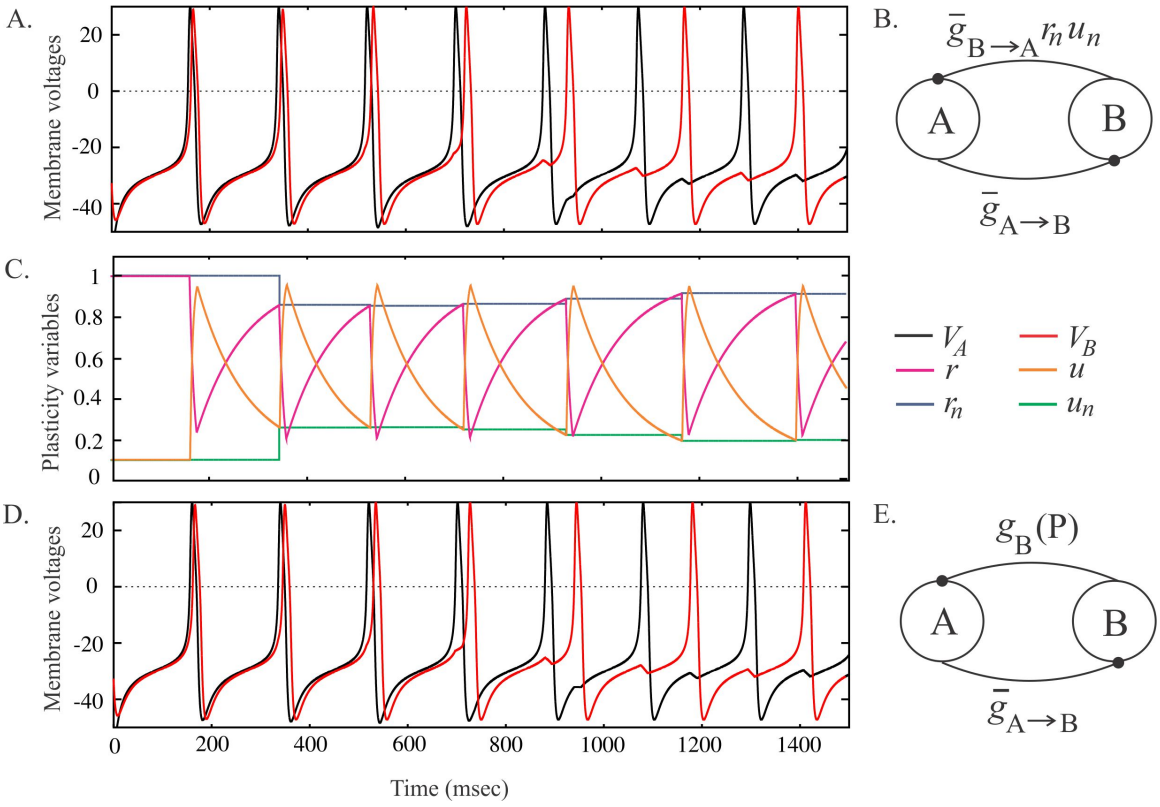

Figure 3.3 Two-cell network with synaptic plasticity in one synapse. A. Voltage traces obtained from simulations of the M-L neurons when the A to B synapse is of fixed strength and B to A synapse changes according to the plasticity model (2.15). C. The evolution of the plasticity variables r, u, r_n, and u_n according to the activity of neuron B. D. Voltage traces obtained from simulations of the M-L neurons when the A to B synapse is of fixed strength and B to A synapse changes according to the steady-state plasticity profiles given by the equations (2.16) B & E. Network connectivity diagram corresponding to the simulations shown in A&D. The parameter values for the plasticity variables are $\tau_1 = 2, \tau_2 = 190, \tau_3 = 2, \tau_4 = 190$.

variables from cell B to cell A

$$\begin{aligned}
\phi_{n+1} &= \frac{Q_0}{P_0}\left[1-Z_B\left(\frac{P_0}{Q_0}(1-Z_A(\phi_n,\bar{g}_{B\to A}r_nu_n)-\phi_n)\right)\right]-1+Z_A(\phi_n,\bar{g}_{B\to A}r_nu_n)+\phi_n \\
r_{n+1} &= 1-(1-r_ne^{-t_a/\tau_1}) \\
&\qquad \exp\left[-\left(Q_0\left(1-Z_B\left(\frac{P_0}{Q_0}(1-Z_A(\phi_n,\bar{g}_{B\to A}r_nu_n)-\phi_n)\right)\right)-t_a\right)/\tau_2\right] \qquad (3.21)\\
u_{n+1} &= U-(U-1+(1-u_n)e^{-t_a/\tau_3}) \\
&\qquad \exp\left[-\left(Q_0\left(1-Z_B\left(\frac{P_0}{Q_0}(1-Z_A(\phi_n,\bar{g}_{B\to A}r_nu_n)-\phi_n)\right)\right)-t_a\right)/\tau_4\right].
\end{aligned}$$

The first equation is the same as (3.11) except that now Z_A is a function of two arguments. The second and third equations are computed using (2.15) over one cycle. The complicated expressions in the exponential of both equations are the time $Q_n - t_a$ recast in terms of ϕ_n, r_n, u_n where Q_n is given in equation (3.20).

Next, we derive the map for case ii where the synapse from neuron A to neuron B has a constant strength at each cycle while the synaptic strength from neuron B to A changes according to the steady-state plasticity function $g_B(x)$. The voltage traces of the neurons A and B obtained from simulations are shown in Figure 3.3D. In this case, instead of the depression and facilitation variables, we can use the cycle length of one of the neurons to derive the activity map. We assume that we know the values ϕ_n and P_n. Then, the phase of neuron B in cycle n can be found by using (3.7) as

$$\theta_n = (P_n - \phi_n P_0)/Q_0. \qquad (3.22)$$

Plugging this into (3.6) immediately yields the expression for the cycle length of neuron B in cycle n as

$$Q_n = Q_0\left[1 - Z_B\left((P_n - \phi_n P_0)/Q_0\right)\right]. \qquad (3.23)$$

We can now obtain the phase of neuron A (3.3) in cycle $n+1$ using equation (3.8) as

$$\phi_{n+1} = (Q_n - d\tau_n)/P_0 = (Q_n - \theta_n Q_0)/P_0. \qquad (3.24)$$

We can use this phase to obtain the cycle length of neuron A in cycle n+1 as

$$P_{n+1} = P_0 \left[1 - Z_A(\phi_{n+1}, g_B(Q_n))\right]. \tag{3.25}$$

Similar to equation (3.18), the period of neuron A is determined by Z_A which is a function of two variables. However, in this case the synaptic strength received by neuron A in cycle $n+1$ depends directly on the cycle length of neuron B in cycle n. The map for the activity of the network can be obtained by plugging the equations (3.22) and (3.23) into (3.24) and (3.25) as

$$\begin{aligned}
\phi_{n+1} = &\frac{Q_0}{P_0}\left[1 - Z_B\left(\frac{P_0}{Q_0}(1 - Z_A\left(\phi_n, g_B\left(Q_0\left[1 - Z_B\left(\frac{P_n - \phi_n P_0}{Q_0}\right)\right]\right)\right) - \phi_n)\right)\right] \\
&-1 + Z_A\left(\phi_n, g_B\left(Q_0\left[1 - Z_B\left(\frac{P_n - \phi_n P_0}{Q_0}\right)\right]\right)\right) + \phi_n \\
P_{n+1} = &P_0\left[1 - Z_A\left(\frac{Q_0}{P_0}\left[1 - Z_B\left(\frac{P_n - \phi_n P_0}{Q_0}\right)\right] - \frac{P_n}{P_0} + \phi_n,\right.\right. \\
&\left.\left. g_B\left(Q_0\left[1 - Z_B\left(\frac{P_n - \phi_n P_0}{Q_0}\right)\right]\right)\right)\right].
\end{aligned} \tag{3.26}$$

Hence, the map (3.21) is reduced to a 2D map for the phase and cycle length of neuron A. A fixed point (ϕ^*, r^*, u^*) of the 3D map (3.21) corresponds to a 1:1 solution. This 1:1 solution is also represented by a fixed point of the 2D map (3.27) which occurs at (ϕ^*, P^*), where P^* is the steady-state value obtained from (3.18) at (ϕ^*, r^*, u^*).

To assess numerically the existence and stability of the fixed points of both the 2D map (3.27) and the 3D map (3.21), consider two identical neurons coupled with asymmetric synapses. Let the synaptic strength from neuron A to B be fixed at $\bar{g}_{A\to B} = 0.1$. We use parameters for the plasticity variables that yield the steady-state plasticity function $g_B(P)$ with a peak at the period 169.5, as shown in Figure 2.3. Denote the steady-state network period and phase of neuron A from the 3D map (case i) as P_{dyn} and ϕ_{dyn}, respectively, and the corresponding values from the 2D map (case ii) as P_{ss} and ϕ_{ss}. Similarly, for static coupling, denote the steady-state network period as P_{st} and phase of neuron A as ϕ_{st}.

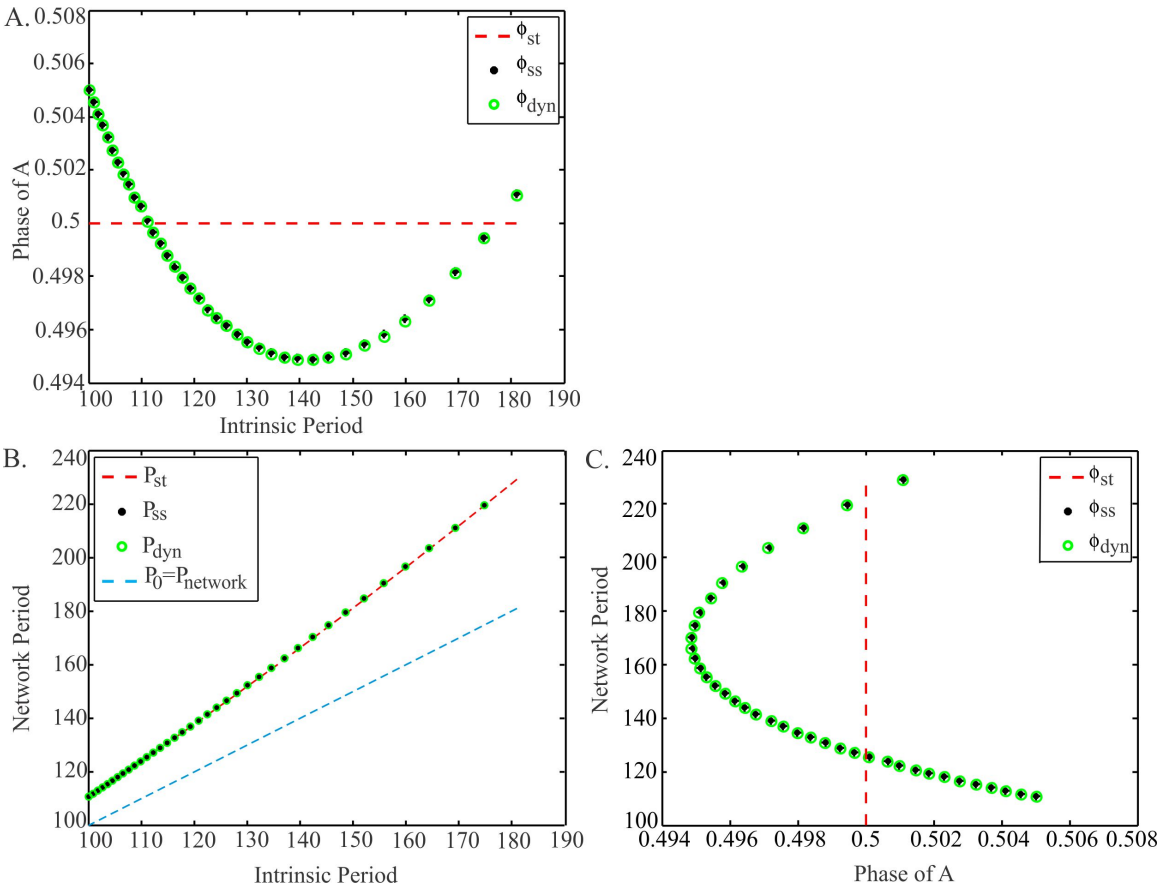

Figure 3.4 A comparison of the 1D (3.11), 2D (3.27) and 3D (3.21) maps. A. The phase of the neuron A, ϕ_{st} from map (3.11), ϕ_{dyn} from map (3.21), ϕ_{ss} from map (3.27), shown as a function of the intrinsic period of both neurons (changed simultaneously). B. The network period as a function of intrinsic periods corresponding to the same maps. C. The relation between the network period and the phase of A for the same maps. The phase of A reaches a minimum (black dashed line) at the network period equal to the preferred period of neuron B. The results of the two maps with plasticity (3.21) and (3.27) overlap in all panels.

Figure 3.4 shows the steady-state phase of neuron A and the network period obtained from the 1D map (3.11), the 3D map (3.21) and the 2D map (3.27), for a set of intrinsic periods P_0 (varied simultaneously in both cells). In Figure 3.4A, the steady-state phase of neuron A is plotted as a function of P_0. The maps with plasticity (cases i and ii) yield the same steady-state phase of neuron A; this phase is not constant but is a function of the intrinsic period (green and black), in contrast to the static case where the network always has an anti-phase solution (dashed red line). This variation in phase depends on the values of the steady-state plasticity profile $g_B(P)$ (further explained below). Figure 3.4B compares the steady-state network period obtained from the three maps. The periods obtained from the maps with plasticity are again the same and they are slightly different than the periods obtained from the static map. The blue dashed line is the $x = y$, i.e., $P_0 = P_{network}$ line. The network period is always larger than the intrinsic period in all cases, due to the selection of the PRC (that the inhibitory input always delays the next firing time). Figure 3.4C relates the steady-state phase of neuron A with the network period.

We now examine how the steady-state phase of neuron A changes with respect to changes in the intrinsic period. The phase of neuron A depends on the value of the synaptic strength received from neuron B at the steady state. This value is determined by Q^*, the steady-state firing period of neuron B, which equals the steady-state network period P^*. When this value equals $\bar{g}_{A\to B} = 0.1$, then anti-phase solutions occur. This happens for two sets of coupled neurons, where the red dashed line intersects green and black curves (Figs. 6A and 6C). Between these two points, the synaptic strength received by neuron A, given by $g_B(Q^*)$, is larger than $\bar{g}_{A\to B}$. Since the cells are identical, the neurons must give equal amount of response (so that their steady-state firing periods will be equal) for a steady-state solution to occur. When both synaptic strengths are equal, both neurons have steady-state phases at 0.5. However, if $g_B(Q^*) > \bar{g}_{A\to B}.$, then neuron A receives stronger synaptic input

than neuron B. This difference can be balanced if neuron A receives this synaptic input at a phase that yields less response. As the PRCs of the neurons are decreasing around the phase 0.5, neuron A needs to phase lock at a phase smaller than 0.5. This explains why phase of neuron A decreases between these intersection points. Similar argument holds when $g_B(Q^*) < \bar{g}_{A\to B}$.

The phase of neuron A reaches a minimum when the synaptic strength reaches a maximum. As can be seen in Figure 2.3, the synaptic plasticity profile has its peak at 169.5. Therefore, the minimum phase of neuron A is observed at the network period 169.5 (Figure 3.4C). The network period of 169.5 is obtained when two cells with the intrinsic periods 141.8 are coupled (Figure 3.4B).

CHAPTER 4

DISCRETE MAPS DESCRIBING THE DYNAMICS OF A TWO-CELL RECURRENT NETWORK WITH SYNAPTIC PLASTICITY IN BOTH DIRECTIONS

Let both reciprocal synapses have short-term plasticity. The map involving the synaptic plasticity variables (2.15) that generalizes (3.21) would now be 5D. But given the results from the previous section showing that the simplified map using the steady-state synaptic plasticity profiles provides the same stable output, we derive only the 2D map associated with the latter. We again start with the intrinsic phase ϕ_n (3.3) and cycle length P_n of neuron A in cycle n. The equation (3.22) can still be used to obtain the phase of neuron B, θ_n, in cycle n. However, the cycle length of neuron B is now given by the equation

$$Q_n = Q_0[1 - Z_B(\theta_n, g_A(P_n))] \tag{4.1}$$

in cycle n, since the synapse from neuron A to B also has plasticity and depends on P_n. The cycle length P and intrinsic phase ϕ of neuron A in cycle $n+1$ is given by

$$\begin{aligned}
\phi_{n+1} &= \Pi_1(\phi_n, P_n) = \frac{1}{P_0}(Q_n - P_n + P_0\phi_n) \\
&= \frac{Q_0}{P_0}\left[1 - Z_B\left(\frac{1}{Q_0}(P_n - P_0\phi_n), g_A(P_n)\right)\right] - \frac{P_n}{P_0} + \phi_n \\
P_{n+1} &= \Pi_2(\phi_n, P_n) = P_0\left[1 - Z_A(\phi_{n+1}, g_B(Q_n))\right] \\
&= P_0\left[1 - Z_A\left(\frac{Q_0}{P_0}\left[1 - Z_B\left(\frac{1}{Q_0}(P_n - P_0\phi_n), g_A(P_n)\right)\right] - \frac{P_n}{P_0} + \phi_n,\right.\right. \\
&\qquad \left.\left. g_B\left(Q_0\left[1 - Z_B\left(\frac{1}{Q_0}(P_n - P_0\phi_n), g_A(P_n)\right)\right]\right)\right)\right]
\end{aligned} \tag{4.2}$$

Equation (4.3) determines the values of P and ϕ when both synapses have plasticity. In the case where the two cells are identical, $Z_A(\cdot) = Z_B(\cdot) = Z$, this map simplifies

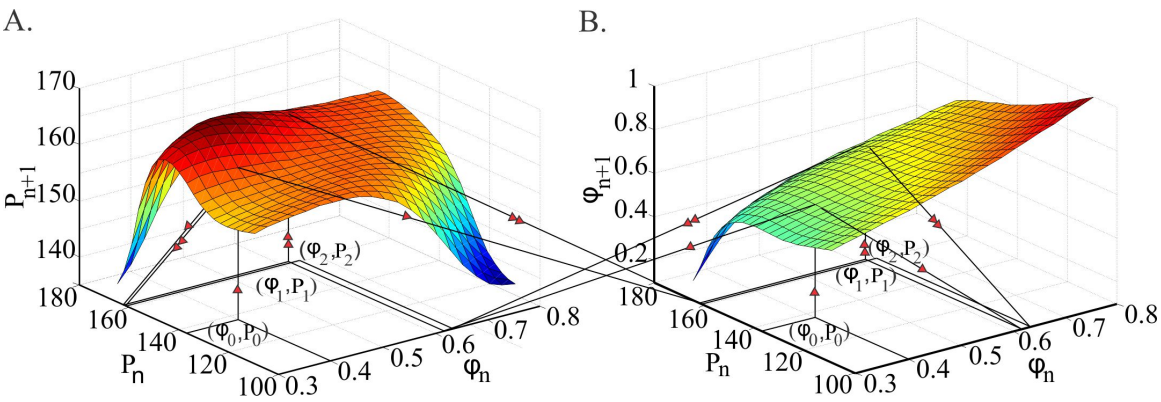

Figure 4.1 Cobwebbing diagram of the 2D map (4.3) for two identical cells ($P_0 = Q_0$) and distinct synaptic plasticity profiles ($P_A = 150, P_B = 190$) shown in two coordinate systems. The period P_1 and the phase ϕ_1 of neuron A in cycle 1 is obtained by evaluating the initial condition (ϕ_0, P_0) on the period surface $P_{n+1} = \Pi_2(\phi_n, P_n)$ (A) and the phase surface $\phi_{n+1} = \Pi_1(\phi_n, P_n)$ (B).The point (ϕ_1, P_1) is then projected back to the $x-y$ axis in in both coordinate systems and mapped to the point (ϕ_2, P_2) with the same procedure. Lines with one arrow correspond to the first and lines with two arrows correspond to the second iteration.

to

$$
\begin{aligned}
\phi_{n+1} &= \Pi_1(\phi_n, P_n) = \frac{1}{P_0}(Q_n - P_n + P_0\phi_n) \\
&= 1 - Z\left(\frac{P_n}{P_0} - \phi_n, g_A(P_n)\right) - \frac{P_n}{P_0} + \phi_n \\
P_{n+1} &= \Pi_2(\phi_n, P_n) = P_0\left[1 - Z(\phi_{n+1}, g_B(Q_n))\right] \\
&= P_0\left[1 - Z\left(1 - Z\left(\frac{P_n}{P_0} - \phi_n, g_A(P_n)\right) - \frac{P_n}{P_0} + \phi_n,\right.\right. \\
&\qquad \left.\left. g_B\left(P_0\left[1 - Z\left(\frac{P_n}{P_0} - \phi_n, g_A(P_n)\right)\right]\right)\right)\right].
\end{aligned}
\tag{4.3}
$$

We now explore whether these equations yield stable fixed points and, if so, how changes in the synaptic profiles affect the resulting phase- and period-locking of the network.

For simplicity, instead of using equation (2.16) for $g(P)$, we assume that the steady-state synaptic profiles obey Gaussian functions $g_A(\cdot)$ (for the A to B synapse) and $g_B(\cdot)$ (for the B to A synapse) (2.17) with peaks (preferred periods) P_A and P_B, respectively. Equations (4.3) define two surfaces $\Pi_1(\phi_n, P_n)$ and $\Pi_2(\phi_n, P_n)$ which

can be plotted in $\mathbb{R}^3$. We plot two 3D coordinate systems to be able to visualize the evolution of the 2D map. We show three iterations of the map (4.3) in Figure 4.1. The values (ϕ_n, P_n) in cycle n are located on the $x-y$ axes. These values are mapped through the surfaces $P_{n+1} = \Pi_2(\phi_n, P_n)$ (Figure 4.1A) and $\phi_{n+1} = \Pi_1(\phi_n, P_n)$ (Figure 4.1B) to the next iteration points (ϕ_{n+1}, P_{n+1}) in cycle $n+1$. Start with the initial condition (ϕ_0, P_0) which is shown in both coordinate systems. The image of (ϕ_0, P_0) on the surface $\phi_{n+1} = \Pi_1(\phi_n, P_n)$ gives the next phase value ϕ_1, and the image of (ϕ_0, P_0) on the surface $P_{n+1} = \Pi_2(\phi_n, P_n)$ gives the next cycle length P_1 (shown by the vertical lines with one arrow). These ϕ_1 and P_1 values are located respectively on the x and y axes of both coordinate systems (shown by the inclined lines with one arrow). The point (ϕ_1, P_1) is then located on the $x-y$ axes in both coordinate systems and mapped to the point (ϕ_2, P_2) by the same procedure (shown by the lines with two arrows). We are able to geometrically observe the iterations (only three shown) approach to a fixed point; hence this is a generalization of cobwebbing for the 2D map.

The fixed point equations of the map (4.3) in a 1:1 firing condition are

$$\begin{aligned} P^* &= Q_0\left[1 - Z_B\left(\frac{P^* - P_0\phi^*}{Q_0}, g_A(P^*)\right)\right] \\ P^* &= P_0\left[1 - Z_A\left(\frac{Q_0}{P_0}\left[1 - Z_B\left(\frac{P^* - P_0\phi^*}{Q_0}, g_A(P^*)\right)\right] - \frac{P^*}{P_0} + \phi^*,\right.\right. \\ &\qquad \left.\left. g_B\left(Q_0\left[1 - Z_B\left(\frac{P^* - P_0\phi^*}{Q_0}, g_A(P^*)\right)\right]\right)\right)\right]. \end{aligned} \tag{4.4}$$

These simplify to

$$\begin{aligned} P^* &= P_0\left[1 - Z\left(\frac{P^*}{P_0} - \phi^*, g_A(P^*)\right)\right] \\ P^* &= P_0\left[1 - Z\left(\phi^*, g_B(P^*)\right)\right] \end{aligned} \tag{4.5}$$

for identical cells.

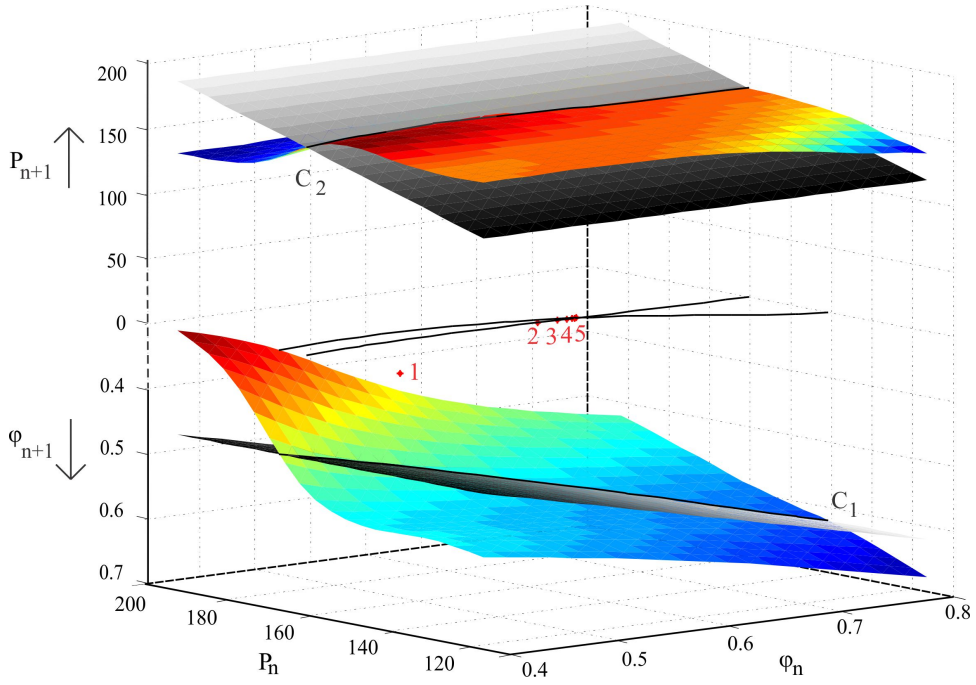

Figure 4.2 Fixed points of 2D (4.3) map when P0=Q0 obtained by solving (4.5). The surfaces for the evolution of period and phase of the 2D map with synaptic preferred periods $P_A = 150$, $P_B = 190$ are drawn above and below the $z = 0$ plane denoted by the axes $z_1 = P_{n_1}$ and $z_2 = \phi_{n+1}$, respectively. The equality $P_n = P_{n+1}$ is satisfied when the surface $z_1 = \Pi_2(x, y)$ (colored surface on top) and the plane $z_1 = y$ (gray-scaled plane on top) intersect. Similarly, the equality $\phi_n = \phi_{n+1}$ is satisfied when the surface $z_2 = \Pi_1(x, y)$ (colored surface on bottom) intersects the plane $z_2 = x$ (gray-scaled plane on bottom). These intersections yield the two black curves above and below the $z = 0$ plane. The fixed point of the map lays on the intersection of the two fixed point curves. The projections of these curves on the $z = 0$ plane are shown together with the iterates (red dots) approaching to the fixed point at their intersection in the order enumerated in the figure.

The fixed point of this 2D map occurs when $\phi_n = \phi_{n+1}$ and $P_n = P_{n+1}$. We can visualize how the fixed point is obtained. For this purpose, we plot the surfaces for the evolution of phase and period (previously drawn on separate coordinate axes in 4.1) on the same coordinate axis, above and below the $z = 0$ plane, and denote by the axes z_1 and z_2 , respectively in Figure 4.2. The equality $\phi_n = \phi_{n+1}$ is satisfied when the surface $z_1 = \Pi_1(x, y)$ and the plane $z_1 = x$ intersect. Denote this intersection curve as C_1. Similarly, the equality $P_n = P_{n+1}$ is satisfied when the surface $z_2 = \Pi_2(x, y)$ intersects the plane $z_2 = y$ (denoted as C_2). These intersection curves C_1 and C_2 are shown in black above and below the $z = 0$ plane. The fixed point of the map lies on both curves; hence it lays on the intersection of C_1 and C_2. The projections of C_1 and C_2 on the $z = 0$ plane are shown in the figure together with the iterations (red dots) approaching to the fixed point at their intersection.

The stability of the fixed point can be examined using the Jacobian of the 2D map (4.3). If the eigenvalues of the Jacobian at the fixed point are located inside the unit circle, the fixed point is stable. For our choice of parameter values, the fixed point can be shown to be stable.

In Section 4.1, assuming both synapses obey steady-state plasticity profiles, we examine how changes in these profiles determine the network period and relative phase relations. In Section 4.2, we find conditions for a network to be able to keep a fixed firing period but vary the relative firing phase between its neurons, and vice versa.

4.1 Different Plasticity Profiles

Having determined a method for calculating the steady-state network period and phase, we now determine how these quantities depend on various network parameters. For simplicity, in this section we consider identical neurons. We use the 2D map (4.3) to obtain the network phase and period when both synapses have plasticity. For

comparison, we also obtain the same from the 1D map (3.14), when the synaptic strength is fixed. We are interested in how differences in the plasticity profiles of the two synapses affects the network period and phase of neuron A (Figures 4.3.A1 and 4.3.B1). The distinct plasticity profiles (Figure 4.3.A1) are produced by simply shifting one profile along the intrinsic period axis.

In the non-identical case, the plasticity profiles are chosen to approach to the same value at the tails (Figure 4.3.A1) and, therefore, for small (and large) intrinsic periods, $\phi_{ss} = 0.5$ due to identical synaptic strengths (Figure 4.3.A3). As the intrinsic period is increased, the difference between $g_A(P)$ and $g_B(P)$ first increases until $P = P_A$ and then decreases to zero when $P = P_{eq}$ (Figure 4.3.A1). This causes ϕ_{ss} to increase from 0.5 to 0.58 until $P_{ss} = P_A$ and then decrease to 0.5 again when $P_{ss} = P_{eq}$ (Figure 4.3.A3), since the weaker synapse from B to A is balanced by a phase that yields more response (more detail is explained in Section 3.2). For firing periods greater than P_{eq}, the opposite relation holds, causing ϕ_{ss} first to decrease to 0.41 and then increase back to 0.5. In contrast to ϕ_{ss} varying between 0.41 and 0.58, ϕ_{st} is always fixed at 0.5 due to identical neurons and synapses. Since the values of the plasticity profiles at the tails are less than the strength $\bar{g} = 0.1$ of the static synapses, P_{ss} is slightly smaller than P_{st} for small (and large) intrinsic periods (Figure 4.3.A2). For a range of intermediate intrinsic periods, when the network synapses have plasticity, P_{ss} is almost equal to the network period with static synapses P_{st} (Figure 4.3.A2). The balancing effects of the two synaptic profiles ($g_A(P)$ being greater, $g_B(P)$ being smaller than $\bar{g}$ for $P_{ss} < P_{eq}$ and $g_A(P)$ being smaller, $g_B(P)$ being greater than $\bar{g}$ for $P_{ss} < P_{eq}$) causes P_{ss} and P_{st} to be almost equal for intermediate intrinsic periods. Thus, this choice of synaptic plasticity profiles provides the network the ability to produce a range of distinct phase relationships as the network period changes (Figure 4.3.A3). Note that the steady-state network period remains almost equal to its value as if no plasticity is included (Figure 4.3.A2).

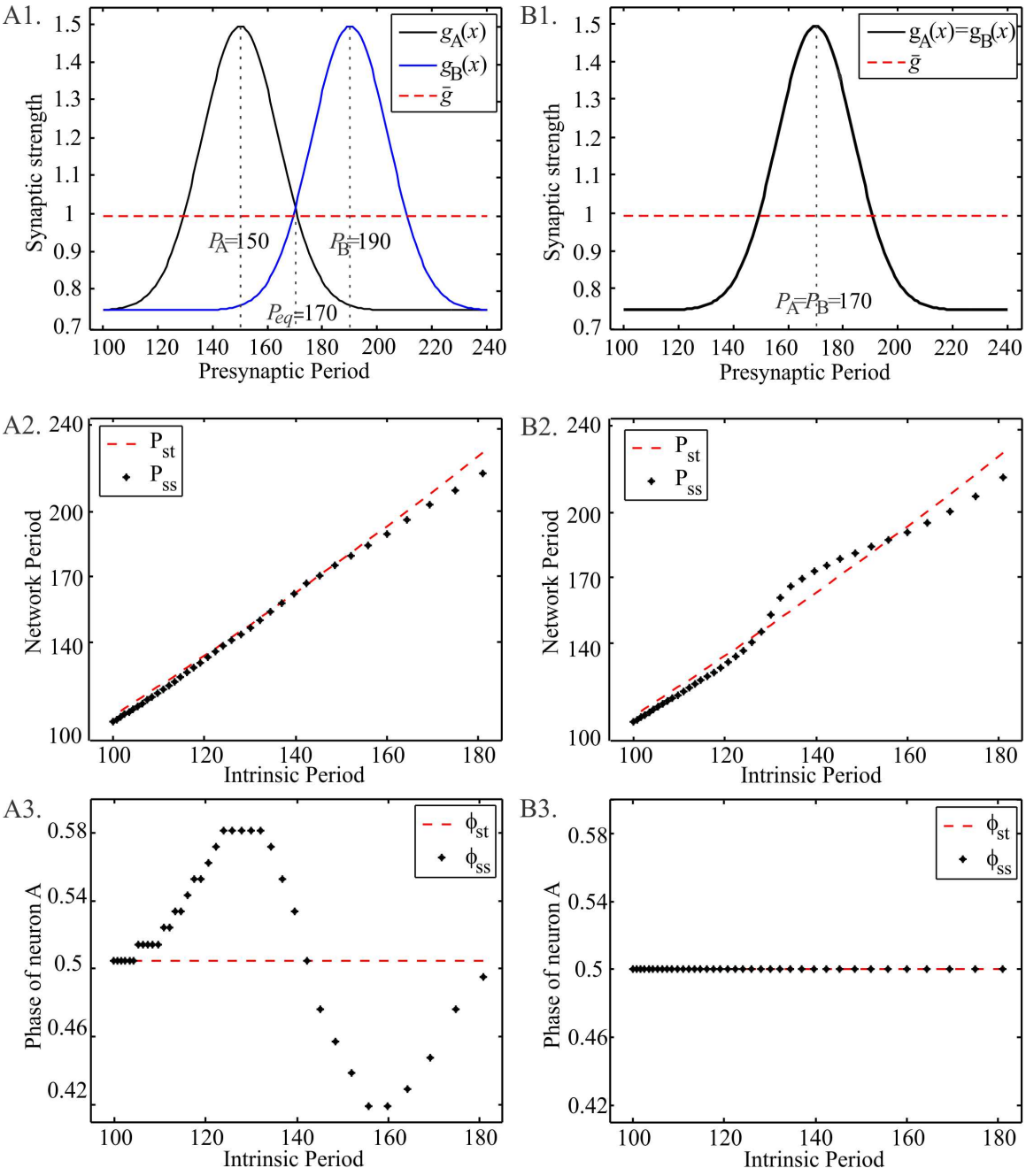

Figure 4.3 Period and phase locking when both synapses follow the synaptic plasticity profile. Dashed line in all panels shows the case with two static synapses. A1. Synaptic plasticity profiles of the two synapses chosen to have different preferred periods at 150 and 190. A2. Network period as a function of the intrinsic periods. A3. Phase $\tilde{\phi}$ of neuron A with respect to B as a function of intrinsic period. B1-B3. Same as A1-A3 but with identical synaptic plasticity profiles (preferred period at 170).

In the case of identical plasticity profiles, the neurons have the same preferred periods and the values of the plasticity profiles again approach 0.075 at the tails (Figure 4.3.B1). This causes P_{ss} to be smaller than P_{st} for small and large intrinsic periods (Figure 4.3.B2). For intermediate firing periods, the opposite holds. In contrast to the almost linear change in P_{st}, P_{ss} changes nonlinearly as a function of the intrinsic periods. Also, in contrast to the nonlinear change in P_{ss}, the phase of neuron A is fixed at 0.5, because both the neurons and their plasticity profiles are identical (Figure 4.3.B3). Hence, depending on the choice of plasticity profiles, the network coupled with synaptic plasticity can have the same period but different relative phases (Figure 4.3 A1-A3), or the same phases but different periods compared to the network coupled with static synapses (Figure 4.3 B1-B3).

4.2 Conditions for Period or Phase Constancy

Short term synaptic plasticity profiles are subject to change by neuromodulation and other long-term modifications [22]. In the previous section, we showed that as the synaptic plasticity profile changes, the network can maintain the network period or the relative activity phases among the network neurons. In this section, we examine the conditions on the steady-state synaptic plasticity profiles that would allow the network to maintain either a constant period or a constant phase.

For this purpose, we make use of the fixed point equations for identical cells (4.5) obtained from the 2D map. The phase ϕ^* in equations (4.5) stand for the intrinsic phase of neuron A (3.3). We use equation (3.16) and rewrite equations (4.5) as implicit functions of the steady-state phase of A $\tilde{\phi}$, network period P and synaptic preferred periods P_A and P_B as

$$F_1(P_A, P_B, \tilde{\phi}, P) = P - P_0 \left[1 - Z \left(\frac{P - \tilde{\phi} P}{P_0}, g_A(P) \right) \right]$$

$$F_2(P_A, P_B, \tilde{\phi}, P) = P - P_0 \left[1 - Z\left(\frac{P - \tilde{\phi}P}{P_0}, g_B(P)\right)\right]$$

Let $F(P_A, P_B, \tilde{\phi}, P) = \Big(F_1(P_A, P_B, \tilde{\phi}, P), F_2(P_A, P_B, \tilde{\phi}, P)\Big)$. At the fixed point, $F(P_A, P_B, \tilde{\phi}, P) = (0, 0)$. We would like to solve this equation for P_A and P_B as a function of P and $\tilde{\phi}$. Using the Implicit Function Theorem, the condition that needs to be satisfied is $\det\left(D_{P_A,P_B}F\right) \neq 0$ at $\left(P_A^*, P_B^*, \tilde{\phi}^*, P^*\right)$ where

$$D_{P_A,P_B}F\Big|_{(P_A^*,P_B^*,\tilde{\phi}^*,P^*)} = \left[\begin{array}{cc} \frac{\partial F_1}{\partial P_A} & \frac{\partial F_1}{\partial P_B} \\ \frac{\partial F_2}{\partial P_A} & \frac{\partial F_2}{\partial P_B} \end{array}\right]_{(P_A^*,P_B^*,\tilde{\phi}^*,P^*)} \tag{4.6}$$

The function F_1 does not depend on P_B, hence $\frac{\partial F_1}{\partial P_B} = 0$. So, for the determinant to be nonzero, both $\frac{\partial F_1}{\partial P_A}$ and $\frac{\partial F_2}{\partial P_B}$ have to be nonzero. These terms are given as

$$\begin{aligned} \frac{\partial F_1}{\partial P_A}\Big|_{(P_A^*,P_B^*,\tilde{\phi}^*,P^*)} &= P_0 \frac{\partial Z}{\partial y}\left(\frac{P^*(1-\tilde{\phi}^*)}{P_0}, g_A(P^*)\right)\frac{\partial g_A}{\partial P_A} \\ \frac{\partial F_2}{\partial P_B}\Big|_{(P_A^*,P_B^*,\tilde{\phi}^*,P^*)} &= P_0 \frac{\partial Z}{\partial y}\left(\frac{P^*\tilde{\phi}^*}{P_0}, g_B(P^*)\right)\frac{\partial g_B}{\partial P_B}. \end{aligned}$$

One condition for the determinant to be nonzero is $\partial Z/\partial y(x,y)|_{(P_A^*,P_B^*,\tilde{\phi}^*,P^*)} \neq 0$; that is, the response of the neuron to perturbations should change with the change in the strength of the perturbation. This is a standard assumption on phase response curves with small perturbations. The other two conditions to be satisfied are $\partial g_A/\partial P_A|_{(P_A^*,P_B^*,\tilde{\phi}^*,P^*)} \neq 0$ and $\partial g_B/\partial P_B|_{(P_A^*,P_B^*,\tilde{\phi}^*,P^*)} \neq 0$, which, upon using equation (2.17), are equivalent to $P_A \neq P^*$ and $P_B \neq P^*$, respectively. In other words, the network period should be different than the synaptic preferred periods.

Under these three conditions, the Implicit Function Theorem guarantees that P_A and P_B can be expressed in terms of ϕ and P near $(P_A^*, P_B^*, \tilde{\phi}^*, P^*)$. More precisely, there are neighborhoods U of $(\tilde{\phi}^*, P^*)$ and W of (P_A^*, P_B^*) such that, for

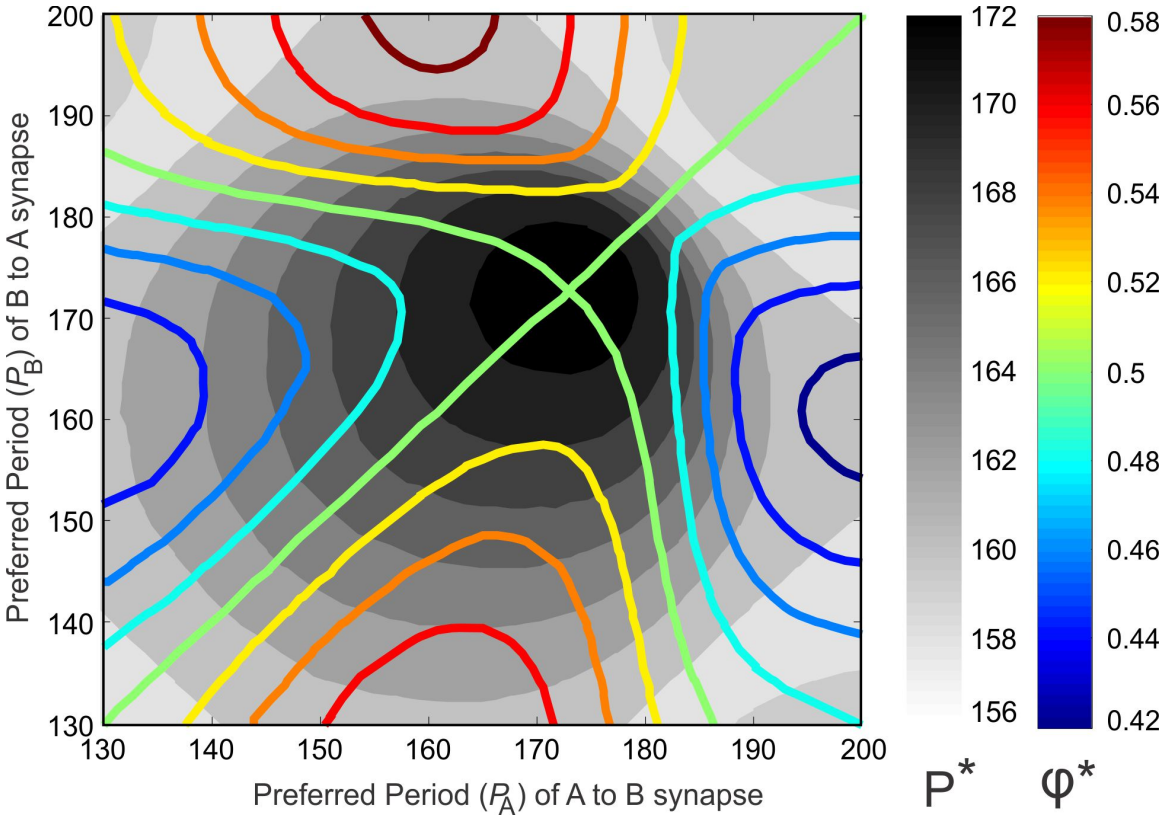

Figure 4.4 Period and phase locking for different steady-state synaptic plasticity profiles. The steady-state network period (gray) and phase (colored) are shown as a function of different steady-state synaptic plasticity profiles. Colored curves correspond to level sets of the phase. The edges of the gray bands correspond to the level sets of the network period. The plasticity profile of each synapse is marked by its preferred period.

each $(\tilde{\phi}, P) \in U$, there exists a unique $(P_A, P_B) \in W$ such that $F(P_A, P_B, \tilde{\phi}, P) = F(P_A(\tilde{\phi}, P), P_B(\tilde{\phi}, P), \tilde{\phi}, P) = 0$. Hence, there is a unique function $h = (h_1, h_2) : U \to W$ such that $F(h_1(\tilde{\phi}, P), h_2(\tilde{\phi}, P), \tilde{\phi}, P)$ for every $(\tilde{\phi}, P) \in U$.

We can interpret this result in two ways. First, around the fixed point $(P_A^*, P_B^*, \tilde{\phi}^*, P^*)$, we can choose $(\tilde{\phi}', P^*)$ such that P^* is fixed and $\tilde{\phi}' \neq \tilde{\phi}^*$, for which there exists $(P_{A'}, P_{B'})$ that satisfy the fixed point equations (4.5). Hence, for a specific P^*, around a point with a phase $\tilde{\phi}'$, there exist synaptic preferred periods $P_{A'}$ and $P_{B'}$ that enables the network to stay on the level set of P^* while setting the phase equal to a new value $\tilde{\phi}'$. In other words, it is possible to keep the network period constant and set the network phase to a new value by changing the synaptic plasticity profiles of the network neurons.

The second interpretation is that, around the fixed point $(P_A^*, P_B^*, \tilde{\phi}^*, P^*)$, we can choose a $(\tilde{\phi}^*, P')$ such that $\tilde{\phi}^*$ is fixed and $P' \neq P$, and can find $(P_{A'}, P_{B'})$ that satisfy the fixed point equations (4.5). This enables the network to stay on the level set for a specific $\tilde{\phi}^*$, while changing the network period to a new value P'.

In the example demonstrated in Figure 4.4, the intrinsic periods of the two neurons are kept constant but the two synaptic plasticity profiles are allowed to vary. As before, the synaptic plasticity profiles are changed only by shifting them along the $x-$axis. We keep track of different synaptic plasticity profiles by the values of the synaptic preferred periods P_A and P_B (the peak of the profile). Figure 4.4 shows the changes in the network period and phase as the synaptic plasticity profiles of the neurons are varied. The neurons are identical with an intrinsic period P_0 of 137. The colored curves are subsets of the level sets of the phase; the phase of the network is fixed on a curve with a specific color. The edges of the gray bands correspond to the level sets of the network period. These level sets inform us about how the network can maintain a specific period but have different phase relations, or vice versa, through varying the combination of synaptic preferred periods.

4.3 Networks of Non-Identical Neurons

We now examine a network of two non-identical M-L neurons. The neurons are chosen to have different intrinsic periods by applying different levels of external current but otherwise use the same parameters. We consider the two cases where the synapses are static or they follow steady-state synaptic plasticity profiles and compare the predictions of the 1D map (3.11) and the 2D map (4.3) with the simulations of the corresponding model equations. We let the preferred period of the A to B synapse be $P_A = 150$ and from neuron B to A be $P_B = 190$ for the case with synaptic plasticity. The results are shown in Figure 4.5.

Note that the maps continue to give good predictions when the neurons are not necessarily identical. The difference between the simulations (filled circles) and the map predictions (open circles) is indistinguishable in most cases. The diagonal corresponds to coupling of identical neurons. Moving away from the diagonal, the difference between the intrinsic periods of the neurons increases and eventually prevents the neurons to phase lock in a 1:1 manner because the fixed point equation (3.12) is not satisfied anymore. These are the limits of the region shown in Figure 4.5. Observe that the limits determined by the map and the simulations overlap except at one single case shown only by an open circle in Figure 4.5C and 4.5D. Here, the map predicts that a 1:1 solution exists while the simulation does not converge to that. In this case, the simulation shows that the firing order between the neurons is not preserved which violates the 1:1 firing assumption of the map.

The phase of neuron A equals 0.5 on the diagonal in the static coupling case (Figure 4.5.A). It decreases (resp. increases) linearly as Q_0 moves down (resp. up) from the diagonal. This behavior can be predicted by perturbing equation (3.12) around the identical network solution. In the identical network, where $P_0 = Q_0$, the activity phases ($\tilde{\phi}^*, \tilde{\theta}^* = 0.5$), and the intrinsic phases ($\phi^* = \theta^* = 0.598$) of the two neurons are equal and hence $Z_A(\phi^*) = Z_B(\theta^*)$. If the solution is perturbed such that

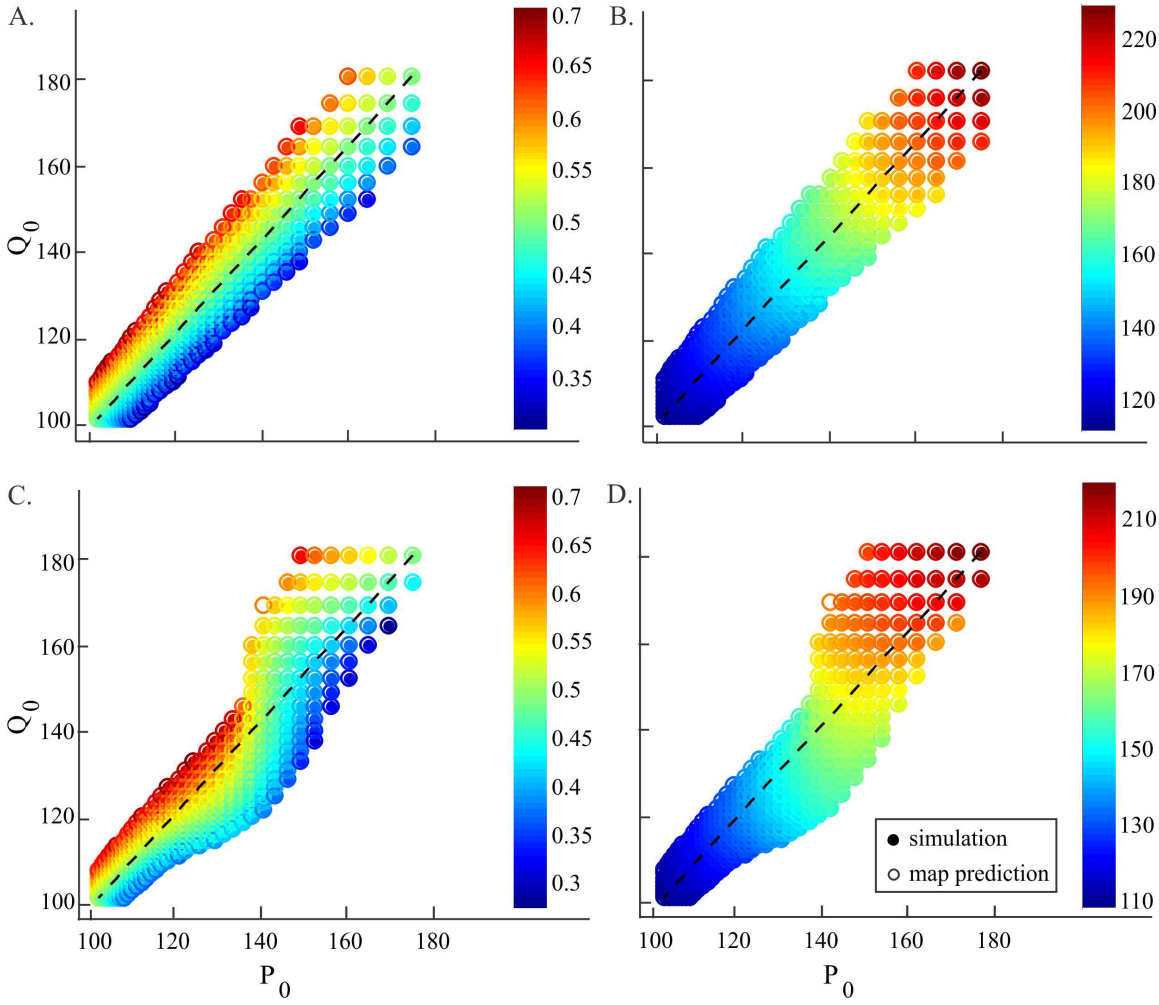

Figure 4.5 Coupling of non-identical M-L neurons. The phase of neuron A (A and C) and the period of the network (B and D) for coupled neurons with different intrinsic periods are shown for static synapses (A and B; $\bar{g} = 0.1$) and when the network follows the synaptic plasticity profile (C and D; $P_A = 150$, $P_B = 190$). The axes are the intrinsic periods of the two neurons. Plasticity adds nonlinearity to the period and phase distribution. Filled circles denote simulation results whereas open circles denote the map predictions. The map yields predictions very close to the simulations in most cases.

$P_0 > Q_0$, then the response of neuron A to synaptic inputs from neuron B must be smaller than the response of neuron B for the equation (3.12) to be satisfied. The PRC of the neurons has a negative slope at this intrinsic phase ϕ^* (Figure 2.3). So, the intrinsic phase ϕ of neuron A in the perturbed solution must be smaller than ϕ^* for $Z_A(\phi)$ to be smaller than $Z_A(\phi^*)$. As the function (3.16) relating ϕ and $\tilde{\phi}$ is monotone increasing, the activity phase $\tilde{\phi}$ of neuron A in the perturbed solution must also be smaller than $\tilde{\phi}^*$. Hence, as the difference $P_0 - Q_0$ increases (resp. decreases), the phase of neuron A decreases (resp. increases). The period of the network increases linearly as the intrinsic periods increase in the static coupling case (Figure 4.5B). Due to symmetry in the synaptic strengths, the distribution of the period is symmetric with respect to the diagonal.

When the synapses are plastic, some 1:1 phase-locked solutions that existed with static coupling no longer exist, while new solutions may emerge (Figures 4.5.C and 4.5.D). Due to asymmetry in the synaptic plasticity profiles, the upper bound for the difference in intrinsic periods that allow a 1:1 phase-locked solution varies. This can be seen by comparing the circles in the top row and rightmost column of Figure 4.5.C and 4.5.D. At the right top corner, $P_0 = Q_0 = 181$, and the network has an anti-phase solution. If Q_0 is fixed while P_0 decreases, the network continues to phase lock in a 1:1 solution for $P_0 \geq 152.1$. On the other hand, if P_0 is fixed while Q_0 decreases, then the network phase locks in a 1:1 solution only when $Q_0 \geq 174.8$. Although the absolute difference between the intrinsic periods are equal, different plasticity profiles causes convergence in one case but not the other. This can be understood by considering equations (4.4). For the identical cell case where $P_0 = Q_0 = 181$, the network period is equal to $P^* = 219.5$. Due to the selection of the plasticity profiles, $g_A(P^*) < g_B(P^*)$, since P^* is close to $P_B = 190$ than it is to $P_A = 150$. As a result, neuron A receives stronger synaptic input from neuron B at the steady state (as $g_B(P^*)$ determines $g_{B\to A}$). The firing periods of both neurons must be equal at

the fixed point. This is only possible if neuron B receives synaptic input at a phase that yields a larger response than that of neuron A. Hence, although the neurons are identical, the difference in their plasticity profiles causes a phase locking solution different than anti-phase. Assume that the solution is (ϕ, P) when the identical solution is perturbed such that $Q_0 > P_0$. Then the relation $g_A(P) < g_B(P)$ will still hold as P will stay close to P^*. In this case, the synaptic strength received by neuron A will be larger while its intrinsic period will be smaller than that of B. These two opposing effects will let the network continue having a solution until the difference between the intrinsic periods are too large to be compensated and the equations (4.4) are not satisfied. On the other hand, if the identical solution is perturbed such that $P_0 > Q_0$, then the synaptic strength received by neuron A and its intrinsic period will both be larger than those of neuron B. The phase of neuron B must increase further and yield a larger response to compensate these adding effects. But when the PRC reaches a maximum in absolute value and starts to decrease, there would be no phase value that would compensate these effects and the network will not be able to have a 1:1 solution. This explains why the limits of the regions in the case with synaptic plasticity are not symmetrical.

In general, whether the equations (4.4) are satisfied or not depends on the intrinsic periods P_0, Q_0 and the values of the PRCs as in the static map case. But in this case the values of the PRCs are also determined by two factors, the phase of inhibition received, and its strength- which is determined by the network period. Hence, the phase of neuron A is a determined both by the interaction of intrinsic periods and the plasticity profiles. This is also responsible for the nonlinearity in the distribution of phase. The level curves of phase are nonlinear in the case with synaptic plasticity as opposed to the linear level curves in the static coupling case.

CHAPTER 5

RECURRENT NETWORKS OF TWO QIF NEURONS COUPLED WITH DEPRESSING SYNAPSES

Poincaré maps describing the activity of a two-cell neuronal network are studied in [36]. The roles of synaptic depression is studied by comparing the phase locking of reciprocally coupled neurons with and without the depression property. We extend this analysis in this chapter. We show that bistable phase locking solutions are possible in networks with depressing synapses compared to static synapses in Section 5.1. We also perform bifurcation analysis in Section 5.2 on the map defined in [36].

The activity in a network of two neurons when the synapses are static is defined in [36] in the same way as we define the 1D static map (3.11) in Chapter 3, except with slight differences in notation. The map (3.11) we define is for the intrinsic phase ϕ of neuron A. We call the intrinsic phase of neuron B as θ. We define the intrinsic phase as the time since the neuron fires until it receives synaptic inhibition from the neuron it is connected to, normalized by its intrinsic period. On the other hand, the way the phase of a neuron is defined differs in the two studies. It is defined in [36] as the phase it gives synaptic inhibition to the neuron it synapses onto and the map is obtained for the phase θ of neuron A. For consistency, we will adjust the maps and the notation in [36] to the current study.

The map in [36] for the activity of two neurons when the synapses are static is equivalent to the map (3.11) which we rewrite here

$$\begin{aligned} \phi_{n+1} &= \Pi(\phi_n) \\ &= \frac{Q_0}{P_0}\left[1 - Z_B\left(\frac{P_0}{Q_0}(1 - Z_A(\phi_n) - \phi_n)\right)\right] - 1 + Z_A(\phi_n) + \phi_n. \end{aligned} \tag{5.1}$$

The condition for a fixed point is

$$P_0(1 - Z_A(\phi^*)) = Q_0(1 - Z_B(\theta^*)). \tag{5.2}$$

Now assume that the synapse from A to B has a fixed strength, while the synapse from B to A is depressing. If the short-term depression property of the B to A synapse follows the short-term synaptic plasticity model (2.12), then the map for the phase of neuron A and the depression variable of B can be obtained using the same approach in Chapter 3 as

$$\begin{aligned}
\phi_{n+1} &= \Pi_1(\phi_n, r_n) \\
&= \frac{Q_0}{P_0}\left[1 - Z_B\left(\frac{P_0}{Q_0}\left(1 - \phi_n - Z_A(\phi_n, g_{B\to A} r_n)\right)\right)\right] - 1 + Z_A(\phi_n, g_{B\to A} r_n) + \phi_n \\
r_{n+1} &= \Pi_2(\phi_n, r_n) \\
&= 1 - (1 - f r_n)\exp\left(-\frac{Q_0}{\tau_r}\left(1 - Z_B\left(\frac{P_0}{Q_0}(1 - \phi_n - Z_A(\phi_n, g_{B\to A} r_n))\right)\right)\right).
\end{aligned} \tag{5.3}$$

Here, $g_{B\to A}$ is the maximal synaptic conductance from B to A which is a constant. Observe that this map is similar to the map (3.21) with synaptic plasticity, except that there is only depression, and the model describing depression is different in this case. The fixed points of the map (5.3) satisfy

$$\begin{aligned}
Q_0\left[1 - Z_B\left(\frac{P_0}{Q_0}\left(1 - \phi^* - Z_A(\phi^*, g_{B\to A} r^*)\right)\right)\right] &= P_0\left[1 - Z_A(\phi^*, g_{B\to A} r^*)\right] \\
Z_B\left(\frac{P_0}{Q_0}\left(1 - \phi^* - Z_A(\phi^*, g_{B\to A} r^*)\right)\right) &= 1 - \frac{\tau_r}{Q_0}\ln\left(\frac{1 - f r^*}{1 - r^*}\right).
\end{aligned} \tag{5.4}$$

We extend the discussion in [36] on the relationship between the maps (5.1) and (5.3). We follow the same approach to distinguish the parameter notation for the synaptic strength in the static and the depressing synapse cases. We denote the total synaptic strength from B to A in the static map (5.1) by $\bar{g}_{B\to A}$. When there is depression from B to A, the maximal synaptic conductance in the map (5.3) is

denoted by $g_{B\to A}$, and the total synaptic strength is given by the product $g_{B\to A}r_n$ in cycle n.

The relationship between the maps (5.1) and (5.3) is obtained in [36] by comparing the fixed point equations (5.2) and (5.4). The two maps yield the same steady-state phase ϕ^* of neuron A if the following two equations are satisfied:

$$\begin{aligned} r^* &= \frac{1-\exp(\frac{P_0}{\tau_r}(1-Z_A(\phi^*,\bar{g}_{B\to A})))}{1-f\exp(\frac{P_0}{\tau_r}(1-Z_A(\phi^*,\bar{g}_{B\to A})))} \\ g_{B\to A} &= \frac{\bar{g}_{B\to A}}{r^*}. \end{aligned} \tag{5.5}$$

These equations define a relationship between the maps (5.1) and (5.3) as follows. The steady-state phase ϕ^* obtained from the 1-D map (5.1) when the synaptic strength form B to A equals $\bar{g}_{B\to A}$ can also be obtained from the 2-D map (5.3) if the maximal synaptic strength equals $\bar{g}_{B\to A}/r^*$ where r^* is given by the first equation in (5.5).

Assume that the 1-D map (5.1) when the synaptic strength from B to A equals $\bar{g}_{B\to A}$ yields a steady-state phase ϕ^* of neuron A. The response $Z_A(\phi^*,\bar{g}_{B\to A})$ of neuron A to perturbations received at the phase ϕ^* can be obtained from its PRC given by the equation (2.8). This determines the steady-state period P^* of neuron A, which is the same as the steady-state firing period of B. This period is given by the expression $P_0(1-Z_A(\phi^*,\bar{g}_{B\to A}))$. To be able to have the same steady-state solution with the 2D map (5.1), the phase and period must equal ϕ^* and P^*, respectively. We can evaluate equation (2.13) at the period value P^* to determine the steady-state value r^* of the depression variable which is given as the first equation in (5.5). From the second equation in (5.5), we find the maximal synaptic conductance $g_{B\to A}$ from B to A as $\bar{g}_{B\to A}/r^*$. Then, the 2-D map with the maximal synaptic conductance from B to A equals $g_{B\to A}$ must yield the fixed point (ϕ^*,r^*). Similarly, assume that the 2-D map with the synaptic conductance from B to A equals $g_{B\to A}$ is used to obtain a fixed point of (ϕ^*,r^*). Then the 1-D map can be used with the synaptic strength from B to A equal to $\bar{g}_{B\to A}=g_{B\to A}r^*$ to obtain the same steady-state phase of ϕ^*.

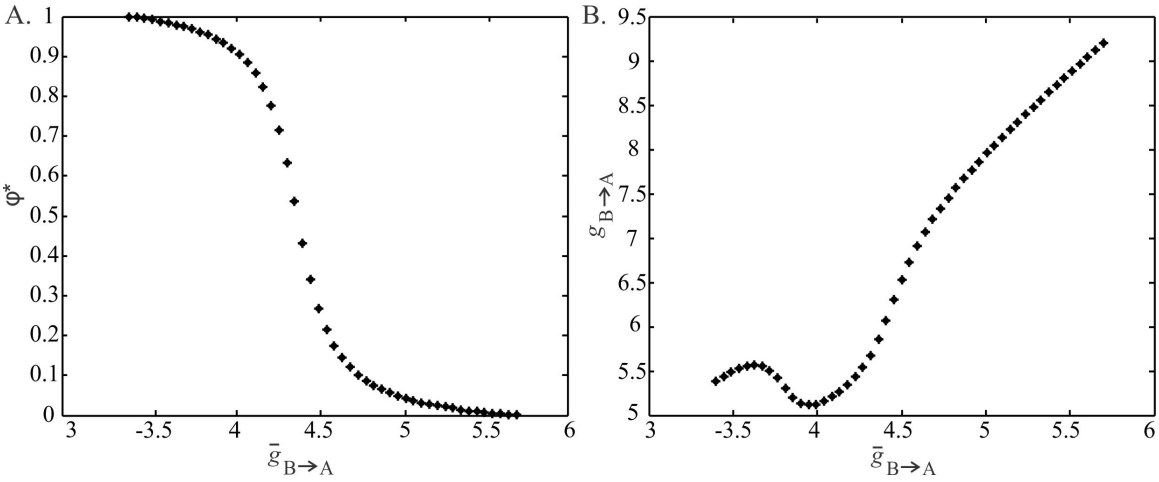

Figure 5.1 Phase locking of QIF neurons with static synapses. A. Steady-state intrinsic phase of neuron A obtained from the map (5.1) as a function of the synaptic coupling strength $\bar{g}_{B\to A}$. The synaptic strength from A to B is constant. The steady-state phase of neuron A decreases as $\bar{g}_{B\to A}$ is increased. B. The relationship between the synaptic strengths of the static map (5.1) and the depressing map (5.1) obtained from equations (5.5). For a given synaptic strength of the static map, the strength of the depressing map that yields the same phase locking is found. The relationship between the strengths of the two maps not being 1-1 causes bistability with the depressing map.

5.1 Bistability with Depression

In this section, we discuss how depressing synapses can produce bistable phase locking solutions. Suppose that the 1-D map (5.1) is used to obtain the steady-state phase ϕ^* of neuron A when it is coupled to B with reciprocal static synapses. As discussed above, the value r^* of the depression variable can be obtained from the first equation of (5.5). Denote by r_g^* and r_h^* the values of the depression variable at the steady state when the neurons are coupled with static synaptic strengths of $\bar{g}_{B\to A}$ and $\bar{h}_{B\to A}$, respectively. Assume that the equality

$$\frac{\bar{g}_{B\to A}}{r_g^*} = \frac{\bar{h}_{B\to A}}{r_h^*} = g_{B\to A} \tag{5.6}$$

is satisfied, i.e., the ratios of the static synaptic strengths to the depression variables are equal to the same value of $g_{B\to A}$. Then, this means that there is more than one solution to the 2-D map when the maximal synaptic conductance from B to A equals

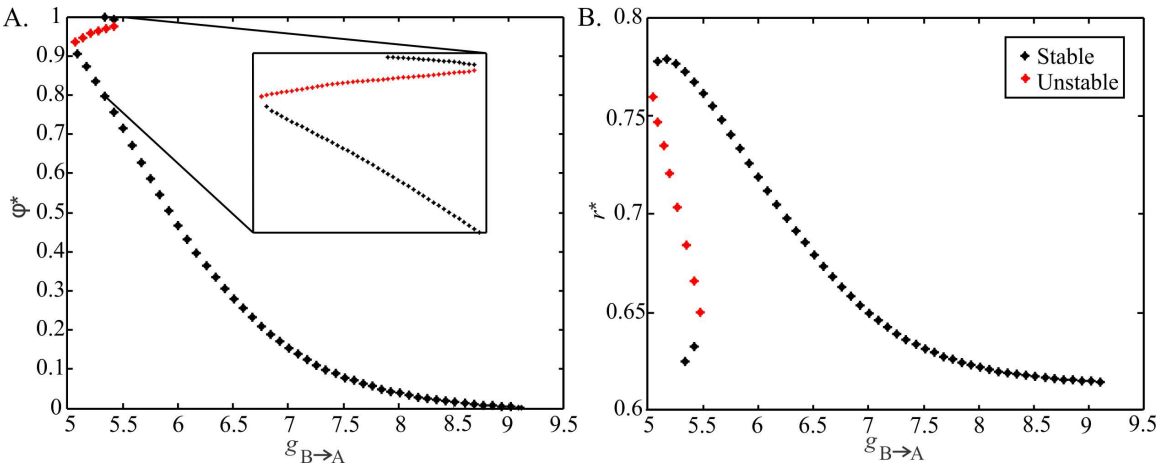

Figure 5.2 Phase locking of QIF neurons with depressing synapses obtained from the map (5.3). A. Steady-state intrinsic phase of neuron A when $g_{A\to B}$ is fixed and $g_{B\to A}$ is varied. The phase is not monotonically decreasing as a function of the synaptic coupling strength due to the existence of depression. There exist a region of bistability as shown in the inset plot. B. The steady-state value of the depression variable as a function of $g_{A\to B}$.

$g_{B\to A}$. The network coupled with depressing synapses of maximal conductance $g_{B\to A}$ would yield both of the fixed points (ϕ_g^*, r_g^*) and (ϕ_h^*, r_h^*). If both of these fixed points are stable, then, the network has bistable solutions.

We now consider QIF neurons. We first find where the network phase locks when the synapses are static using the map (5.1). We then let the synapses from cell B to A be depressing and use the map (5.3) to find phase locking. We observe the relation between the two maps and find whether we have bistability.

Consider two identical neurons and let the parameters governing the individual neuron dynamics be $V_{tA} = V_{tB} = 7$, $V_{rA} = V_{rB} = -8$. Let the synaptic strength from A to B be fixed at $\bar{g}_{A\to B} = 4$. Let the total synaptic conductance $\bar{g}_{B\to A}$ from B to A vary in a range from 3.3 to 5.6. The steady-state phase ϕ^* of neuron A obtained from the map (5.1) as a function of $\bar{g}_{B\to A}$ is shown in Figure 5.1A.

Having obtained the phases from the static map (5.1), we use the first equation in (5.5) to determine the value of the depression variable at the steady state. We set the parameters governing the depression dynamics as $f = 0.5$ and $\tau_r = 5$, i.e.,

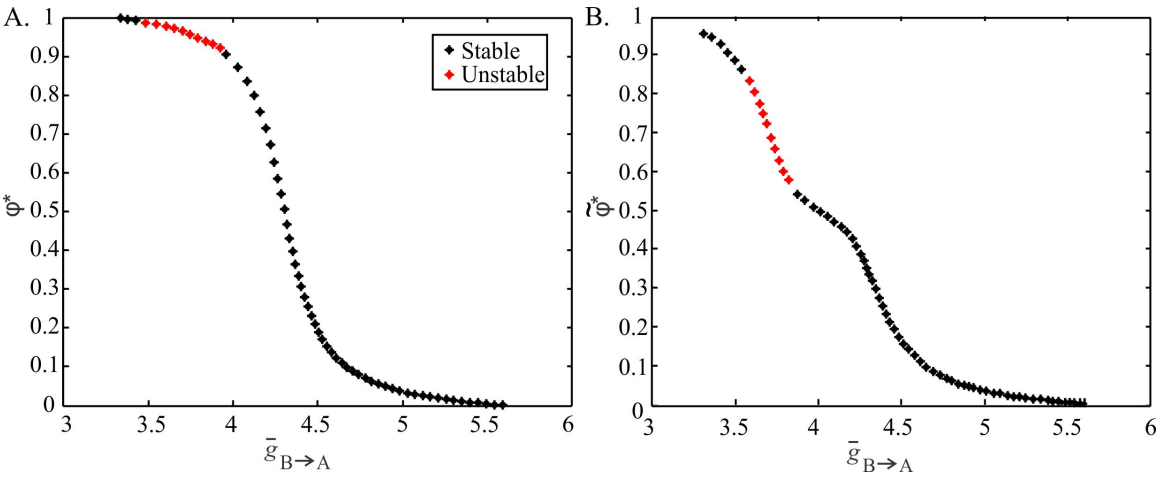

Figure 5.3 The equivalence of the fixed points of the maps (5.1) and (5.3). A. The steady-state intrinsic phase of neuron A obtained from the depressing map (5.3) is equivalent to the phase obtained from the static map (5.1) (compare with Figure 5.1) when plotted as a function of $\bar{g}_{B\to A} = g_{B\to A} r^*$. B. The activity phase $\tilde{\phi}^*$ of neuron A.

whenever the neuron spikes, the strength of the synapses decreases to half of its current value. It recovers to 1 with a time constant $\tau_r = 5$. We use the second equation in (5.5) to find the value of the maximal synaptic strength necessary to obtain the same phase locking from the depressing map (5.3). The relationship between the two synaptic conductances is shown in Figure 5.1B.

We see that there are some values of $\bar{g}_{B\to A}$, that yields the same $g_{B\to A}$ value. In other words, there exist more than one value of $\bar{g}_{B\to A}$ corresponding to a $g_{B\to A}$. This means that there is more than one solution to the 2-D map for these values of synaptic conductance. We now plot the steady-state phase values obtained from the 2-D map. We let $g_{B\to A}$ change in a range from 5 to 9.1 which is determined by the equations (5.5) as shown in Figure 5.1B. Figure 5.2 shows the fixed points of the map (5.3) as a function of $g_{B\to A}$. The steady-state phases ϕ^* are shown in Figure 5.2A and the values of the depression variable is shown in Figure 5.2B. The stability of the fixed points can be found numerically which is explained in the next section. The stable solutions are shown in black and the unstable solutions are shown in red in the figure.

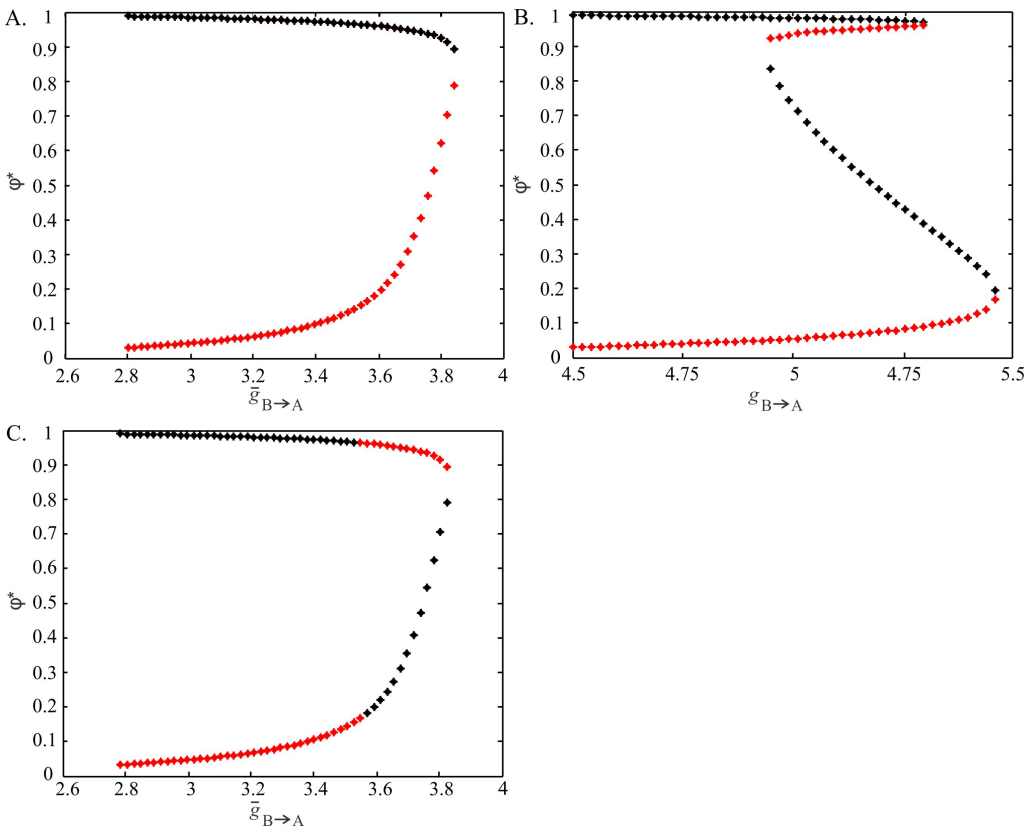

Figure 5.4 Phase locking of non identical QIF neurons with static (5.1) and depressing (5.3) maps. A. Steady-state intrinsic phase of neuron A obtained from the static map (5.1) as a function of $\bar{g}_{B\to A}$ when $\bar{g}_{A\to B}$ is constant. There are two fixed points, the larger of which is stable. B. Steady-state intrinsic phase of neuron A obtained from the depressing map (5.3) as a function of $g_{B\to A}$ when $\bar{g}_{A\to B}$ is constant. Existence of depression causes bistability for larger $g_{B\to A}$. C. Steady-state intrinsic phase of neuron A obtained from the depressing map (5.3) as a function of $\bar{g}_{B\to A} = g_{B\to A} r^*$. The fixed points of the two maps are equivalent although the stability of these points do not match.

For $g_{B\to A}$ large, there are three fixed points, two of which are stable. Therefore, the network has bistability for this range of synaptic strength. The inset plot shows the zoom in the bistability region. For completeness, we plot the results of the 2-D map as a function of the total synaptic conductance $\bar{g}_{B\to A} = g_{B\to A} r^*$ in Figure 5.3A. The fixed points agree with the ones obtained from the 1-D map (5.1) which is shown in Figure 5.1A. Some solutions obtained from the 2-D map are unstable while all the solutions obtained from the 1-D map are stable.

We now analyze the relationship between $\bar{g}_{B\to A}$ and $g_{B\to A}$ (Figure 5.1B) to understand how bistability is achieved. As we discussed above, if there are two distinct synaptic conductances $\bar{g}_{B\to A}$ and $\bar{h}_{B\to A}$ for the static map such that the equality (5.6) holds, then the depressing map would yield bistability. This is possible only if $\bar{g}_{B\to A}$ and $g_{B\to A}$ have a non-monotonic relationship. We now analyze what determines the relationship between the two conductances and find conditions for bistability to occur.

As the synaptic strength $\bar{g}_{B\to A}$ is increased, the phase of neuron A decreases (Figure 5.1A). The firing period of the network at the steady state is determined by this phase through the PRC of neuron A. The PRC of a QIF neuron first increases and then decreases in absolute value with increasing phase (Figure 2.3B). Therefore, the network period P^* first increases and then decreases as $\bar{g}_{B\to A}$ is increased. The steady-state value of depression r^* is an increasing function of P^* (Figure 2.2B). So, r^* first increases and then decreases with increasing $\bar{g}_{B\to A}$, too.

The networks coupled with larger synaptic strengths yield smaller steady-state phases of neuron A (Figure 5.1A). The PRC is increasing in amplitude for this range of phases. Therefore, for larger synaptic strengths, r^* decreases as $\bar{g}_{B\to A}$ is increased. The synaptic strength $g_{B\to A}$ equals the ratio $\bar{g}_{B\to A}/r^*$. Hence, for larger synaptic strengths, $g_{B\to A}$ is always an increasing function of $\bar{g}_{B\to A}$, since the numerator $\bar{g}_{B\to A}$ is increasing and the denominator r^* is decreasing.

On the other hand, for smaller synaptic strengths, the phase locking occurs at larger phases (Figure 5.1A), where the PRC is decreasing in amplitude with increasing phase. Here, increasing $\bar{g}_{B\to A}$ would yield a smaller phase, a larger period, and a larger r^* value. In this case, whether $g_{B\to A}$ is an increasing or a decreasing function of $\bar{g}_{B\to A}$ depends on the increase rate of r^* with respect to the increase rate of $\bar{g}_{B\to A}$. When the PRC has a larger derivative, the increase in r^* is large, causing a decrease in

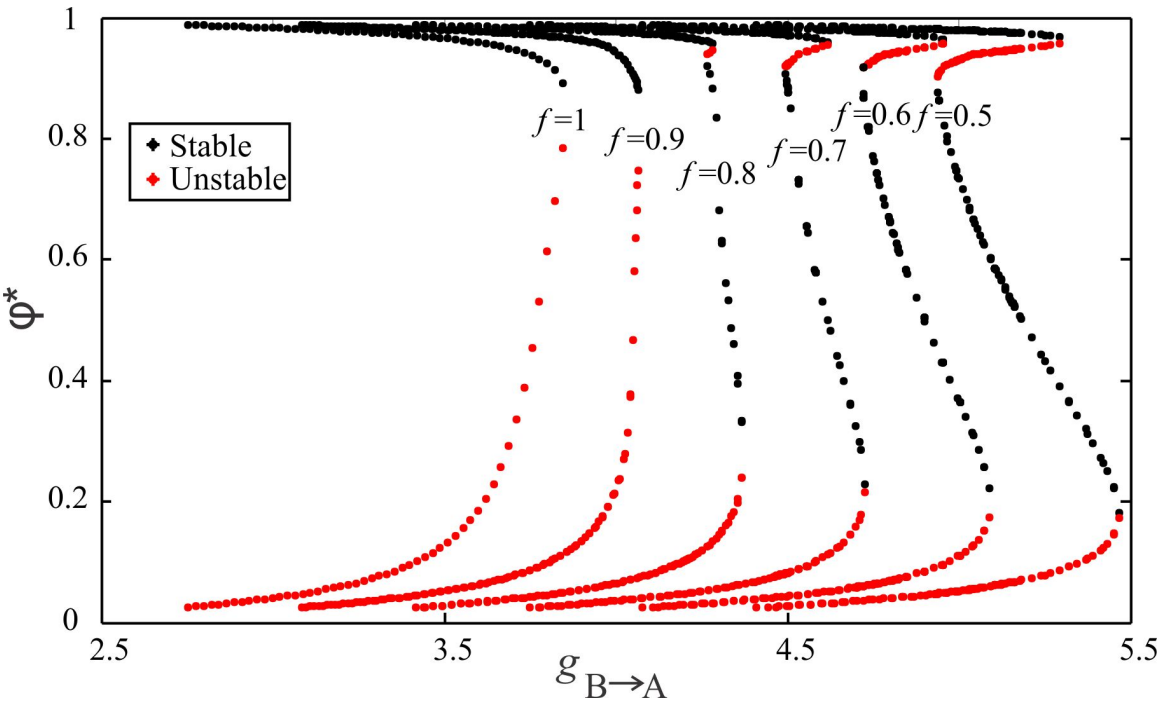

Figure 5.5 The dependence of bistability on the parameters that govern synaptic depression. The region of bistability increases from left to right as f is decreased. Similar behavior is observed when τ is increased.

$g_{B\to A}$. The non-monotonicity between the two conductances is observed for smaller $\bar{g}_{B\to A}$ (5.1.B) and bistability occurs for synaptic conductances falling in this range.

We repeat this procedure of finding the fixed points for non-identical neurons. Let $V_{tB} = 9$ and keep $g_{A\to B}$ and the rest of the parameters governing the neuron and plasticity dynamics the same. The static map (5.1) yields two fixed points for each $\bar{g}_{B\to A}$ in the range from -3.8 to -2.8 (Figure 5.4A). The larger fixed point is stable while the smaller one is unstable. Using the set of equations (5.5), we find that the value of the maximal synaptic conductance $g_{B\to A}$ has to be in the range from -5.5 to -4.5 to obtain the same fixed points from the dynamic map (5.3). The fixed points of this map is shown in Figure 5.4B. For large and small $g_{B\to A}$ values, there are two fixed points, the larger of which is stable and the other one is unstable, as in the case of the static map. However, for intermediate $g_{B\to A}$ values, there are four fixed points, two of which are stable. Therefore, the network has bistability for this range

of synaptic conductances. The fixed points of the depressing map is shown in the $\bar{g}_{B\to A} = r^* g_{B\to A}$ axis for comparison with the solutions of the static map in Figure 5.4C. Although the fixed points are the same, the stability of the solutions do not match, which is not guaranteed by the equations (5.5).

For bistability to occur, the depression variable must be strong enough to cause a decrease in $g_{B\to A}$. So, if the fraction parameter f is large or the time constant τ is small, r^* will not increase much with increasing network period. Its effect will be negligible in determining $g_{B\to A}$ and bistability will not be possible. Figure 5.5 demonstrates the change in the bistability region as the parameter f is varied. Smaller values of f correspond to more depressing synapses and the region of bistability increases from left to right as f is decreased (Figure 5.5). A similar increase in the bistability region is observed as τ is increased. Also, existence of bistability is possible for phases where the PRC is increasing in amplitude and it depends on the derivative of the PRC in this range. Hence, its existence is determined by the interaction of neuronal and synaptic dynamics together.

We have first obtained the fixed points of the 1-D map and used the equations (5.5) to obtain the same steady-state phase values using the 2-D map. This process can also be reversed. For any given $g_{B\to A}$, we can first obtain the phase locked solutions of the network from the 2-D map and can find $\bar{g}_{B\to A}$ from the equations (5.5) that would result in the same solutions of the 1-D map.

5.2 Bifurcation Analysis

Although there is an equivalence between the two maps in terms of the fixed points, the stability of these solutions may differ. The condition for stability of the static map is given in (3.13). We find the stability condition of the depressing map (5.3) in this section.

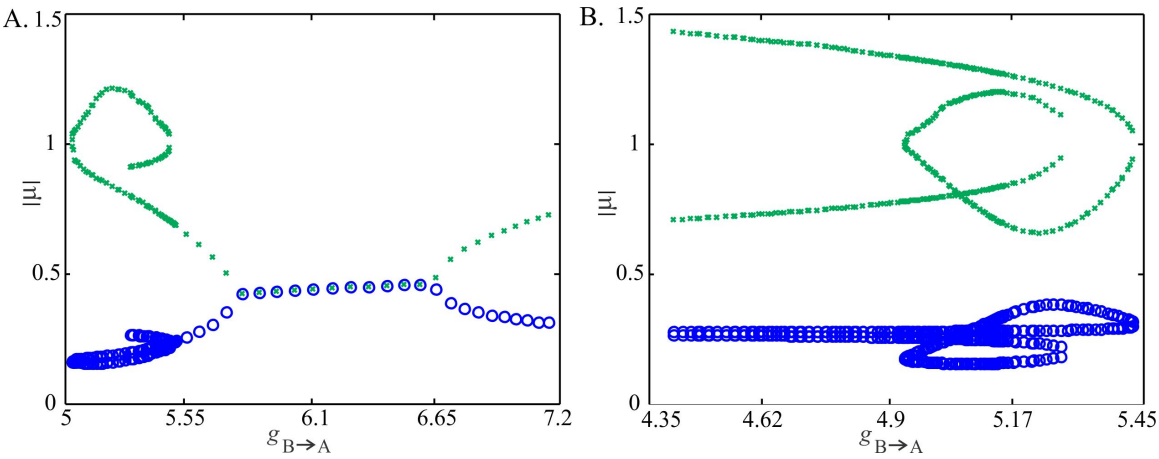

Figure 5.6 The dependence of bistability on the eigenvalues of the depressing map (5.3). A. The absolute values of the eigenvalues of the 2D map (5.3) for identical neurons. B. The absolute values of the eigenvalues of the 2D map (5.3) for non-identical neurons. The absolute values of the two eigenvalues of the depressing map are shown in different colors. The absolute values overlap for imaginary eigenvalues. The fixed points are stable when both eigenvalues are less than 1 in absolute value. One of the eigenvalues is greater than 1 for some $g_{B\to A}$ and this creates unstability via saddle-node bifurcation.

A fixed point $x^* = (\phi^*, r^*)$ of the map Π corresponds to a limit cycle L_0 of the underlying neuronal dynamics. The multipliers μ_1 and μ_2 of the Jacobian matrix A of the map Π determine the type of the fixed point x^*.

If none of the multipliers lie on the unit circle, i.e., $\{\mu \in \mathbb{C} : |\mu| = 1\} = \emptyset$, then the point x^* is said to be hyperbolic [41]. The hyperbolicity condition can be violated in three ways. If one of the eigenvalues, say μ_1, passes through 1, then a saddle-node bifurcation occurs. If μ_1 passes through -1, then a flip bifurcation occurs. If both eigenvalues μ_1 and μ_2 are complex and $|\mu_1| = |\mu_2| = 1$, then a Neimark-Sacker bifurcation occurs. To analyze the bifurcations of the map Π, we first find the multipliers. The Jacobian of the map (5.3) is given by

$$A = \begin{pmatrix} \frac{\partial \Pi_1}{\partial \phi} & \frac{\partial \Pi_1}{\partial r} \\ \frac{\partial \Pi_2}{\partial \phi} & \frac{\partial \Pi_2}{\partial r} \end{pmatrix}.$$

The partial derivatives are

$$\begin{aligned}
\frac{\partial \Pi_1}{\partial \phi} &= (Z_B'(\theta)+1)\left(\frac{\partial Z_A}{\partial \phi}(\phi, \bar{g}_{B\to A} r)+1\right) \\
\frac{\partial \Pi_1}{\partial r} &= (Z_B'(\theta)+1)\frac{\partial Z_A}{\partial r}(\phi, \bar{g}_{B\to A} r) \\
\frac{\partial \Pi_2}{\partial \phi} &= \frac{P_0}{\tau_r} Z_B'(\theta)(1-fr)\left(1+\frac{\partial Z_A}{\partial \phi}(\phi, \bar{g}_{B\to A} r)\right)\exp\left(\frac{Q_0}{\tau_r}\left(1-Z_B(\theta)\right)\right) \\
\frac{\partial \Pi_2}{\partial r} &= \left(f+\frac{P_0}{\tau_r} Z_B'(\theta)(1-fr)\frac{\partial Z_A}{\partial r}(\phi, \bar{g}_{B\to A} r)\right)\exp\left(\frac{Q_0}{\tau_r}\left(1-Z_B(\theta)\right)\right)
\end{aligned} \tag{5.7}$$

where $\theta = \frac{P_0}{Q_0}(1-\phi-Z_A(\phi, \bar{g}_{B\to A} r))$ and Z_B' denotes derivative with respect to ϕ. The PRC of the QIF model neuron is given in Equation (2.8). Taking derivatives of the PRCs of neurons A and B yields

$$\begin{aligned}
Z_B'(\theta) &= \frac{\sec^2(Q_0\theta + \bar{g}_{A\to B}\tan V_{r_B})}{1+(\tan(Q_0\theta+\bar{g}_{A\to B}\tan V_{r_B})+\bar{g}_{A\to B})^2} - 1, \\
\frac{\partial Z_A}{\partial \phi}(\phi, \bar{g}_{B\to A} r) &= \frac{\sec^2(P_0\phi + \bar{g}_{B\to A}\tan V_{r_A})}{1+(\tan(P_0\phi+\bar{g}_{B\to A}\tan V_{r_A})+\bar{g}_{B\to A})^2} - 1, \\
\frac{\partial Z_A}{\partial r}(\phi, \bar{g}_{B\to A} r) &= \frac{\bar{g}_{B\to A}}{P_0(1+(\tan(P_0\phi+\bar{g}_{B\to A}\tan V_{r_A})+\bar{g}_{B\to A} r)^2)}.
\end{aligned}$$

We evaluate the Jacobian matrix A for a the fixed points of the 2-D map. The absolute values of the two eigenvalues corresponding to each fixed point is shown in Figure 5.6. When the eigenvalues are both complex, their absolute values are equal. We see that the absolute value of one of the eigenvalues exceed 1 when $g_{A\to B}$ is large. We find that it equals 1 at the bifurcation point hence this is a saddle-node bifurcation. The dependence of stability on the depression parameters f and τ_r can be seen in Equations (5.7) and (5.8). Hence, the existence of bistability depends heavily on these parameters.

CHAPTER 6

THE EFFECT OF A HYPERPOLARIZATION-ACTIVATED INWARD CURRENT IN A NEGATIVE-LEAK CONDUCTANCE OSCILLATOR

In this chapter, we use Negative-Leak model (2.6), a simple conductance-based model, to study how oscillations are generated by the interaction of several ionic currents in a single neuron and how these currents effect the networking properties of the neurons.

Regenerative inward currents are known to be important for the generation of neuronal oscillations. Roles of these currents on the generation of oscillations are studied in [5] by replacing it with a simplified linearized current, which they call the Negative-Leak current. The aim of this study is to understand the mechanisms of slow oscillations underlying neuronal bursting which involve such regenerative currents. We extend this study in this chapter by considering some additional properties and the networks of N-L model neurons.

We study the networking properties of Negative-Leak neurons in Section 6.1. We compare the M-L and N-L models in Section 6.2. Finally, we study how the properties of the ionic currents effect the oscillations in a single N-L neuron in Section 6.3.

6.1 Networks of N-L Neurons

In this section, we consider the networking properties of two N-L neurons (2.6). Our aim is to explore the role of network interactions in the generation of oscillations with I_{N-L} for coupled neurons. We would like to use the Poincaré maps we developed in Chapter 3 to predict the coupled network's period and phase relations. We couple two N-L neurons with inhibitory synapses where the synaptic current from neuron j to i by $I_{j\to i} = g_{syn}s_i(V_i - V_{syn})$. The dynamic variable s_i is governed by the equation

$$\frac{ds_i}{dt} = \frac{1-s_i}{\tau_1}\mathrm{H}(V_j - V_{th}) + \frac{-s_i}{\tau_2}\mathrm{H}(V_{th} - V_j) \tag{6.1}$$

where τ_1 and τ_2 are rise and decay time constants for the synaptic variable.

We first let the synapses have fast rise and decay and set $\tau_1 = \tau_2 = 1$. We do simulations using XPPAUT for two identical N-L neurons. The intrinsic period of the neurons A and B are $P_0 = Q_0 = 719.4$ and the intrinsic burst durations ($V > V_{th}$) are $b_0 = q_0 = 314.8$. The neurons fire in anti-phase when coupled with identical synaptic conductance of $\bar{g}_{A\to B} = \bar{g}_{B\to A} = 0.01$. We next check whether the map (3.11) is able to predict this activity. For this purpose, we generate the PRC of the N-L neurons using perturbations of the form (2.9). The map yields the steady state intrinsic phase $\phi^* = 0.48$. The network period evaluated at this intrinsic phase is obtained to be $P^* = 694.2$. Using Equation (3.1) we find the activity phase $\tilde{\phi}^*$ to be at 0.5. The network period and phase obtained from the map are consistent with the simulations. However, although there is a change in the burst duration of the neurons when coupled, this is not captured by the map. This is because the existing techniques we developed so far do not take into account the changes in the burst duration of the neurons. We assumed either instantaneous spikes or spikes with a constant burst duration. These maps gave accurate results in M-L or QIF neurons since the fixed burst duration assumption is satisfied. Yet, to be able to have a better understanding of the network behavior when the burst duration is not fixed, this should be included in the map as a variable. We now derive a map that takes the changing burst duration into account.

In order to derive a map for the network activity that tracks the changes in the burst duration, we need a burst response curve apart from a PRC. We numerically calculate the 1^{st} and 2^{nd} order PRCs (Z^1 and Z^2) and BRCs (W^1 and W^2) of a N-L model neuron for perturbations in the form (2.9). If the perturbation is received after the offset of the burst, then it does not effect the current cycle's burst duration and $W^1 = 0$. We assume that the neuron does not receive a perturbation during its burst, hence we ignore the first order BRC. We also observe that the 2^{nd} order PRC

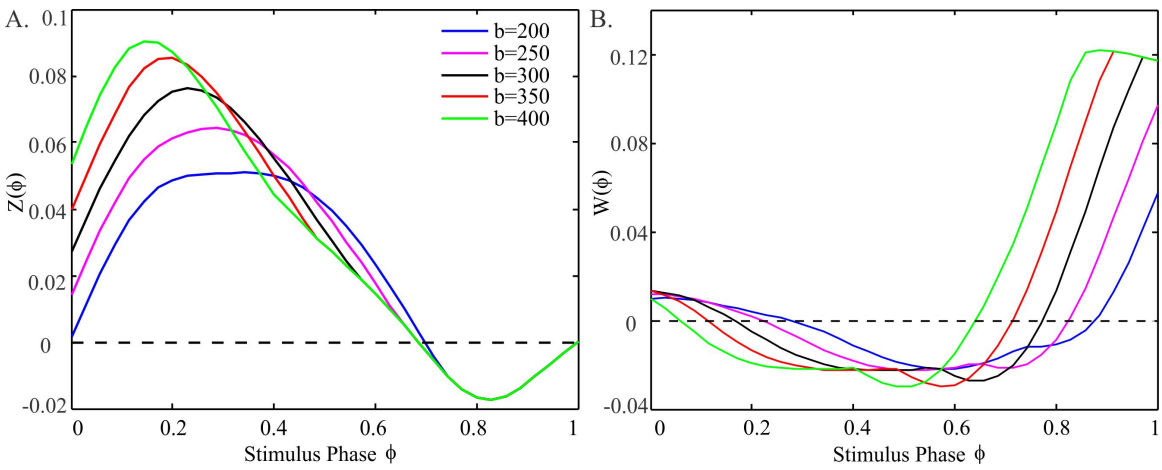

Figure 6.1 Responses of the N-L model neuron to perturbations. A. Phase response curve, changes in the cycle period due to perturbations. B. Burst response curve, changes in the burst duration due to received perturbations.

is negligibly small, so we also ignore Z^2. In this case, we denote the 1^{st} order PRC with Z_A (respectively Z_B) and 2^{nd} order BRC with W_A (respectively W_B) for neuron A (respectively B). The PRCs and BRCs for a N-L model neuron for a set of burst durations are shown in Figure 6.1.

We take the 1st order PRC and 2nd order BRC into account and derive the map for network activity accordingly. The cycle periods for the neurons A and B are

$$\begin{aligned} P_n &= P_0\,(1 - Z_A(\phi_n, q_n)) \\ Q_n &= Q_0\,(1 - Z_B(\theta_n, b_{n+1}))\,, \end{aligned}$$

and the burst durations are

$$\begin{aligned} b_{n+1} &= b_0\,(1 - W_A(\phi_n, q_n)) \\ q_{n+1} &= q_0\,(1 - W_B(\theta_n, b_{n+1}))\,, \end{aligned}$$

in cycle n, where ϕ and θ are defined in 3.3 and 3.4. Starting with ϕ_n and q_n, one can obtain

$$\theta_n = \frac{P_0}{Q_0}\left[1 - Z_A(\phi_n, q_n) - \phi_n\right] \tag{6.2}$$

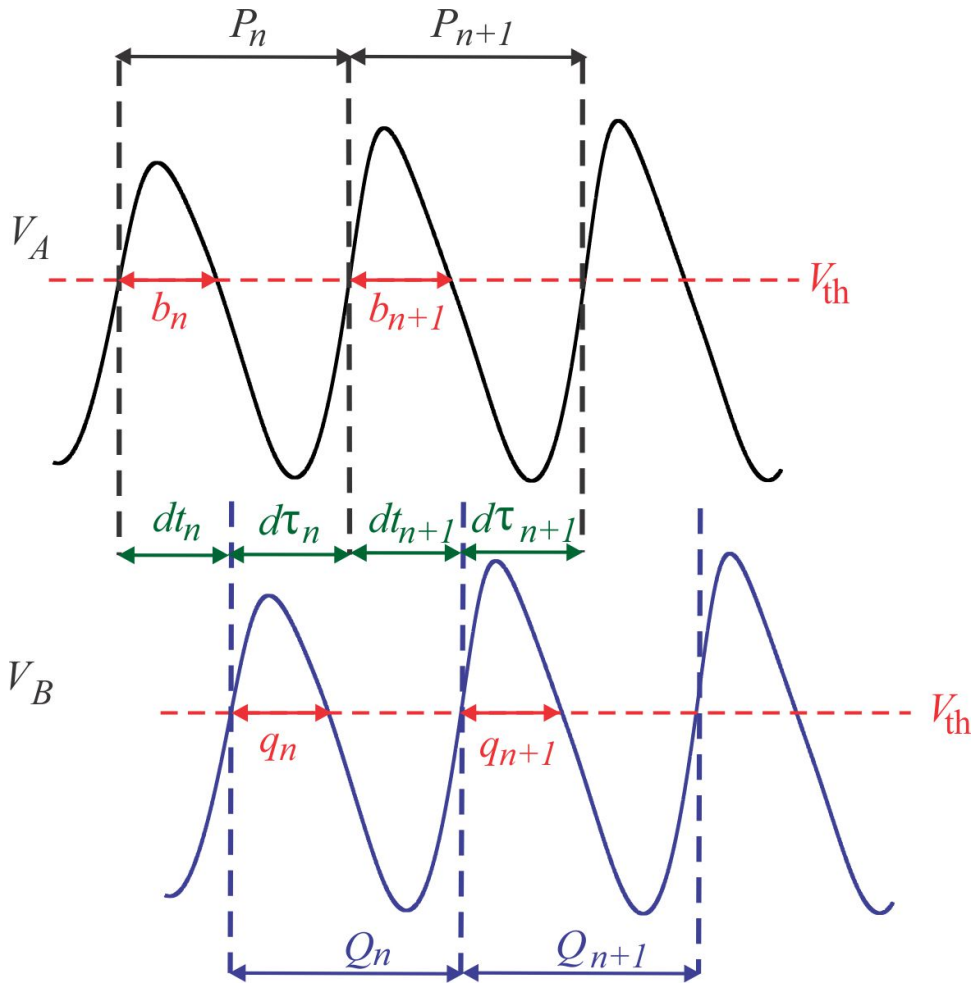

Figure 6.2 Schematic diagram of the map variables. In addition to the cycle lengths P_n, Q_n of the neurons A and B, the burst durations b_n, q_n are also included in the map as variables. Changes in the burst duration of the oscillations due to coupling are captured by the map.

by plugging Equation (6.2) into (3.9). Then using Equations (6.2) and (3.10) together with (6.2) gives the values of ϕ and q in the next cycle. Then, the map for the network activity with changing burst duration is given by

$$\begin{aligned} \phi_{n+1} &= \frac{Q_0}{P_0}\left[1 - Z_B\left(\frac{P_0}{Q_0}\left[1 - Z_A(\phi_n, q_n) - \phi_n\right], b_0\left(1 - W_A(\phi_n, q_n)\right)\right)\right] \\ &\quad -1 + Z_A(\phi_n, q_n) + \phi_n \qquad (6.3) \\ q_{n+1} &= q_0\left[1 - W_B\left(\frac{P_0}{Q_0}\left[1 - Z_A(\phi_n, q_n) - \phi_n\right], b_0\left(1 - W_A(\phi_n, q_n)\right)\right)\right] \end{aligned}$$

The map variables and their relations are shown in Figure 6.2. A similar map for a two cell network activity that takes into account the BRC is also derived in [62] and the conditions for stable solutions are analyzed in the case that the BRC effects are zero.

To be able to apply the map to N-L model neurons, we obtain PRCs and BRCs for perturbation durations changing from $\sigma = 200$ to $\sigma = 400$ with increments of 25. We let the synaptic strength $a = 0.01$ and use perturbations of the form (2.9). Hence, we generate PRC and BRC matrices of size 36×9 (number of phase points $\times$ burst durations). The PRCs and BRCs grow in amplitude as the duration of the perturbation is increased (Figure 6.1). If the effects of the BRC is neglected, i.e., if $W_A = W_B = 0$, then this map simplifies to the static map (3.11).

The map (6.3) yields $\phi^* = 0.48$ for the intrinsic phase and $q^* = 321.8$ for the burst duration. The network period is obtained to be $P^* = 694.9$ and the activity phase $\tilde{\phi}$ to be 0.5. The map correctly predicts the change in the burst duration when the network is coupled. Observe that the PRC is positive and the BRC is negative at the intrinsic phase ϕ^*. This is consistent with the decrease in the network period and the increase in the burst duration when the cells are coupled.

Although this map gives accurate results with synapses that rise and decay fast, it does not generalize to synapses with slow rise and decay. To demonstrate this, we show an example. We take the same network of neurons, keeping the intrinsic neurons' parameters the same and only changing the time constants to $\tau_1 = 140$ and $\tau_2 = 200$. This causes the synapses to rise and decay slowly. Simulation shows that this network has bistability, as both synchrony and anti-phase being solutions. We concentrate on the anti-phase solution since we assumed that the burst durations do not overlap in the derivation of the map (6.3). From simulation, the period and burst duration at the steady state are obtained to be 610 and 252, respectively. Knowing the period and the activity phase of the neuron A from simulations, we find its intrinsic phase

to be 0.42 from Equations (3.1) and (3.3). The PRC of the neuron is positive at this intrinsic phase for different perturbation durations (Figure 6.1.A). This is consistent with the simulations. However, the BRC has a negative value at 0.42 (Figure 6.1.B). This would yield a longer burst duration which is not consistent with the simulations. As the perturbation duration is increased, the PRC increases in amplitude. One might expect that this would decrease the intrinsic phase of the neuron enough to fall in the positive region of the BRC and cause the burst duration to decrease. However, as the perturbation duration is increased, the region where the BRC is negative shifts to the left (Figure 6.1.B). So, with longer perturbation durations (corresponding to synapses with slow rise and decay), this negative region shifts more to the left, making it almost impossible for the burst duration to decrease.

The reason that this map does not apply to synapses with longer durations is that the first order BRC effects are ignored in the derivation. Although the burst durations of the neurons do not overlap in the anti-phase solution, the synapses continue longer and the neuron receives synaptic input during its burst. The effect of the synaptic input that the neuron receives during its burst is included in the first order BRC. Therefore, the map needs also include first order BRCs to generalize to study synapses with longer durations.

6.2 N-L Model Compared with the M-L Model

We study how the N-L model compares with the M-L model (2.5). For this purpose, we take a M-L neuron and replace I_{Ca} with I_{N-L}. We keep the K^+ and the leak currents in the M-L model (2.5), and replace the Ca^{2+} current with a $N-L$ current. Hence, the equations for the N-L model are as follows

$$\begin{aligned} \frac{dV}{dt} &= (I_{app} - I_L - I_K - I_{N-L})/C \\ \frac{dw}{dt} &= \frac{w_\infty - w}{\tau_w(V)}. \end{aligned} \tag{6.4}$$

Note that this model is equivalent to the basic N-L model (2.6) except that applied current is included here.

We start with a M-L model that gives stable oscillations. To be able to compare the two models, we choose the same values for the parameters that are common in both models. We let $I_{app} = 70$, $g_K = 8$, $g_L = 2$, $E_K = -84$, $E_L = -60$, $c = 20$, $V_c = 12$, $v_4 = 17.4$ and $\phi = 0.0067$. Setting the remaining parameters of the M-L model as $v_1 = -1.2$, $v2 = 18$, $g_{Ca} = 4$ and $E_{Ca} = 120$ yields to stable oscillations. We now find the correct parameters for the N-L model that would imitate the M-L model. We choose the N-L parameters so that two criteria are satisfied. The first criterion is that the locations of the fixed point of the M-L and N-L models should match. And the second criterion is that the characteristics of the two fixed points should be the same, i.e., their eigenvalues should match.

We now consider the first criterion. To be able to find the fixed point of the M-L model accurately, we first increase the value of ϕ. This yields slower potassium kinetics which causes the oscillations to die out and the solution to approach the stable focus (V_M, w_M) whose value is numerically obtained to be $(6.769, 0.3541)$. To be able to match the fixed point (V_N, w_N) of the N-L model with the point (V_M, w_M), we solve w_N in terms of V_N on the V-nullcline. This yields

$$w_M = \frac{I_{app} - g_L(V_M - E_L) - g_{N-L}(V_M - E_{N-L})}{g_K(V_M - E_K)}. \tag{6.5}$$

This defines a relationship between g_{N-L} and E_{N-L} that has to be satisfied since the rest of the parameters are already determined.

The second criteria reads as follows. The linearizations of the V-nullclines of the two models should match around the fixed point. This would yield the same type of fixed point, since the w-nullcline is the same in both models. Denote the i, jth entries of the Jacobian of the M-L model by $M_{i,j}$ and the Jacobian of the N-L model

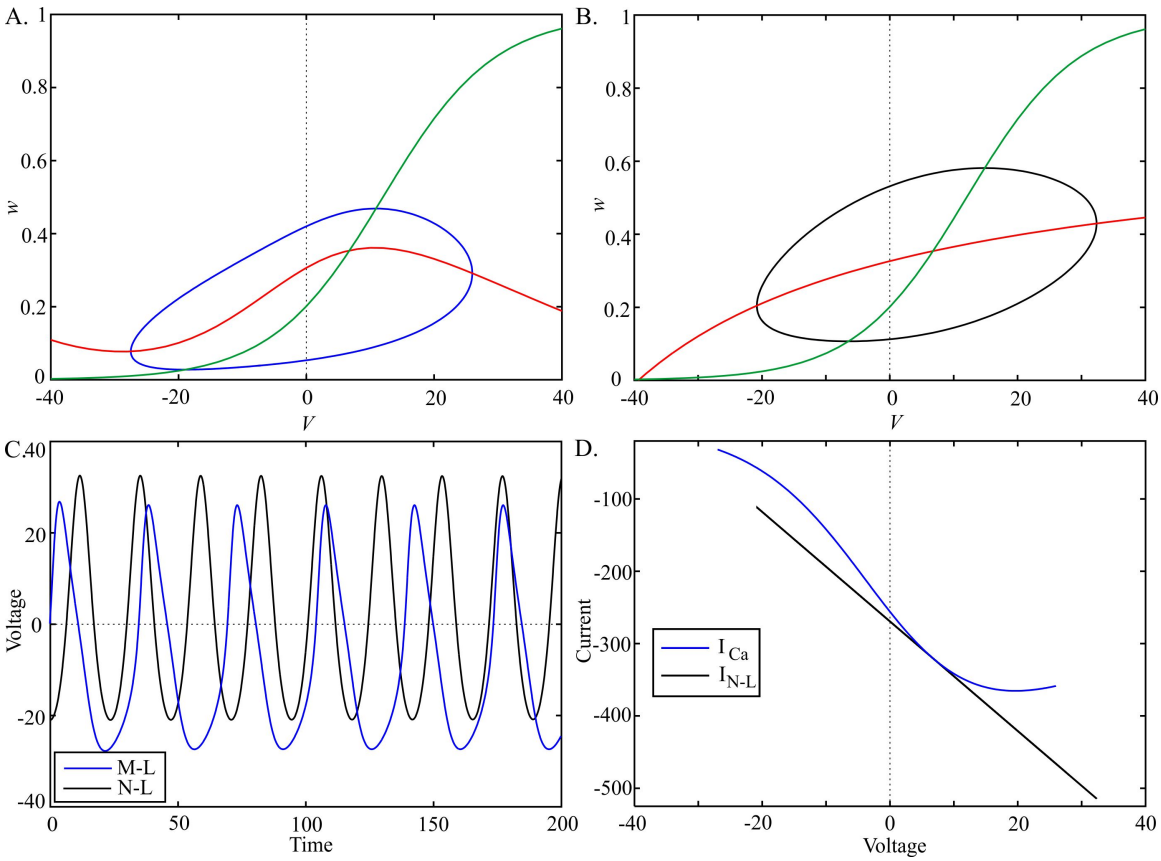

Figure 6.3 Oscillations obtained from N-L model (2.6) compared to M-L model (2.5).

by $N_{i,j}$. Then, we have

$$\begin{aligned}
M_{1,1} &= (-g_L - g_K w - g_{Ca}(m_\infty(V) + m'_\infty(V)(V - E_{Ca})))/c \\
N_{1,1} &= (-g_L - g_K w - g_{N-L})/c \\
M_{1,2} &= N_{1,2} = -g_K(V - E_K)/c \\
M_{2,1} &= N_{2,1} = \frac{w'_\infty(V)\tau(V) - \tau'(V)w_\infty(V)}{\tau^2(V)} \\
M_{2,2} &= N_{2,2} = \frac{-1}{\tau(V)}.
\end{aligned}$$

The entries are the same except for the first ones. For the characteristics of the fixed points to be the same, we need the two Jacobians to be equal. Therefore,

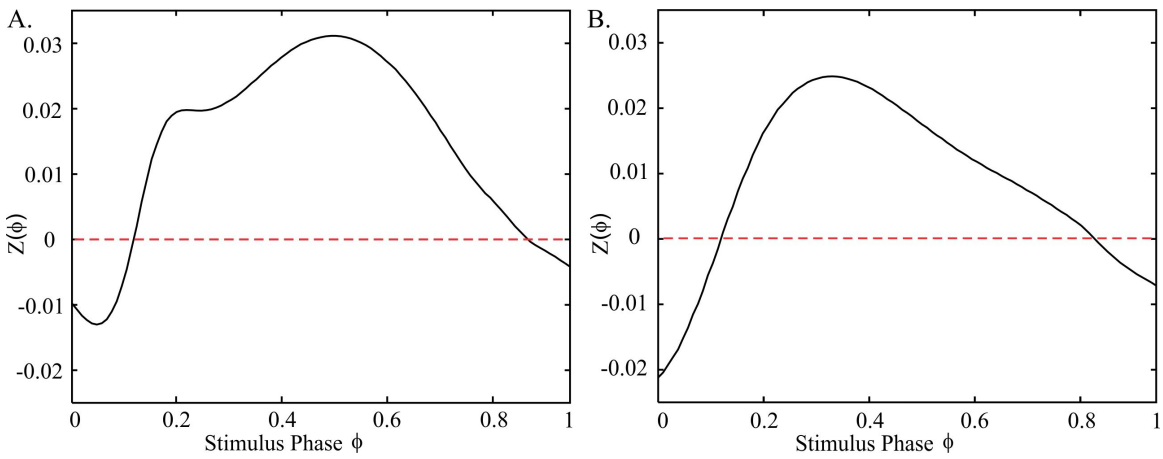

Figure 6.4 Comparison of the PRC obtained from N-L model (2.6) and M-L model (2.5) obtained from applying perturbation of same shape and amplitude. A. PRC of the N-L model. B. PRC of the M-L model.

setting $M_{1,1} = N_{1,1}$ and solving for g_{N-L} gives the second criterion as

$$g_{N-L} = g_{Ca}(m_\infty(V) + m'_\infty(V)(V - E_{Ca})). \tag{6.6}$$

This determines a unique g_{N-L} value since the parameters for the Ca^{2+} are already determined. Plugging into the parameters for I_{Ca} we get $g_{N-L} = -7.572$. We plug this value into the first criterion (6.5) to obtain the value of $E_{N-L} = -35.57$.

Numerically solving the N-L equations yields the same stable focus at (V_M, w_M). By decreasing back the value of ϕ for the M-L and N-L models, we obtain oscillations in both of the models. The period and the amplitude of the N-L oscillations heavily depend on the value of ϕ, while the oscillations of the M-L model are not affected much. We choose the value of 0.1312 for ϕ that yields oscillations from N-L model whose period and amplitude best match with those of the M-L oscillations. The oscillations obtained from the two models are shown in Figure 6.3.A. The approximation of I_{Ca} of the M-L model by I_{N-L} is shown in Figure 6.3.B. The nullclines and the stable limit cycle of the M-L and N-L models are shown in Figure 6.3.C and in Figure 6.3.D, respectively.

The comparison of the phase response curves of the M-L (2.5) and N-L (2.6) models with the above parameters is gives in Figure 6.4. The two models have PRCs qualitatively similar.

6.3 Effects of the h-current on N-L Model Neurons

We now consider the effects of the h-current on N-L model neurons. The N-L model with h-current is given by

$$\begin{aligned} \epsilon\frac{dV}{dt} &= (I_{app} - I_K - I_{N-L} - I_h)/C \\ \frac{dw}{dt} &= \frac{w_\infty(V) - w}{\tau_w(V)} \\ \frac{dh}{dt} &= \frac{h_\infty(V) - h}{\tau_h(V)} \end{aligned} \tag{6.7}$$

where $I_K = \bar{g}_K w(V - E_K)$, $I_{N-L} = \bar{g}_{N-L}(V - E_{N-L})\mathrm{H}(V - E_{N-L})$ and the h-current $I_h = \bar{g}_h h(V - E_h)$ are the ionic currents governing the membrane potential. We let the $N-L$ current be nonzero only for voltages above its reversal potential E_{N-L}, which is achieved by the Heaviside function $\mathrm{H}(x)$. The activation variable h has a steady-state curve which is in general a decreasing sigmoidal function of the membrane potential. For ease of computation, we will use a piecewise linear function instead, which is given by $h_\infty(V) = \min\left(\frac{V-V_U}{V_L-V_U}, 1\right)\mathrm{H}(V_U - V)$. The function h_∞ takes the value of one for voltages smaller than V_L and the value of zero for voltages greater than V_U. It changes from 1 to 0 linearly between these two voltages. The voltages V_L and V_U determine the slope of the middle piece of the function, which we denote by $h_{slope} = \frac{1}{V_L - V_U}$. They also determine the half-activation voltage $h_{mid} = \frac{V_U + V_L}{2}$. The function h_∞ can be rewritten in terms of these variables as $h_\infty(V) = \min\left(h_{slope}(V - h_{mid} + \frac{1}{2h_{slope}}), 1\right)\mathrm{H}(h_{mid} - \frac{1}{2h_{slope}} - V)$.

The steady-state function w_∞ is defined in the same way as in the M-L Equations (2.5). We let the time constants governing w dynamics be a step function given by

$$\tau_w(V) = \begin{cases} \tau_{w1}, & V < V_c \\ \tau_{w2}, & V > V_c, \end{cases} \tag{6.8}$$

where $V_c > E_{N-L}$. Finally, the time constant governing the h dynamics is

$$\tau_w(V) = \begin{cases} \tau_{h1}, & V < V_U \\ \tau_{h2}, & V > V_U. \end{cases} \tag{6.9}$$

The contribution of the h-current to the oscillations in N-L model has been studied in [5] to some extend. They assumed that the h-current depends on an instantaneous function V. Here, we assume that it depends on a dynamic variable h. There are parameter regimes that yield stable oscillations with the N-L model (2.6). However, these oscillations are not very robust to perturbations. Addition of the h-current increases the size of the basin of attraction of these periodic solutions. Also, in some parameter regimes, no oscillations are possible and only a stable fixed point exists without the h-current. Addition of the h-current is necessary to have stable oscillations. The phase planes for the models (2.6) and (6.7) are shown in Figure 6.5. When the model consists of the K and $N-L$ currents only, there exist a stable fixed point at $V = E_K$ (Figure 6.5). The addition of h-current moves the V-nullcline upwards and stable oscillations emerge (Figure 6.5). We now find conditions for the h-current that enables the oscillations to exist.

The V-nullcline ($\mathcal{N}_V$) is obtained by setting the first equation in (6.7) equal to zero. We define $f(V,w,h) \equiv -\bar{g}_K w(V-E_K) - \bar{g}_{N-L}H(V-E_{N-L})(V-E_{N-L}) - \bar{g}_h h(V-E_h)$. Then, $\mathcal{N}_V$ is given by the equation $f(V,w,h) = 0$. Similarly, the w-nullcline ($\mathcal{N}_w$) and the h-nullcline ($\mathcal{N}_h$) are given by $w = w_\infty(V)$ and $h = h_\infty(V)$, respectively. We define $g_h \equiv \bar{g}_h h$.

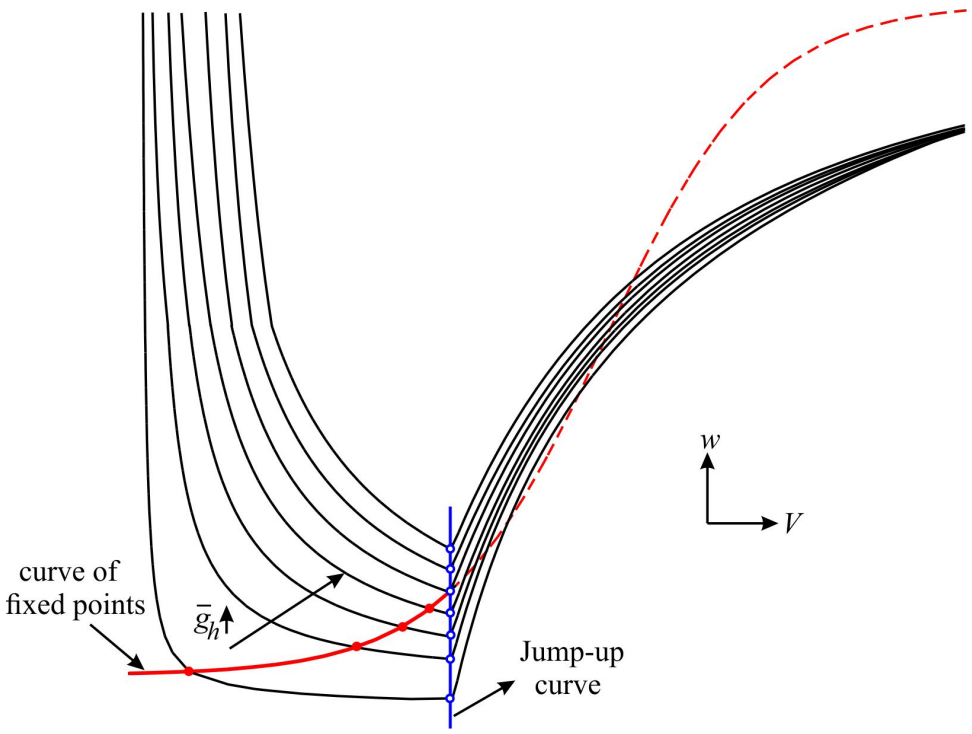

Figure 6.5 Phase plane for N-L model with h-current.

Consider first $g_h = 0$. In this case, since I_{N-L} is nonzero for voltages greater than E_{N-L}, the only contribution to the V-dynamics for $V < E_{N-L}$ is from I_K. So, the V-nullcline is given by $\bar{g}_K w(V - E_K) = 0$ for $V < E_{N-L}$. Therefore, $\mathcal{N}_V$ consists of the lines $w = 0$ and $V = E_K$. Then, $\mathcal{N}_V$ and $\mathcal{N}_w$ intersect at $(V, w) = (E_K, w_\infty(E_K))$ on the $V - w$ plane which creates a stable fixed point. Every trajectory approaches this fixed point. The V-nullcline starts taking positive values at $V = E_{N-L}$ due to the contribution of I_{N-L}. Since w_∞ is positive and close to 0 near E_{N-L}, the two nullclines intersect in a small neighborhood of E_{N-L} which creates an unstable fixed point to the right of E_{N-L}. Our aim is to find conditions on the h-current that will cause the two fixed points to vanish and enable the oscillations to exist when included in the model.

When the h-current is included, the V-nullcline is given by the equation $\bar{g}_K w(V - E_K) + g_h(V - E_h) = 0$ for $V < E_{N-L}$. Let $w_1(V, h)$ denote the value of w on $\mathcal{N}_V$. Then, solving the nullcline equation for w yields $w_1(V, h) = -\frac{g_h(V-E_h)}{\bar{g}_K(V-E_K)}$. The

conductances $\bar{g}_h$ and $\bar{g}_K$ are positive, h is a decreasing function and $E_K < V < E_{N-L}$, by assumption. Hence, w_1 is a decreasing function of V for $V < E_{N-L}$.

On the other hand, for $V > E_{N-L}$, the V-nullcline is given by $\bar{g}_K w(V - E_K) + g_h(V - E_h) + \bar{g}_{N-L}(V - E_{N-L}) = 0$. Solving for w gives that $w_1(V, h) = -\frac{g_h(V-E_h)}{\bar{g}_K(V-E_K)} - \frac{\bar{g}_{N-L}(V-E_{N-L})}{\bar{g}_K(V-E_K)}$ on $\mathcal{N}_V$. If $\bar{g}_h$ is not very large, w_1 is an increasing function of V for $V > E_{N-L}$. Hence, w_1 reaches a minimum when $V = E_{N-L}$.

Let $w_2(V)$ denote the value of w on $\mathcal{N}_w$. Then, $w_2(V) = w_\infty(V)$. Since $w_1(V)$ reaches a minimum at $V = E_{N-L}$, the nullclines $\mathcal{N}_V$ and $\mathcal{N}_w$ intersect if the value $w_1(E_{N-L})$ is smaller than or equal to the value $w_2(E_{N-L})$. Hence the condition for the fixed points to vanish and the oscillations to exist is given by

$$\bar{g}_h h_\infty(E_{N-L}) \geq \frac{g_K w_\infty(E_{N-L})(E_{N-L} - E_K)}{E_h - E_{N-L}}. \tag{6.10}$$

The right hand side of the inequality is positive. A necessary condition to be satisfied is that $h_\infty(E_{N-L}) > 0$. This implies that V_U must lie above E_{N-L}. The following proposition summarizes the conditions for the existence of oscillations.

Proposition 1. The relation that needs to be satisfied between the h and the $N - L$ currents for the existence of oscillations is given as follows:

- If $h_{mid} - \frac{1}{2h_{slope}} < E_{N-L}$, then there is a stable fixed point and no oscillations exist.
- If $h_{mid} + \frac{1}{2h_{slope}} < E_{N-L} < h_{mid} - \frac{1}{2h_{slope}}$, then oscillations exist if $\bar{g}_h \geq \frac{g_K w_\infty(E_{N-L})(E_{N-L}-E_K)}{(E_h-E_{N-L})h_{slope}(E_{N-L}-h_{mid}+1/2h_{slope})}$.
- If $h_{mid} + \frac{1}{2h_{slope}} > E_{N-L}$, then oscillations exist if $\bar{g}_h \geq \frac{g_K w_\infty(E_{N-L})(E_{N-L}-E_K)}{E_h-E_{N-L}}$.

We assume that the condition (6.10) for the existence of oscillations is satisfied and we analyze the dynamics of the oscillations. We make some assumptions for the

time constants governing the dynamics. For the w time constants, we assume that $\tau_{w1} = \mathcal{O}(1)$, while $\tau_{w2} = \mathcal{O}(\epsilon)$, where $\epsilon << 1$. We also assume that τ_{h1} and τ_{h2} are both $\mathcal{O}(1)$. These assumptions yield a singularly perturbed system where V is a fast variable and h is a slow variable. The dynamics of w are on the same order as h, for $V < V_c$, while they are on the same order as V for $V > V_c$. The singular perturbation parameter $\epsilon << 1$ being small will allow us to use techniques of geometric singular perturbation theory. Under these assumptions, Equations (6.7) take the form

$$\begin{aligned} \epsilon V' &= f(V, w, h) \\ \epsilon w' &= \epsilon \mathrm{H}(V_c - V)\frac{w_\infty - w}{\tau_{w1}} + \mathrm{H}(V - V_c)\frac{w_\infty - w}{\tau_{w2}} \\ h' &= \frac{h_\infty - h}{\tau_h(V)}. \end{aligned} \tag{6.11}$$

We now construct and analyze the singular solutions of the reduced equations which are appropriately scaled versions of (6.7) when $\epsilon = 0$. We first consider the system of equations for $V < V_c$. Restricting the equations (6.11) for $V < V_c$ and setting $\epsilon = 0$ gives the slow reduced equations as

$$\begin{aligned} 0 &= f(V, w, h) \\ w' &= \frac{w_\infty - w}{\tau_{w1}} \\ h' &= \frac{h_\infty - h}{\tau_h(V)}. \end{aligned} \tag{6.12}$$

The fast reduced equations for $V < V_c$ are obtained by rescaling time in (6.11) by letting $\tau = t/\epsilon$ and then setting $\epsilon = 0$. This yields

$$\begin{aligned} \dot{V} &= f(V, w, h) \\ \dot{w} &= 0 \\ \dot{h} &= 0. \end{aligned} \tag{6.13}$$

where $\dot{}$ denotes the derivatives with respect to τ. The first equation in (6.12) implies that when $V < V_c$, the singular solution is forced to lie on the V-nullcline $f(V, w, h) = 0$. So, when the neuron is not active, its dynamics are determined by the dynamics of the slow variables w and h. The fast equations (6.13) imply that while the voltage changes, the w and h variables stay constant.

Restricting the equations (6.11) for $V > V_c$ and setting $\epsilon = 0$ gives the slow reduced equations for $V > V_c$ as

$$\begin{aligned} 0 &= f(V, w, h) \\ 0 &= \frac{w_\infty - w}{\tau_{w1}} \\ h' &= \frac{h_\infty - h}{\tau_h(V)}. \end{aligned} \tag{6.14}$$

The fast reduced equations for $V > V_c$ are obtained by rescaling time in (6.11) by letting $\tau = t/\epsilon$ and then setting $\epsilon = 0$. This yields

$$\begin{aligned} \dot{V} &= f(V, w, h) \\ \dot{w} &= \frac{w_\infty - w}{\tau_{w1}} \\ \dot{h} &= 0. \end{aligned} \tag{6.15}$$

We denote the slow manifold determined by w and g_h for $V < V_c$ by $\mathcal{M}$. The fact that the solution lies on $\mathcal{N}_V$ and is determined by w and g_h enables us to use the equality $f(V, w, g_h) = 0$ to write V as a function of the slow variables. The neuron stays on the slow manifold until it reaches the minimum point of $\mathcal{N}_V$. From this point the cell leaves the slow manifold $\mathcal{M}$ and enters the active state. Since the minimum of $\mathcal{N}_V$ occurs at $V = E_{N-L}$, the cell jumps to the active phase at $V = E_{N-L}$. Hence, on the slow manifold, the membrane voltage is below E_{N-L}, therefore $I_{N-L} = 0$ and $\mathcal{N}_V$ is determined by I_K and I_h only. Therefore, solving the N_V equation for V yields

$$V = \frac{\bar{g}_K w E_K + g_h E_h}{\bar{g}_K w + g_h} := g(w, g_h). \tag{6.16}$$

When the membrane potential reaches E_{N-L} on $\mathcal{N}_V$, the neuron jumps to the active state and leaves the slow manifold. Therefore, the curve $g(w, g_h) = E_{N-L}$ determines the jump-up curve ($\mathcal{J}$). As g_h increases, the V-nullcline is shifted up in the $V - w$ phase plane (Figure 6.5), so the w value corresponding to the minimum of $\mathcal{N}_V$ increases. Hence, this curve has a positive slope and determines the border of $\mathcal{M}$ on the left (Figure 6.6).

Consider now the fixed points which exist when the condition (6.10) is not satisfied. We locate the stable fixed points on the slow manifold $\mathcal{M}$. When $g_h = 0$, the V-nullcline has a minimum at $(V = E_{N-L}, w = 0)$ on the $V - w$ phase plane. Therefore, the jump-up curve passes through the point $(0, 0)$ on the $w - g_h$ slow manifold. For this value of g_h, there exists a stable fixed point at $(E_K, w_\infty(E_K))$. Therefore, the fixed point when $g_h = 0$ passes through the point $(w_\infty(E_K), 0)$ on the slow manifold. As g_h increases, the contribution of the h-current moves the V-nullcline upwards. This causes the fixed points to have a larger w value with increasing g_h. So, the curve of fixed points ($\mathcal{F}$) has a positive slope. The fixed points no longer exist when the condition (6.10) is satisfied. At this point, the minimum of the V-nullcline which occurs at E_{N-L} just hits the w-nullcline. Therefore, the curves $\mathcal{F}$ and $\mathcal{J}$ intersect at the point $w_\infty(E_{N-L})$ and $\mathcal{F}$ does not exist for larger w values. The curve of fixed points $\mathcal{F}$ is the projection of $\mathcal{N}_w$ on $\mathcal{M}$ (red curve in Figure 6.5).

The flow on $\mathcal{M}$ is a function of w' and h' which are both functions of V. We have already located $\mathcal{N}_w$ on $\mathcal{M}$. Plugging the function (6.16) into the third equation of (6.12), we can locate $\mathcal{N}_h$ and determine the direction field on $\mathcal{M}$. Depending on the choice of h_{mid} and h_{slope}, $\mathcal{N}_h$ can divide $\mathcal{M}$ into regions where h' is either positive or negative. We now determine the location of $\mathcal{N}_h$ on $\mathcal{M}$. We first determine where $\mathcal{J}$ and $\mathcal{N}_h$ intersect. On the h-nullcline, the equation $h = h_\infty(V)$ is satisfied. On the jump-up curve, we have $V = E_{N-L}$. Hence, the value of h at the intersection of N_h and $\mathcal{J}$ is given by $h = h_\infty(E_{N-L})$. The value of w at this intersection can be found

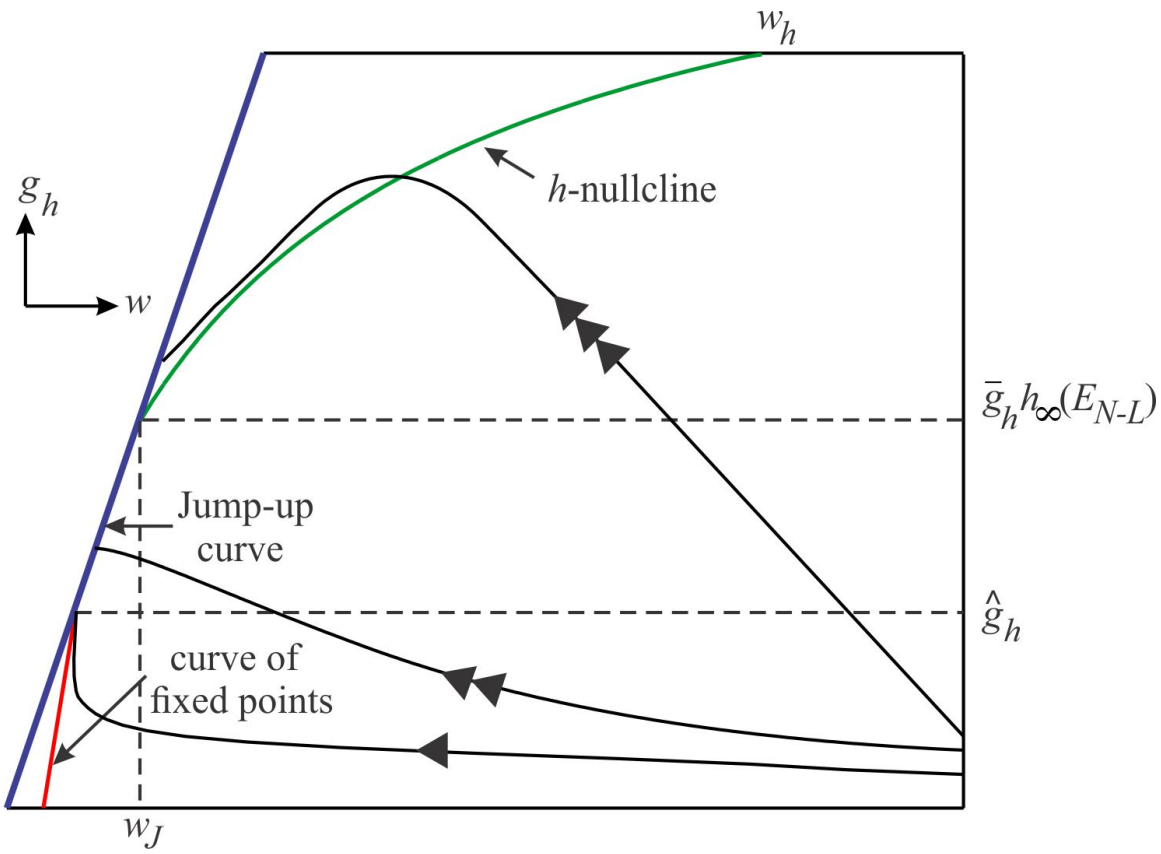

Figure 6.6 The jump-up curve, fixed point curve and h-nullcline on the slow manifold $\mathcal{M}$. The curve of fixed points is the projection of $\mathcal{N}_V$ on $\mathcal{M}$.

by solving the function $V = g(w, g_h)$ for w when $V = E_{N-L}$ and $g_h = \bar{g}_h h_\infty(E_{N-L})$. This gives the value of w as

$$w_J = \frac{-\bar{g}_h h_\infty(E_{N-L})(E_{N-L} - E_h)}{\bar{g}_K(E_K - E_{N-L})}.$$

Consider now the $h = 1$ line. The membrane potential V changes on this line as a function of w. If V is smaller than V_L on this line, then, $h_\infty = 1$. Then the equality $h = h_\infty(V)$ which defines $\mathcal{N}_h$ is satisfied. The function $h_\infty(V)$ equals 1 for $V \geq V_L$ and starts decreasing for larger voltages. Therefore, $h' = h_\infty - h = 0$ when $V \geq V_L$ on $h = 1$ and $\mathcal{N}_h$ hits the $h = 1$ line at $V = V_U$. The w value for this point can be found by using the function (6.16) as

$$w_h = \frac{g_h(V_L - E_h)}{\bar{g}_K(E_K - V_L)}.$$

The derivative of $\mathcal{N}_h$ can be evaluated using chain rule

$$\begin{aligned}\frac{dh}{dw} &= \frac{dh}{dV}\cdot\frac{dV}{dw} \\ &= h_{slope}\cdot\frac{\bar{g}_K E_K(\bar{g}_K w + g_h h) - \bar{g}_K(\bar{g}_K w E_K + g_h h E_h)}{(\bar{g}_K w + g_h h)^2} \\ &= h_{slope}\cdot\frac{\bar{g}_K g_h(E_K - E_h)}{(\bar{g}_K w + g_h)^2}.\end{aligned}$$

The denominator is always positive. The numerator is negative since $E_K < E_h$. So, $\mathcal{N}_h$ has a positive slope, since h_{slope} is also negative. These findings determine the location of $\mathcal{N}_h$ on the slow manifold $\mathcal{M}$.

The slow manifold $\mathcal{M}$ is shown in Figure 6.5. The trajectories enter $\mathcal{M}$ from the bottom right corner. They all reach the jump-up curve $\mathcal{J}$. The trajectories depend on the relation between the time constants governing the w and h dynamics. If $\tau_{w1} << \tau_{h1}$, then the trajectory goes horizontally, without much change in h until it reaches $\mathcal{N}_w$, from there on, it goes vertically until it reaches $\mathcal{J}$ and jumps to the active state (curve with one arrow). If $\tau_{w1} >> \tau_{h1}$, then the both w and h values increase until the trajectory reaches $\mathcal{N}_h$. The h value starts decreasing when it crosses $\mathcal{N}_h$ and reaches $\mathcal{J}$ above the point $(w_h, \bar{g}_h h_\infty(E_{N-L})$ (curve with three arrows). Finally, the trajectory would follow a path between these two cases if τ_{w1} and τ_{h1} are of the same order of magnitude (curve with two arrows).

CHAPTER 7

DISCUSSION

7.1 Conclusions and Discussion

In the analysis of an oscillatory network, the steady-state activity of the network can often be reduced to the study of a return map. The advantage of using maps is that it often allows the network dynamics to be understood by tracking empirical observable characteristics such as period and phase. Here, we derive such a map for a two-cell network coupled with inhibitory synapses with the goal of understanding how short-term synaptic plasticity and other factors determine the network period and the relative activity phase of the two neurons. Our results show that the information on the network period and phase can be obtained using maps that keep track of readily observable network variables such as the intrinsic periods of the neurons involved, their phase response curves and the synaptic plasticity profiles: relationships describing how synaptic strength depends on input frequency. These variables can be readily determined experimentally with "feed-forward" measurements where the input is controlled by the experimenter and the output is measured. For example, the strength of a synapse can be measured at all frequencies simply by driving the presynaptic neuron at different rates and measuring the postsynaptic current. In fact, the current study was motivated by our experimental measurements of these types of network variables in the crab stomatogastric pyloric network [55, 56, 82].

There are several prior works that utilize PRCs and map based techniques to understand phase locking [2, 14, 17, 20, 36, 45, 58, 61, 63, 65, 72, 85, 88]. Of particular interest is the result of Cui et al. [14] who use a functional PRC (fPRC) that is calculated from actual experimental measurements of Aplysia pacemaker neurons. Cui et al. show that the fPRC differs from the single pulse PRC (as was used in this

paper) due to accommodation of the pacemaker neurons. They then go on to use the fPRC to study phase-locking in a coupled network by deriving a map that encodes how a neuron responds to a period input that arrives a fixed time after the firing of the cell. By linearizing about a fixed point of their 1D map, they find conditions for the existence and stability of 1:1 phase-locked solutions. Their predictions from the fPRC method are better matched to simulations than predictions from a conventional single-pulse PRC. Importantly, their fPRC methods do not depend on the exact shape of the PRC but rather on the effect on the cycle period based on the time the input was given. This is a statistic that is easily found in experiments. Moreover, their results are obtained from combing feed-forward processes as opposed to directly studying a feed-back map, what they call open-looped versus closed-looped.

Our results complement those of Cui et al. in the sense that we relate cycle to cycle changes in the period independent of how those changes arise, allowing us to also use experimentally obtainable information to derive the maps. Our maps are also based on assumptions that are consistent with Cui et al.'s assumption that the closed-loop behavior of a system can be predicted by knowing the open-looped behavior of some of its components. Our results extend those of Cui et al. and other prior works in that we allow the timing of inputs to vary on a cycle by cycle basis that is determined by the synaptic plasticity profile of the pre-synaptic neuron. This results in a higher dimensional map arising by specifically considering the dynamics of synaptic facilitation and depression on a cycle by cycle basis. This yields a 3D map when plasticity is present only in one direction of the two-cell network, or a 5D map if present in both directions. When we used the steady-state synaptic plasticity profile, both cases reduce to a 2D map. For this 2D map, we derived a geometric method that generalizes cobwebbing in a 1D map to allow us to study the existence and stability of fixed points. For a generic 1D map, $\Pi(x)$, the intersection of the curve $y = \Pi(x)$ with the curve $y = x$, and the slope at that point, determine existence and

stability of the fixed point. In our generalized 2D case, given maps $\Pi_1(x, y)$ and $\Pi_2(x, y)$, it is the intersection of these surfaces with appropriate planes that yield two curves. It is the intersection of the projection of these two curves onto a common plane that determines existence of the fixed point. Stability is more complicated than just checking the slopes at the point of intersection. We showed how it could depend on both the PRC and the synaptic plasticity profile.

In this study, we considered a general form of short-term synaptic plasticity which is a combination of short-term facilitation and depression. We modeled such a synapse using an ad hoc model as described previously [48]. The advantage of this model is that the extent to which facilitation or depression is a dominant factor can be simply determined by changing the model parameters. Our analysis progressed through a network of two neurons with static synapses, the same network but with one synapse having plasticity and finally with both synapses showing plasticity. The analysis of a two-cell network with static synapses yields a 1D map [17, 36]. Including synaptic plasticity increases the dimension of the map because variables underlying synaptic dynamics must be tracked as well. The change in synaptic strength due to the plasticity means that the PRCs of the neurons also change. Our analysis shows that these higher-dimensional maps can accurately predict the steady state phase and period of the network, as seen in comparisons with numerical simulations of the underlying ODEs.

In experimental measurements, synaptic plasticity profiles are often measured using repetitive input pulses or waveforms and reported at steady state, i.e., the steady-state strength of the synapse is known for each stimulation frequency [24, 25, 82]. In most cases, the mechanisms that underlie these synaptic dynamics are unknown and it is therefore impossible to track how synaptic strength changes as a function of frequency on a cycle-to-cycle basis. One of the interesting findings from our work is that the prediction of the higher-dimensional map obtained when using

dynamics of the synapse is the same as a lower-dimensional map that uses only the steady-state plasticity profile. In other words, the network output is dependent on the steady-state strength independent of the mechanisms through which this synaptic strength is actually generated. In turn, this allows an experimentalist to understand the effects of, say a synaptic neuromodulator, on the network output simply by understanding the effect on a single component such as the synaptic plasticity profile.

The results of our maps help us understand the role of synaptic dynamics in determining the relative phase between two neurons in an oscillatory network. For example, neurons in the crustacean pyloric oscillatory network, involve multiple reciprocally inhibitory connections. Pyloric oscillations are quite stable in individual preparations and are generated by a pacemaker group of neurons (AB/PD) which make reciprocally inhibitory connections with a single follower neuron, LP. The analysis of this reciprocally inhibitory network provided the motivation for the current study. As in other rhythmic motor networks, the pyloric network neurons maintain a constant phase relationship even when these phases are measured in different animals [8]. Surprisingly this tight phase relationship is maintained despite a large variability in the pyloric cycle period (1-2.5 s) across preparations. In fact, different preparations differ both in the intrinsic periods of the neurons involved as well as the synaptic plasticity profiles. The results of the current study indicate that the pyloric network could maintain constant phase relationships, even in different animals, by tuning the synaptic plasticity profiles along the level sets of phase (Figure 4.4). Alternatively, if the relative activity phases of the neurons involved in producing the network oscillations are not an essential component of the network output, but the network must maintain a constant period, the maps we have derived can be used to establish the relationships that could produce a constant frequency output. These are plausible strategies for all rhythmic motor networks in which the output is tightly constrained by the proper phase of muscle movements to produce meaningful behavior.

An interesting implication of our results is that if the network period coincides with the synaptic preferred periods, it is not possible to uniquely prescribe the synaptic profiles in terms of the network period and the relative phase of the neurons (Equation 4.6). If the level sets of phase, described in Figure 4.4, provide a unique rule for the network to tune its synaptic plasticity profiles for phase maintenance, then the network period should avoid the synaptic preferred periods. Additionally, by avoiding the periods at which the synaptic strengths are maximal, the network can operate with a larger degree of flexibility and perhaps more efficiently. This is in fact the case for the synapses between the AB/PD pacemaker neurons and the follower LP neuron in the crustacean pyloric network. The network period is around 1-2.5 s, in a range of values that is larger than the preferred periods of the synapses (~ 0.5 Hz) [82]. Hence, our findings give an insight for this experimentally observed fact.

We have shown using Poincaré map approach that bistability can occur in networks of neurons having depressing synapses in Chapter 5. The depression is strong enough to yield bistability in the examples we show. However, we do not observe bistability in Chapters 3 and 4, where we use Morris-Lecar model neurons and a plasticity model different than in Chapter 5. In these cases, the plasticity alters the phase and period relationships of the neurons but is not strong enough to cause bistability. Since the PRCs of the M-L and QIF models we use are qualitatively the same, it could be possible to observe bistability in M-L neurons if stronger plasticity dynamics are assumed.

We have generalized the map for the network activity for neurons that have changing burst durations. An equivalent map based on PRCs and BRCs is derived in [62] and conditions for stability are analyzed. However, the effects of the BRC are ignored in the analysis. We show with an example that our map yields results consistent with simulations when both PRC and BRC effects are included.

We have studied how a regenerative inward current can be replaced with a $N-L$ current in M-L neurons. We have shown that the oscillations and the PRCs obtained from the two models are qualitatively similar. We have also studied the contribution of the h-current in obtaining oscillations and derived necessary conditions in the N-L model.

In conclusion, we have shown that the frequency-dependent information on synapses can be combined with the PRCs of oscillatory neurons to predict the activity period and phases of a coupled network using maps derived from empirically observable relationships.

7.2 Future Work

The Poincaré map methods we derived for predicting the network activity can be extended to include heterogeneity. Although we studied coupling of non-identical neurons to some extend, the heterogeneity was limited. Networks of an oscillatory and a non-oscillatory neuron can be studied with this approach.

In our map derivations, we assumed that the neurons have first order PRCs. In other words, we assumed that a perturbation received at on oscillatory cycle of a neuron has an effect only on that current cycle. This assumption can be relaxed to include possible effects of a perturbation to consequtive oscillatory cycles and to define maps that make use of second or third order PRCs.

Real neuronal systems include noise in their electrical activity. It is possible to study robustness of neuronal networks to noise by using these Poincaré map methods. In this case, we need to use stochastic functions for the PRCs of the neurons and the short-term plasticity functions of the synapses.

These methods can be applied to a real biological network, such as the pyloric network, to predict its activity. For example, a map for the activity of the simplified network consisting of the PD and LP neurons can be derived. Due to

the heterogeneities in cellular and synaptic properties, these neurons do not fire in anti-phase relation. The burst durations of these cells and the time delay between their bursts change with the network frequency [34]. A feedback map derived using our methods can be used to predict the phase relationships among these neurons.

The pyloric network is subject to extensive neuromodulation. The effects of six different neuromodulators on the membrane properties of the pyloric neurons [76] and the network output [77] were analyzed. It was shown that all of these modulators activated the same voltage dependent current while different subsets of cells were targeted by each of the substances, causing a different network response each time. The strength and the short-term dynamics of the synapses in the pyloric network were shown to be altered by neuromodulators such as dopamine, octopamine, serotonin [38] and proctolin [90]. Although the effects of the neuromodulators on the network components were mostly identified, their role on the network output is complicated and hard to predict. The feedback map derived for the pyloric network activity, can be used to understand how experimentally observable effects of modulation on synaptic and cellular properties change the network output. Hence, the effects of cell properties and synaptic dynamics that change with neuromodulatory effects on phase maintenance can be analyzed.

To derive such a map, the experimental data obtained in Nadim Lab. for the synaptic properties from LP to PD and from PD to LP can be used. These data correspond to the steady-state values of the synaptic properties. The parameters in the equations of the synaptic plasticity variables r and u can be fit using an optimization technique and comparing the synaptic output to data.

Biophysical models for PD and LP [47, 63, 72] can be used to obtain the PRCs of these two cells numerically. The PD neuron is an intrinsic oscillator. Its PRC can be obtained by giving perturbations that imitate synaptic inputs with changing strength and peak phase. As the LP neuron is not an intrinsic oscillator, the method

given in [7, 19] for obtaining PRCs of non-oscillatory neurons can be used. This is done by first giving a perturbation to the neuron which causes it to start bursting. Then several further perturbations are given at the same phase in successive cycles. The responses of the cell are averaged to obtain the steady-state response which is called the functional phase response curve (fPRC). The PRCs of the PD and LP neurons obtained from experiments can also be used.

Other properties, such as the dependence of the synaptic peak time on firing frequency can also be taken into account. However, as more properties are included in the map, the dimension of the map increases. As explained in Chapter 4, if the dynamics of the depression and facilitation variables in the reciprocal synapses are to be included, a 5D map would be needed. Using the steady-state profiles would simplify it to a 2D map. In addition to the plasticity, if the changes in the time course of the synapse are also considered, this would increase the dimension of the map by at least one dimension. Also, the PRC used in such a map would depend on three variables, the phase, strength and the time course of the synaptic perturbation received.

The information for the PRC of the cells, either obtained from experimental data or from biophysical models, and the dynamics of the synaptic properties obtained experimentally can be incorporated in a Poincaré map, to predict the steady-state activity of the network. The existence and stability of the fixed points of these maps can be analyzed. The results can be compared with the phase locked solutions of the real biological system.

This tool allows one to check various properties of the network which are hard or impossible to test experimentally. For example, the response of the PD neuron for synaptic inputs with changing peak phases and the dependence of synaptic peak phase on the LP firing frequency can be obtained experimentally, but it is hard (or not possible) to test their consequences in the feedback network, when they are coupled.

By manipulating the model parameters and comparing the results of the map for these parameters, it is possible to understand their roles in the phase locking of the feedback network.

This model can be used to understand the effects of neuromodulation on the activity of neuronal networks. For example, the effects of the neuromodulators such as proctolin or dopamine on the synaptic strength of the LP to PD synapses have been identified [58, 59]. This information can be used in the feedback map to analyze the effects of these neuromodulators on the network frequency and phasic relationships. The map derived for a two cell network can be generalized for a three cell network enabling a more involved analysis of the maintenance of the tri-phasic pyloric rhythm.

The map derived in Chapter 6 for the neurons whose burst duration is not fixed yields accurate results for synapses with fast rise and decay. However, to study the network activity when synapses have slow rise and decay, other methods are needed. Geometric singular perturbation techniques can be used to define a Poincaré map to show the existence and stability of the modes in such networks.

BIBLIOGRAPHY

[1] L. F. Abbott and W. G. Regehr. Synaptic computation. *Nature*, 431(7010):796-803, 2004.

[2] S. Achuthan and C. C. Canavier. Phase-resetting curves determine synchronization, phase locking, and clustering in networks of neural oscillators. *The Journal of Neuroscience*, 29(16):5218-33, 2009.

[3] C. Ambrosio-Mouser, F. Nadim, and A. Bose. The effects of varying the timing of inputs on a neural oscillator. *SIAM Journal of Applied Dynamical Systems*, 5(1):108-139, 2006.

[4] J. T. Birmingham and D. L. Tauck. Neuromodulation in invertebrate sensory systems: from biophysics to behavior. *Journal of Experimental Biology*, 206:3541-6, 2003.

[5] A. Bose, J. Golowasch, Y. Guan, and F. Nadim. Role of linear and voltage-dependent ionic currents in the generation of slow wave oscillations. *Journal of Computational Neuroscience*, in press.

[6] A. Bose, Y. Manor, and F. Nadim. Bistable oscillations arising from synaptic depression. *SIAM Journal of Applied Mathematics*, 62(2):706-27, 2001.

[7] A. Bose, Y. Manor, and F. Nadim. The activity phase of postsynaptic neurons in a simplified rhythmic network. *Journal of Computational Neuroscience*, 17(2):245-61, 2004.

[8] D. Bucher, A. A. Prinz, and E. Marder. Animal-to-animal variability in motor pattern production in adults and during growth. *The Journal of Neuroscience*, 25(7):1611-9, 2005.

[9] C. C. Canavier and S. Achuthan. Pulse coupled oscillators and the phase resetting curve. *Mathematical Biosciences*, 226(2):77-96, 2010.

[10] C. C. Canavier, D. A. Baxter, J. W. Clark, and J. H. Byrne. Control of multistability in ring circuits of oscillators. *Biological Cybernetics*, 80(2):87-102, 1999.

[11] C. C. Canavier, R. J. Butera, R. O. Dror, D. A. Baxter, J. W. Clark, and J. H. Byrne. Phase response characteristics of model neurons determine which patterns are expressed in a ring circuit model of gait generation. *Biological Cybernetics*, 77(6):367-80, 1997.

[12] C. C. Canavier, F. G. Kazanci, and A. A. Prinz. Phase resetting curves allow for simple and accurate prediction of robust n:1 phase locking for strongly coupled neural oscillators. *Biophysical Journal*, 97(1):59-73, 2009.

[13] K. P. Carlin, K. E. Jones, Z. Jiang, L. M. Jordan, and R. M. Brownstone. Dendritic l- type calcium currents in mouse spinal motoneurons: Implications for bistability. *European Journal of Neuroscience*, 12:1635-1646, 2000.

[14] J. Cui, C. C. Canavier, and R. J. Butera. Functional phase response curves: a method for understanding synchronization of adapting neurons. *Journal of Neurophysiology*, 102(1):387-98, 2009.

[15] G. Cymbalyuk and A. Shilnikov. Coexistence of tonic spiking oscillations in a leech neuron model. *Journal of Computational Neuroscience*, 18:255263, 2005.

[16] P. S. Dickinson. Neuromodulation of central pattern generators in invertebrates and vertebrates. *Current Opinion in Neurobiology*, 16(6):604-14, 2006.

[17] R. O. Dror, C. C. Canavier, R. J. Butera, J. W. Clark, and J. H. Byrne. A mathematical criterion based on phase response curves for stability in a ring of coupled oscillators. *Biological Cybernetics*, 80(1):11-23, 1999.

[18] J. D. Drover, V. Tohidi, A. Bose, and F. Nadim. Combining synaptic and cellular resonance in a feed-forward neuronal network. *Neurocomputing*, 70(10-12):2041-5, 2007.

[19] K. E. Eastman and H. S. Hock. Bistability in the perception of motion and stationarity: Effects of temporal asymmetry. *Perception & Psychophysics*, 61(6):1055-65, 1999.

[20] G. B. Ermentrout. n:m phase-locking of weakly coupled oscillators. *Journal of Mathematical Biology*, 12:327-42, 1981.

[21] G. B. Ermentrout. Multiple pulse interactions and averaging in systems of coupled neural oscillators. *Journal of Mathematical Biology*, 29:195-217, 1991.

[22] G. B. Ermentrout. Type i membranes, phase resetting curves, and synchrony. *Neural Computation*, 8(5):979-1001, 1996.

[23] G. B. Ermentrout and D. H. Terman. *Mathematical Foundations of Neuroscience.* New York, NY: Springer, 2010.

[24] L. Feng, P. Molnar, and J. V. Nadler. Short-term frequency-dependent plasticity at recurrent mossy fiber synapses of the epileptic brain. *The Journal of Neuroscience*, 23(12):5381-90, 2003.

[25] E. S. Fortune and G. J. Rose. Short-term synaptic plasticity contributes to the temporal filtering of electrosensory information. *The Journal of Neuroscience*, 20(18):7122-30, 2000.

[26] T. Gisiger and M. Boukadoum. Mechanisms gating the flow of information in the cortex: what they might look like and what their uses may be. *Frontiers in Computational Neuroscience*, 5:1-15, 2011.

[27] P. Goel and B. Ermentrout. Synchrony, stability, and firing patterns in pulse-coupled oscillators. *Physica D*, 163:191-216, 2002.

[28] M. S. Goldman, P. Maldonado, and Abbott L. F. Redundancy reduction and sustained firing with stochastic depressing synapses. *The Journal of Neuroscience*, 22(2):584-91, 2002.

[29] D. Golomb and G. B. Ermentrout. Bistability in pulse propagation in networks of excitatory and inhibitory populations. *Physical Review Letters*, 86(18):4179-4182, 2001.

[30] A. A. Grace. Gating of information flow within the limbic system and the pathophysiology of schizophrenia. *The Journal of Neuroscience*, 31:330-341, 2000.

[31] P. J. Hahn and D. M. Durand. Bistability dynamics in simulations of neural activity in high-extracellular-potassium conditions. *Journal of Computational Neuroscience*, 11(1):5-18, 2001.

[32] R. M. Harris-Warrick. Neuromodulation and flexibility in central pattern generator networks. *Current Opinion in Neurobiology*, 21(5):685-92, 2011.

[33] A. L. Hodgkin and A. F. Huxley. A quantitative description of membrane current and its application to conduction and excitation in nerve. *Journal of Physiology*, 117(4):500-44, 1952.

[34] S. L. Hooper. Phase maintenance in the pyloric pattern of the lobster (panulirus interruptus) stomatogastric ganglion. *Journal of Computational Neuroscience*, 4(3):191-205, 1997.

[35] J. Hounsgaard, H. Hultborn, B. Jespersen, and O. Kiehn. Bistability of α-motoneurons in the decerebrate cat and in the acute spinal cat after intravenous 5-hydroxytryptophan. *Journal of Physiology*, 405:345-367, 1988.

[36] X. Huang. *Using Feed-Forward Networks to Infer the Activity of Feedback Neuronal Networks.* PhD thesis, New Jersey Institute of Technology, 2011.

[37] E. M. Izhikevich, N. S. Desai, E. C. Walcott, and F. C. Hoppensteadt. Bursts as a unit of neural information: selective communication via resonance. *Trends in Neurosciences*, 26(3):161-7, 2003.

[38] B. R. Johnson, J. M. Brown, M. D. Kvarta, J. Y. Lu, L. R. Schneider, F Nadim, and R. M. Harris-Warrick. Differential modulation of synaptic strength and timing regulate synaptic efficacy in a motor network. *Journal of Neurophysiology*, 105(1):293-304, 2011.

[39] T. B. Kepler, E. Marder, and L. F. Abbott. The effect of electrical coupling on the frequency of model neuronal oscillators. *Science*, 248(4951):83-5, 1990.

[40] I. Kupfermann. Modulatory actions of neurotransmitters. *Annual Review Neuroscience*, 2:447-65, 1979.

[41] Y. A. Kuznetsov. *Elements of Applied Bifurcation Theory.* New York, NY: Springer-Verlag, 2004.

[42] A. Mamiya and F. Nadim. Dynamic interaction of oscillatory neurons coupled with reciprocally inhibitory synapses acts to stabilize the rhythm period. *The Journal of Neuroscience*, 24(22):5140-50, 2004.

[43] Y. Manor, A. Bose, V. Booth, and F. Nadim. Contribution of synaptic depression to phase maintenance in a model rhythmic network. *Journal of Neurophysiology*, 90(5):3513-28, 2003.

[44] Y. Manor and F. Nadim. Synaptic depression mediates bistability in neuronal networks with recurrent inhibitory connectivity. *The Journal of Neuroscience*, 21(23):946070, 2001.

[45] C. C. Maran, S. K. Canavier. Using phase resetting to predict 1:1 and 2:2 locking in two neuron networks in which firing order is not always preserved. *Journal of Computational Neuroscience*, 24(1):37-55, 2008.

[46] E. Marder and D. Bucher. Understanding circuit dynamics using the stomatogastric nervous system of lobsters and crabs. *Annual Review of Physiology*, 69:291-316, 2007.

[47] E. Marder and R. L. Calabrese. Principles of rhythmic motor pattern generation. *Physiological Reviews*, 76(3):687-717, 1996.

[48] H. Markram, Y. Wang, and M. Tsodyks. Differential signaling via the same axon of neocortical pyramidal neurons. *Proceedings of the National Academy of Sciences of the United States of America*, 95(9):5323-8, 1998.

[49] D. McCormick and H. C. Pape. Noradrenergic and serotonergic modulation of a hyperpolarization-activated cation current in thalamic relay neurones. *Journal of Physiology*, 431:319-42, 1990.

[50] D. McCormick and H. C. Pape. Properties of a hyperpolarization-activated cation current and its role in rhythmic oscillation in thalamic relay neurones. *Journal of Physiology*, 431:291-318, 1990.

[51] J. D. Meiss. *Differential Dynamical Systems.* Philadelphia, PA: SIAM, 2007.

[52] E. B. Merriam, T. I. Netoff, and M. I. Banks. Bistable network behavior of layer i interneurons in auditory cortex. *The Journal of Neuroscience*, 25(26):6175 86, 2005.

[53] C. Morris and H. Lecar. Voltage oscillations in the barnacle giant muscle fiber. *Biophysical Journal*, 35(1):193-213, 1981.

[54] C. Mouser, F. Nadim, and A. Bose. Maintaining phase of the crustacean tri-phasic pyloric rhythm. *Journal of Mathematical Biology*, 57(2):161-81, 2008.

[55] F. Nadim, S. Zhao, and A. Bose. A prc description of how inhibitory feedback promotes oscillation stability. In *Phase Response Curves in Neuroscience*. Springer, 2012.

[56] F. Nadim, S. Zhao, L. Zhou, and A. Bose. Inhibitory feedback promotes stability in an oscillatory network. *Journal of Neuroengineering*, 8(6), 2011.

[57] N. Nadim, Y. Manor, N. Kopell, and E. Marder. Synaptic depression creates a switch that controls the frequency of an oscillatory circuit. *Proceedings of the National Academy of Sciences*, 96(14):8206-11, 1999.

[58] T. I. Netoff, M. I. Banks, A. D. Dorval, C. D. Acker, J. S. Haas, N. Kopell, and J. A. White. Synchronization in hybrid neuronal networks of the hippocampal formation. *Journal of Neurophysiology*, 93(3):1197-208, 2005.

[59] M. P. Nusbaum and M. P. Beenhakker. A small-systems approach to motor pattern generation. *Nature*, 417(6886):343-50, 2002.

[60] M. Oh and V. Matveev. Loss of phase-locking in non-weakly coupled inhibitory networks of type-i model neurons. *Journal of Computational Neuroscience*, 26(2):303-20, 2009.

[61] S. A. Oprisan. Existence and stability criteria for phase-locked modes in ring neural networks based on the spike time resetting curve method. *Journal of Theoretical Biology*, 262(2):232-44, 2010.

[62] S. A. Oprisan and C. C. Canavier. Stability criterion for a two-neuron reciprocally coupled network based on the phase and burst resetting curves. *Neurocomputing*, 65-66:733-9, 2005.

[63] S. A. Oprisan, A. A. Prinz, and C. C. Canavier. Phase resetting and phase locking in hybrid circuits of one model and one biological neuron. *Biophysical Journal*, 87(4):2283-98, 2004.

[64] H-C. Pape. Queer current and pacemaker: The hyperpolarization-activated cation current in neurons. *Annual Review of Physiology*, 58:299326, 1996.

[65] D. D. Pervouchine, T. I. Netoff, H. G. Rotstein, J. A. White, M. O. Cunningham, M. A. Whittington, and N. J. Kopell. Low-dimensional maps encoding dynamics in entorhinal cortex and hippocampus. *Neural Computation*, 18(11):2617-50, 2006.

[66] A. A. Prinz, V. Thirumalai, and E. Marder. The functional consequences of changes in the strength and duration of synaptic inputs to oscillatory neurons. *The Journal of Neuroscience*, 23(3):943-54, 2003.

[67] P. Rabbah and F. Nadim. Synaptic dynamics do not determine proper phase of activity in a central pattern generator. *The Journal of Neuroscience*, 25(49):11269-78, 2005.

[68] H. G. Rotstein, D. D. Pervouchine, C. D. Acker, M. J. Gillies, J. A. White, E. H. Buhl, M. A. Whittington, and N Kopell. Slow and fast inhibition and an h-current interact to create a theta rhythm in a model of ca1 interneuron network. *Journal of Neurophysiology*, 94(2):1509-18, 2005.

[69] J. Rubin and D. Terman. Geometric analysis of population rhythms in synaptically coupled neuronal networks. *Neural Computation*, 12(3):597-645, 2000.

[70] M. A. Schwemmer and T. J. Lewis. The theory of weakly coupled oscillators. In *Phase Response Curves in Neuroscience: Theory, Experiment, and Analysis*. Springer, 2012.

[71] A. Shilnikov, R. L. Calabrese, and G. Cymbalyuk. Mechanism of bistability: Tonic spiking and bursting in a neuron model. *Physical Review E*, 71(5):1539-3755, 2005.

[72] F. H. Sieling, S. Archila, R. Hooper, C. C. Canavier, and A.A. Prinz. Phase response theory extended to nonoscillatory network components. *Physical Review E*, 85:056208, 2012.

[73] F. H. Sieling, C. C. Canavier, and A. A. Prinz. Predictions of phase-locking in excitatory hybrid networks: excitation does not promote phase-locking in pattern-generating networks as reliably as inhibition. *Journal of Neurophysiology*, 102(1):69-84, 2009.

[74] F. K. Skinner, N. Kopell, and E. Marder. Mechanisms for oscillation and frequency control in reciprocally inhibitory model neural networks. *Journal of Computional Neuroscience*, 1(1-2):69-87, 1994.

[75] C. Soto-Trevino, P. Rabbah, E. Marder, and F. Nadim. Computational model of electrically coupled, intrinsically distinct pacemaker neurons. *Journal of Neurophysiology*, 94(1):590-604, 2005.

[76] A. M. Swensen and E. Marder. Multiple peptides converge to activate the same voltage- dependent current in a central pattern-generating circuit. *The Journal of Neuroscience*, 20(18):6752-9, 2000.

[77] A. M. Swensen and E. Marder. Modulators with convergent cellular actions elicit distinct circuit outputs. *The Journal of Neuroscience*, 21(11):4050-8, 2001.

[78] J. Tabak, W Senn, M. J O'Donovan, and J. Rinzel. Modeling of spontaneous activity in developing spinal cord using activity-dependent depression in an excitatory network. *The Journal of Neuroscience*, 20(8):304156, 2001.

[79] A. L. Taylor, J. M. Goaillard, and E. Marder. How multiple conductances determine electrophysiological properties in a multicompartment model. *The Journal of Neuroscience*, 29(17):5573- 86, 2009.

[80] D. Terman, N. Kopell, and A. Bose. Dynamics of two mutually coupled slow inhibitory neurons. *Physica D*, 117:241-75, 1998.

[81] B. Torben-Nielsen, M. Uusisaari, and K. M. Stiefel. A comparison of methods to determine neuronal phase-response curves. *Frontiers in Neuroinformatics*, 4:6, 2010.

[82] H. A. Tseng and F. Nadim. The frequency-dependent response of synapse in an oscillatory network. *Society for Neuroscience Annual Meeting*, 36:489.12, 2010.

[83] G. G. Turrigiano, E. Marder, and L. F. Abbott. Cellular short-term memory from a slow potassium conductance. *Journal of Neurophysiology*, 75(2):963-6, 1996.

[84] G. G. Vetter, J. D. Haynes, and S. Pfaff. Evidence for multistability in the visual perception of pigeons. *Vision Research*, 40:2177-86, 2000.

[85] S. Wang, L. Chandrasekaran, F. R. Fernandez, J. A. White, and C. C. Canavier. Short conduction delays cause inhibition rather than excitation to favor synchrony in hybrid neuronal networks of the entorhinal cortex. *PLoS Computational Biology*, 8(1):e1002306, 2012.

[86] X-J. Wang and J. Rinzel. Alternating and synchronous rhythms in reciprocally inhibitory model neurons. *Neural Computation*, 4:84-97, 1992.

[87] A. T. Winfree. *The Geometry of Biological Time.* New York, NY: Springer-Verlag, 1981.

[88] M. M. Woodman and C. C. Canavier. Effects of conduction delays on the existence and stability of one to one phase locking between two pulse-coupled oscillators. *Journal of Computational Neuroscience*, 31(2):401-18, 2011.

[89] S. Zhao, J. Golowasch, and F. Nadim. Pacemaker neuron and network oscillations depend on a neuromodulator-regulated linear current. *Frontiers in Behavioral Neuroscience*, 4(21):1-8, 2010.

[90] S. Zhao, A. F. Sheibanie, M. Oh, P. Rabbah, and F. Nadim. Peptide neuromodulation of synaptic dynamics in an oscillatory network. *The Journal of Neuroscience*, 31(39):13991-4004, 2011.